

## Design of an automated aerodynamic guide vane mechanism for a micro compressor

**David Carreira Ribeiro**

Thesis to obtain the Master of Science Degree in

### **Mechanical Engineering**

Supervisors: Dr. Christoph Schreiber

Prof. Miguel António Lopes de Matos Neves

### **Examination Committee**

Chairperson: Prof. João Orlando Maques Gameiro Folgado

Supervisor: Prof. Miguel António Lopes de Matos Neves

Member of the Committee: Dr. Hugo Filipe Diniz Policarpo

**November 2019**



To my parents for their unconditional support,



## **Acknowledgments**

It is my great pleasure to acknowledge a sense of gratitude to all people present in the Laboratory for Applied Mechanical Design (LAMD), with whom I learned over these five months. More particular, I thank Dr Christoph Schreiber for having accepted me to carry out this project and for all assistance provided since the beginning.

I would also like to thank Professor M. Matos Neves from Instituto Superior Tecnico for his availability and for having accepted the supervision of this thesis and thus providing me with this experience that I will never forget.

To my colleagues with whom I have learned a lot during these five years and with whom I have shared moments that will mark me for the rest of my life. With them, I learned that the path is always easier when it is not done alone.

Finally, I cannot forget to thank my family for all the support and motivation for the realization of this thesis, especially my father, for always having believed and encouraged me in most of my decisions.



## Resumo

O desenvolvimento de compressores centrífugos é sensível a um conjunto de parâmetros que influenciam o seu desempenho. Uma das formas comuns de melhorar o desempenho de um compressor centrífugo, é através do uso de um conjunto de palhetas-guia de ângulo ajustável que possibilitam o controlo angular do escoamento à entrada do compressor. Se corretamente controladas, estas palhetas permitem aumentar a gama de operação deste tipo de compressores.

Neste projeto, os dois mecanismos de controlo de pequena escala das palhetas-guia existentes no LAMD (um manual e outro automático), foram analisados do ponto de vista teórico e testados experimentalmente. Verificou-se que ambos os sistemas levam a um erro considerável na tarefa de direcionar o fluxo no ângulo escolhido. Isto constitui uma limitação no projeto posterior de compressores centrífugos.

Posteriormente, foi realizado o estudo de possíveis “designs” que pudessem eliminar o erro no ajuste das guias de pequena escala, tendo sido escolhido um mecanismo automático de acionamento direto com seis motores de passo para o controlo das palhetas-guia. Após modelação num software de Computer-Aided Design (CAD), os desenhos do mecanismo foram entregues às oficinas, as quais foram responsáveis pelo respetivo fabrico. Foram realizados em laboratório ensaios experimentais com o novo sistema.

O novo mecanismo elimina significativamente o erro mecânico do sistema automático anterior. Após comparação com os resultados de Computational Fluid Dynamics (CFD), foi possível concluir que o novo mecanismo permitiu uma redução absoluta média do erro no ajuste das IGVs de 30,75%, relativamente aos resultados obtidos para o anterior mecanismo automático.

**Palavras- Chave:** Mecanismo automático, guia de ângulo ajustável, ângulo de escoamento, controle de posição angular, projecto mecânico, micro-compressor





# Abstract

The behaviour of centrifugal compressors is sensitive to several parameters that influence their performance. One way that is typically used to enhance the performance of compressors involves a set of automated, variable Inlet Guide Vanes (IGVs) for compressor inlet flow control. If correctly controlled, those vanes allow increasing the operating range of those compressors.

In this project, the two small-scale guide vane control mechanisms available at LAMD (one manual and one automated geared mechanism) were analysed theoretically and tested experimentally. It was found that both systems lead to a considerable error in the task to direct the flow at the chosen angle. This is a limitation, in the design of the centrifugal compressors.

Subsequently, the study of possible designs that could eliminate the error in the adjustment of small scale IGVs was carried out. An automatic direct drive mechanism with six stepper motors was chosen. After the design in the Computer-Aided Design software (CAD), the drawings of the mechanism were delivered to the workshops which were responsible for the manufacturing of the new mechanism. Experimental tests were carried out in the laboratory with the new system.

The new design significantly eliminates the mechanical error of the previous automated system. After comparison with the Computational Fluid Dynamics (CFD) results, it was possible to conclude that the new mechanism allowed an absolute mean error reduction in the IGVs adjustment of 30.75%, compared to the results obtained for the automated geared mechanism.

**Keywords:** automated mechanism, Variable Inlet Guide Vane, flow angle, angular position control, mechanical design, micro-compressor



# CONTENTS

Acknowledgments.....	iv
Resumo .....	vi
Abstract.....	viii
List of Tables.....	xii
List of Figures .....	xiii
List of Symbols .....	xvi
<b>1. Introduction .....</b>	<b>1</b>
<b>1.1. Motivation .....</b>	<b>1</b>
<b>1.2. Project Overview .....</b>	<b>1</b>
<b>1.3. Objective .....</b>	<b>2</b>
<b>1.4. Thesis Outline .....</b>	<b>3</b>
<b>2. Background.....</b>	<b>4</b>
<b>2.1. IGVs in Compressors .....</b>	<b>4</b>
<b>2.2. IGV Theory .....</b>	<b>6</b>
<b>2.3. Guide Vane Mechanisms .....</b>	<b>8</b>
<b>2.3.1. Guide vane air foils.....</b>	<b>9</b>
<b>2.3.2. Control mechanism .....</b>	<b>10</b>
<b>3. Experimental Investigation .....</b>	<b>14</b>
<b>3.1. Description of the setup .....</b>	<b>14</b>
<b>3.2. Experiment conditions .....</b>	<b>15</b>
<b>3.3. CFD results .....</b>	<b>18</b>
<b>4. Mechanisms Analysis .....</b>	<b>20</b>
<b>4.1. Automated Mechanism .....</b>	<b>20</b>
<b>4.1.1. Description of mechanism.....</b>	<b>20</b>
<b>4.1.2. Key elements and error sources .....</b>	<b>21</b>
<b>4.1.3. Experiment testing with the mechanism .....</b>	<b>31</b>
<b>4.1.4. Analysis Conclusions .....</b>	<b>33</b>
<b>4.2. Manual Mechanism .....</b>	<b>34</b>
<b>4.2.1. Description of mechanism.....</b>	<b>34</b>
<b>4.2.2. Key elements and error sources .....</b>	<b>34</b>
<b>4.2.3. Experiment testing with the mechanism .....</b>	<b>38</b>
<b>4.2.4. Conclusion of the analysis.....</b>	<b>40</b>
<b>5. Solution Finding .....</b>	<b>41</b>

<b>5.1. Requirements</b> .....	41
<b>5.2. Constraints</b> .....	41
<b>5.3. Methodology in design choice</b> .....	42
<b>5.4. Choice of Final Concept</b> .....	45
<b>5.4.1. Lever mechanism</b> .....	46
<b>5.4.2. Direct Drive mechanism</b> .....	52
<b>5.4.3. Conclusion</b> .....	56
<b>6. New IGV Mechanism Design</b> .....	58
<b>6.1. Mechanical Design</b> .....	58
<b>6.1.1. Structural analysis to the vanes</b> .....	58
<b>6.1.2. O-ring choice</b> .....	63
<b>6.1.3. Sizing of the stepper motor</b> .....	65
<b>6.2. Mechanism manufacturing</b> .....	69
<b>6.3. Assembly of the mechanism</b> .....	70
<b>6.4. Control of the mechanism</b> .....	71
<b>7. New Mechanism Test Experiments</b> .....	74
<b>8. Conclusions</b> .....	76
<b>8.1. Achievements</b> .....	76
<b>8.2. Future work</b> .....	77
<b>8. References</b> .....	79
<b>A. Annex</b> .....	81
<b>A.1. KISSsoft Procedure Analysis</b> .....	81
<b>A.2. Technical Drawings</b> .....	85
<b>A.3. Technical data of the motor, controller and arduino</b> .....	93
<b>A.4. Arduino Control Routine</b> .....	96
<b>A.5. Procedure to place baldes (automated part)</b> .....	99
<b>A.6. Procedure to run the experiment (after placing blade angle)</b> .....	100

## List of Tables

Table 1: Absolute error between CFD results of [1] and theoretical values for blade angle.....	19
Table 2: Match between the number of steps and the angle adjusted in stepper motor .....	23
Table 3: Experimentally and theoretical obtained results for the backlash of the gear train (crown gear)	29
Table 4: Error between the experimental data from Automated Mechanism and CFD results .....	33
Table 5: Summary of the error quantification of the sources in the automated system .....	33
Table 6: Summary of the error quantification of the sources in the manual system .....	38
Table 7: Inlet and Outlet pressures of the experiment with manual mechanism .....	38
Table 8: Error between the experimental data from Manual Mechanism and CFD results .....	40
Table 9: Summary of pros and cons of manual and automated system.....	40
Table 10: Error quantification due to manufacturing tolerances in the system calibration task.....	49
Table 11: Summary of inaccuracy sources of the levers mechanism designed.....	51
Table 12: Expected Cost involved in levers mechanism design.....	52
Table 13: Summary of inaccuracy sources of the designed Direct Drive mechanism .....	55
Table 14: Expected Cost involved in Direct Drive mechanism design .....	55
Table 15: Summary of the variables involved in the accuracy of the analysed systems .....	56
Table 16: Metric Decision Table.....	56
Table 17: Conditions used in Catia V5 .....	60
Table 18: Parameters involved in fatigue stress concentration factor computation [32].....	61
Table 19: Corrective parameters for fatigue limit strength [32].....	62
Table 20: Data concerning the existing seal types in the mechanism .....	64
Table 21: System inertia for specific axis .....	67
Table 22: Data concerning the fluids that can be used for testing the system.....	68
Table 23: Torque required by different system components due to friction [37].....	68
Table 24: Summary of torque required by the system to work properly .....	69
Table 25: Inlet and Outlet pressures of the experiment with direct drive mechanism .....	74
Table 26: Mean absolute deviation between the tested mechanisms and CFD, function of the angle adjusted .....	75
Table 27: Mean absolute deviation between the tested mechanisms and CFD, function of the radial position .....	75
Table 28: Gear train dimensions computed in the automated mechanism .....	81

# List of Figures

Figure 1: Example of IGVs actuation (source: [1]).....	1
Figure 2: IGVs control mechanisms used in LAMD .....	2
Figure 3: Different types of compressors and turbomachines .....	4
Figure 4: Centrifugal compressor (source: [4] ).....	4
Figure 5: Main Components of a centrifugal compressor: .....	5
Figure 6: Compressor map representing how the impeller stalling is influenced by IGVs (source: [6]) .....	6
Figure 7: Influence of IGV angle on output work of a centrifugal compressor ( source: ITSM University of Stuttgart) .....	7
Figure 8: Components of a guide vane lever mechanism (source:[10] ).....	8
Figure 9:NACA 0012 Airfoil with its lift and drag coefficient curves ( source:[9]).....	9
Figure 10:Joints (red mark) present in diferentes lever guide vane mechanisms: a) LAMD b) (source: [11] ) c) Piller Blowers&Compressors (source: [12]) .....	11
Figure 11: Geared Mechanism (source: [13]) .....	11
Figure 12:Manual Mechanism to control IGVs present at LAMD .....	12
Figure 13:Different variants of multi actuator control mechanisms (source: [14]) .....	13
Figure 14: Experimental setup of the IGV with the IGV control manual mechanism .....	15
Figure 15: Overview of IGV channel.....	15
Figure 16:Reference axes in the probe manipulation .....	16
Figure 17: Results to figure out center of the IGV channel .....	16
Figure 18: Results to figure out the center hole in the probe .....	17
Figure 19: Method to calculate the flow angle for a given radial position.....	17
Figure 20: IGVs position relative to the probe position.....	18
Figure 21:Angle profiles of CFD and theroretical angles adjusted by the operator with error bars.....	19
Figure 22: Automated control mechanism for IGV present in the LAMD .....	20
Figure 23:Sources of innacuracy in the automated geared system.....	21
Figure 24:SPG1518M0504-102 stepper motor datasheet (source:[16]).....	22
Figure 25: Generic example of a Nema stepper motor torque vs speed chart (source: [18]) .....	22
Figure 26: Backlash on a gear train (source: [19] ) .....	24
Figure 27:Different types of backlash in a gear train (source: [20] ) .....	25
Figure 28:Gear train used in automated mechanism (Gears from Nozag) (source: [22]) .....	25
Figure 29: Results from KISSsoft analysis .....	26
Figure 30:Components contributing to the backlash of the gear train.....	27
Figure 31: Scheme of the test setup used to measure the backlash of the gear train.....	28
Figure 32: Results obtained for circunferential backlash using a system: without springs (left) and with springs (right) .....	28
Figure 33: Dimensional and Geometrical Tolerances of the part used to calibrate the Initial position of the system .....	30
Figure 34: Calibrator used in automated system .....	30

Figure 35: Deviation in blade adjustment caused by the calibrator and manufacturing tolerances.....	31
Figure 36: Deviation between automated mechanism and CFD angle profiles .....	32
Figure 37: Error in the adjustment of the blades angle with the automated system function of radial position .....	32
Figure 38: Sources of inaccuracy due the manufacturing tolerances in manual system .....	34
Figure 39- Angle scale present on cursor .....	35
Figure 40: Dimensional tolerances of parts involved in blade adjustment (source: [26]) .....	35
Figure 41: Scheme used in error calculation .....	36
Figure 42: Dimensional and geometric tolerances presents in blade manufacturing .....	36
Figure 43: Reference axis used to compute the error coming from the distance between cursor and casing grade .....	37
Figure 44: Possible error coming from operator precision to perform the task of adjust blades angle .....	37
Figure 45: Deviation between manual mechanism and CFD angle profile.....	39
Figure 46: Angle error function of the radial position .....	39
Figure 47: Adjacent parts of the assembly constraining IGV build space .....	42
Figure 48: Schematic summary of the steps required to solve the problem .....	42
Figure 49: Steps involved in solution finding stage .....	43
Figure 50: Gears classification according to the position of shaft axes (source: [27]).....	44
Figure 51: Split gearing solution considered.....	45
Figure 52: Lever Solution Design- Cut View .....	46
Figure 53: Solution with Levers and Linear Stepper Motor- External View .....	47
Figure 54: 0012 NACA Shaft .....	47
Figure 55: Grade inscribed in the external surface of the casing .....	48
Figure 56: Relation between lever 1 and Lever 2 .....	48
Figure 57: Inaccuracy in connection between ring and lever 2 .....	48
Figure 58: Connection part between linear actuator and lever 2 .....	49
Figure 59: Absence of gap between the casing and the scale inscribed in the ring reduces the error in the system calibration. ....	49
Figure 60: Different types of linear motors (source:[28]) .....	50
Figure 61: Technical data of linear actuator necessary to compute systems accuracy from Nanotec (source: [28]) .....	50
Figure 62: Error in blade adjustment coming from the linear actuator .....	51
Figure 63: Relation between linear actuator step and blades angle.....	51
Figure 64: Direct Drive Solution Design- Cut View.....	52
Figure 65: Final design of the VIGV direct drive mechanism: External view (left) and Cut View (right)	53
Figure 66: 0012 NACA Shaft of Direct Drive system .....	53
Figure 67: Casing of Direct Drive system.....	54
Figure 68: Calibration of the system with Direct Drive System .....	54
Figure 69: 0012 NACA blade analysed .....	59
Figure 70: Stress in the vane (source: [9]) .....	60

Figure 71: Graph of applied stress over time .....	61
Figure 72: Different types of seal in the mechanism: static (left) and dynamic / almost static (right).....	64
Figure 73: Percentage of O-ring deformation depending on the type of application (source: [33]).....	64
Figure 74:Dimensions table provided by Normatec regarding the elaboration of enclosures for allocation of O-Rings (source: [35]) .....	65
Figure 75: Torque vs Speed Charts of stepper motors with the same size and brand as the chosen one (source:[16] ).....	66
Figure 76:Parts involved in transmitting the movement of the motor stepper to the vane .....	66
Figure 77: Typical acceleration profile in Stepper motors (source: [36]) .....	67
Figure 78: Steps involved in the manufacturing process of the mechanism .....	69
Figure 79: Constituent parts of the new mechanism: Clean parts after ultrasound (left), calibrators mounted on the mechanism (center) and magnified image of an IGV (right) .....	70
Figure 80:Exploded view of the VIGV mechanism .....	71
Figure 81: Connection diagram of the control system .....	72
Figure 82: Interaction between electronic components in the functioning of the new mechanism.....	72
Figure 83:Electronic components constituting the new design .....	73
Figure 84: Mechanism final configuration with the electronic part assembled.....	73
Figure 85: Deviation between tested mechanisms and CFD angle profile with error bars .....	74
Figure 86: Problem prevents correct shaft rotation when adjusting the blade angle .....	77
Figure 87: Relative position of the 3 components of the experimental design susceptible to large deviations .....	78
Figure 88: Data entry regarding the power of the system .....	81
Figure 89: Basic data introduction about the gear train .....	82
Figure 90: Rough Sizing window on KISSsoft .....	82
Figure 91: Fine Sizing window on KISSsoft .....	83
Figure 92: Solutions computed by KISSsoft for gear train .....	83
Figure 93:Intended results from KISSsoft analysis.....	84



# List of Symbols

## Acronyms

ATME	Atelier de l'institut de génie Mécanique.
CAD	Computer Aided Design
CAM	Computer Aided Manufacturing
CFD	Computational Fluid Dynamics
CNC	Computer Numerical Control
IGV	Inlet Guide Vane
LAMD	Laboratory for Applied Mechanical Design
Matlab	Matrix Laboratory
NBR	Nitrile Butadiene Rubber
3D	Three-Dimensions

## Greek Symbols

$\alpha$	Flow angle
$\alpha'$	Angular acceleration
$\alpha''$	Pressure angle
$\beta$	Relative angle between probe and IGV
$\Delta h$	Specific enthalpy
$\delta$	Primitive angle
$\varepsilon$	Error
$\varepsilon_a$	Addendum angle
$\varepsilon_f$	Dedendum angle
$\Sigma$	Shaft angle
$\mu$	Friction coefficient
$\emptyset$	Diameter
$\rho$	Specific mass
$\sigma$	Stress
$\sigma_{applied}$	Applied stress
$\sigma_{max}$	Maximum stress
$\sigma_{min}$	Minimum stress
$\sigma_m$	Mean stress
$\sigma_a$	Alternating stress
$\bar{\sigma}_m$	Corrected mean stress
$\bar{\sigma}_a$	Corrected alternating stress
T	Torque

## Roman Symbols

A	Area
$c_i$	Absolute flow velocity
$C_d$	Drag coefficient
$C_l$	Lift coefficient

$d_m$	Mean deviation
D	Pitch diameter
D'	Equivalent pitch diameter
$D_a$	Crown diameter
$D_a'$	Equivalent crown diameter
$D_b$	Base diameter
$D_b'$	Equivalent base diameter
$D_f$	Root diameter
$D_f'$	Equivalent root diameter
E	Tooth range
$F_l$	Lift force
I	Moment of inertia
i	Gear ratio
g	Geratriz
$h_a$	Addendum
$h_f$	Dedendum
j	Root clearance
$K_a$	Surface factor
$K_b$	Size factor
$K_c$	Loading factor
$K_d$	Temperature factor
$K_e$	Reliability factor
$K_f$	Fatigue stress-concentration factor
$K_t$	Stress concentration factor
L	Length or distance
M	Module
n	Safety factor
P	Pressure
P'	Circular pitch
$P_{ang}$	Angular pitch
$P_t$	Total pressure
$P_{stat}$	Static pressure
$P_\alpha$	Wall pressure
q	Notch sensitivity
r	Radius
S	Tooth thickness
$S_e$	Endurance limit stress
$S_Y$	Yield strength
$S_{UT}$	Ultimate tensile strength
t	time
tan	Tangent
T	Temperature
u	Rotational speed
v	Velocity
$w_{compressor}$	Work generated by a compressor
$w_i$	Relative flow velocity
Z	Number of teeth
Z'	Equivalent number of teeth

# 1. Introduction

## 1.1. Motivation

In the world of turbomachinery, famous companies like Rolls Royce or Pratt and Whitney have vast experience in the engine manufacturing for large scale applications. On the other side, manufacturing of small-scale turbomachines components often appear to be neglected by large industries.

The LAMD focuses on the design and experimental investigation of small scale turbomachines. One part of its research focuses on understanding how the scale influences the design and how to mitigate losses on small scale radial compressors and turbines.

One of the laboratory's tests stands is used to assess the performance of a small scale turbo compressor developed by LAMD. It includes variable IGVs, located in front of the compressor. These have the purpose of directing the fluid-flow to the compressor, as shown in figure [1](#), at the appropriate angle to ensure the most efficient operation. The accuracy in controlling the angle of IGVs is of vital importance as it provides results that are used in the subsequent design of centrifugal compressors.

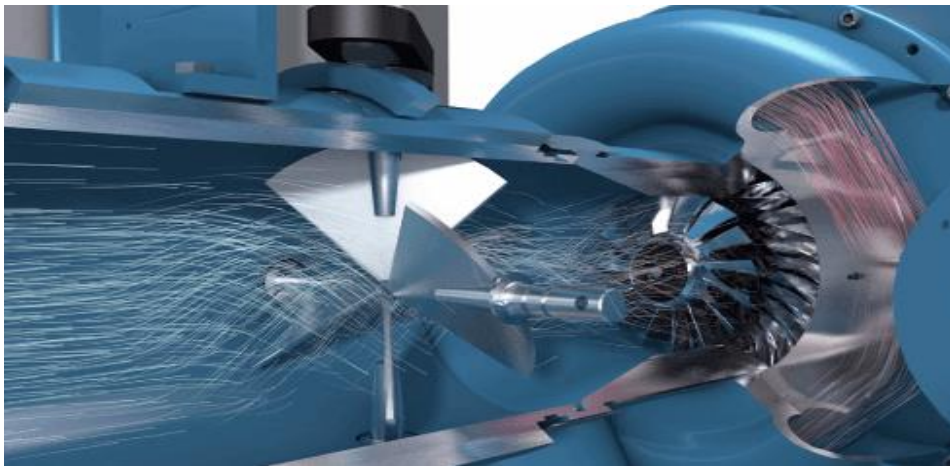


Figure 1: Example of IGVs actuation (source: [1])

## 1.2. Project Overview

At LAMD a set of small scale IGVs that are part of a small scale compressor (large diameter of the compressor is  $\varnothing=14\text{mm}$ ) is available.

In order to control this set of IGVs, an automated geared mechanism (Figure [2a](#)) has been designed and realised. It has been found in Aeschbacher's work [2] and in a preliminary study by Schreiber, that this mechanism was insufficient in terms of accuracy and repeatability.

In order to achieve more precise control in terms of accuracy, repeatability and adjustability, a manual mechanism (Figure 2b) was built that meets the quality criteria, namely allows more precise control in the adjustment of the blade angle.

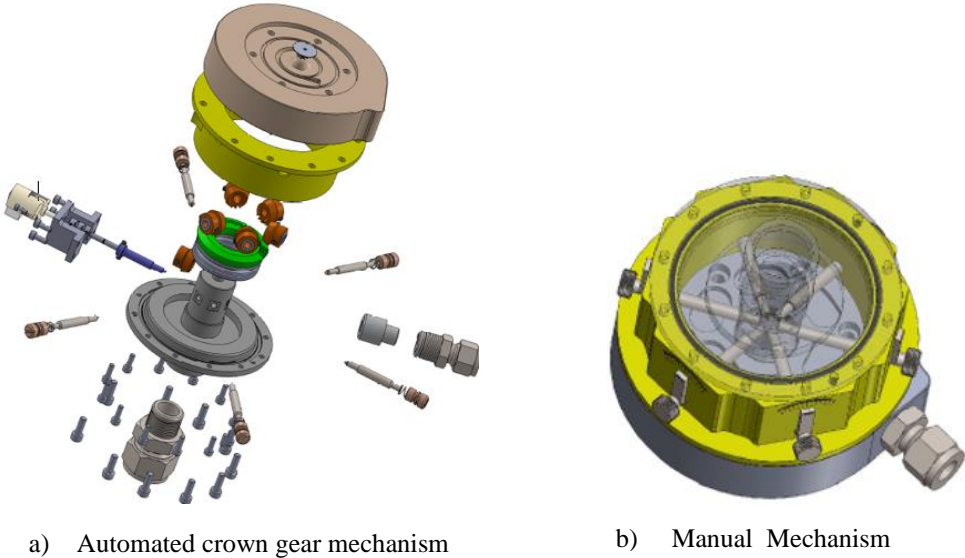


Figure 2: IGVs control mechanisms used in LAMD

Due to the small scale of the application, even manufacturing tolerances play an important role in the final system accuracy.

### 1.3. Objective

The main goal of this thesis is to find a solution that can combine the accuracy of manual mechanism with automated control. This will involve three different steps: problem analysis, solution finding and design.

Based on this, the primary objective of this thesis is to perform an analysis of the failures and limitations, as well as the advantages of both systems regarding accuracy in blades adjustment. In this focus, it is necessary to evaluate also the manual and automated mechanisms from an experimental point of view, taking into account the results of the CFD analysis of Aeschbacher [2].

Once the results obtained have been analysed, a suitable IGV automated control system should be designed. The aim implied in constructing the mechanism is to provide the fulfilment of the design requirements in terms of accuracy, repeatability in the adjustment of the blades. This stage will include the development of advanced actuation mechanism, 3D design and manufacturing drawings. The secondary objective of this thesis involves the assembly, experimental test and validation of the new solution through comparison with the available CFD results.

## 1.4. Thesis Outline

This thesis is composed of eight chapters: Introduction, Background, Experimental Investigation, Mechanisms analysis, Solution Finding, New mechanism design, New Mechanism Experiments and Conclusions.

In the introduction chapter, the motivation and the objectives of the thesis are defined, providing an overview of the main topic that is the focus of the thesis.

The second chapter is the background, where the information regarding the context of the project is introduced. This section provides an overview of the existing compressors to frame the use of variable IGVs in their operation. Also, the general structure of a centrifugal compressor is presented. The purpose of the use of IGVs is explained, and its role in optimizing the design of centrifugal compressors is described.

The experimental investigation chapter is concerned with describing the test bench and the entire apparatus involved in experiments to test the control mechanisms of IGVs. It explains how the results should be processed to assess the accuracy of each of the mechanisms. The CFD results [2] that serve as a reference for experimental comparison are also presented.

The fourth chapter analyses the mechanisms present in the LAMD. Sources of error are identified and quantified for each mechanism. The theoretical maximum error that each source can cause in the task of correctly adjusting the intended angle of the IGVs is calculated. The results of the experiments, which served as final support in assessing the accuracy of each mechanism, are also provided. A survey of the failures and advantages of each design is also performed to help in the solution-finding stage.

The fifth chapter deals with the methodology involved in the choice of the final solution. It includes the presentation of the constraints and requirements involved in the design of the new mechanism. In the decision of the final solution, the two final designs considered, and the factors that led to the choice of the final solution are presented.

The new mechanism's design chapter includes the presentation of the entire process involved in the design and manufacture of the final mechanism. Details of the design of the mechanical and electronic component of the final designed system are provided.

New Mechanism Experiments chapter presents the results obtained from the new mechanism experiments. The results are compared with the values obtained in the tests of the other mechanisms (manual and geared mechanism), and the key points of this assessment are highlighted.

The final chapter concludes the results and experimental mechanisms presented in this thesis and suggests improvements in the test bench that allow a more efficient data acquisition. Some factors can be improved to enable the optimization of centrifugal compressor design.

## 2. Background

This chapter presents a brief review of the background information for this thesis. Firstly, the different types of compressors are distinguished, and compressors that use variable IGVs during their operation are identified. In this section, the fundamental constitution of a centrifugal compressor is presented. Also, the inclusion of the control mechanism of IGVs in its operation is explained. The second section provides information about the purpose of the IGVs and how their use affects the performance of a compressor. The third and final section of this chapter presents the constitution of a control mechanism for IGVs. The different types of existing control mechanisms are also presented in this section.

### 2.1. IGVs in Compressors

In the field of compressors, there is a wide range of different types that can be distinguished [3]. Control of IGVs is generally related to the efficient mapping of centrifugal compressors, which are a particular type of turbomachine (Figure 3).

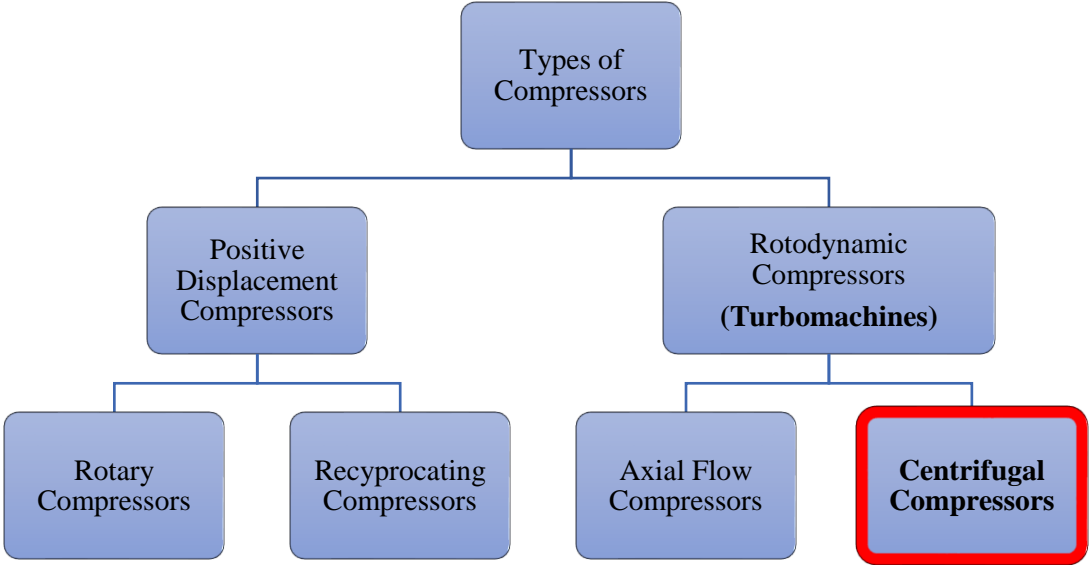


Figure 3: Different types of compressors and turbomachines

Centrifugal compressors are generally characterized by receiving the gas in an axial direction and expelling it in a radial direction. They add work to the fluid by exchange of momentum with the fluid via their characteristically shaped blades, shown in figure 4.



Figure 4: Centrifugal compressor (source: [4] )

The same ones are used in several applications, the most known being turbochargers and gas turbines. A centrifugal compressor consists of the following four major components [5]: inlet, impeller, diffuser, and volute (see figure 5a).

The functions of these different components are detailed below:

**Inlet Pipe:** The entrance to a centrifugal compressor is a single pipe. It is in this component of the centrifugal compressor that the IGVs, to redirect the inlet flow, can be installed. They will be seen later in this chapter.

**Impeller:** the component responsible for receiving the fluid in the axial direction and accelerating and expelling it in the radial direction. The speed of the impeller output flow can reach transonic speeds.

**Diffuser:** the diffuser translates the kinetic energy of the working fluid into potential energy (pressure). It occurs by increasing the cross-sectional area and gradually reducing the flow velocity.

**Volute:** The volute absorbs the flow by redirecting it in the tangential direction and delivers it to the compressor outlet pipe. The flow velocity is further reduced in the flow channel, and the static pressure is increased. The volute can take many different geometric shapes.

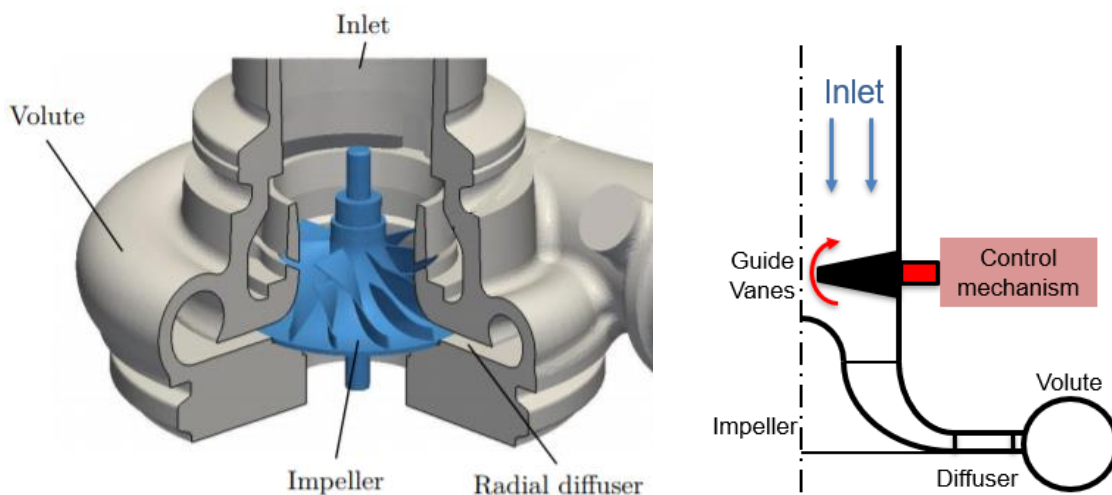


Figure 5: Main Components of a centrifugal compressor:

a) Isometric view (source: [5])      b) Section view

As mentioned above, not rarely IGVs are also used in order to be able to operate with different operating points as explained later in section 2.2. As a result, variable guide vanes are used in the constitution of a centrifugal compressor. For the use of these, a control mechanism is needed to allow the correct adjustment of the IGVs angle (red mark in Figure 5b). It is on this control component that the work developed is focused.

## 2.2. IGV Theory

Regarding IGVs, these can be fixed or variable. Located in front of the impeller eye, they are designed to guide the fluid flow efficiently into the impeller. In this project, the IGVs used are the variable ones, in order to enhance the operating range.

The performance of a compressor can be assessed using a map of the compressor that associates the variables of pressure ratio and volume or mass flow rate. The surge line bounds this map at low flow rates and the choke limit at high flow rates.

The surge line reflects the operating points where the pressure ratio is too high for the volume of fluid flowing. This phenomenon causes the fluid to no longer adheres to the suction side of the compressor blades, leading to the reversal of the fluid flow direction, and thus the discharge process is disturbed. This can be deteriorating for the system and also cause high vibrations and noise. For instance, surge can lead to the complete breakdown of steady flow in the compressor.

When the volumetric flow rate of the fluid is too high for the pressure ratio, and the velocity of the fluid can not be increased further, it means that a choke situation is reached. In a well designed compressor, the maximum volumetric flow is limited by the cross-section at the inlet, where transonic conditions are reached.

Thus, the range of operation between the surge and choke limit defines the operating range of a compressor. It is at this point that the use of IGVs comes in since they allow manipulating the map of the compressor, increasing the range of operation [4]. As variable IGVs are placed in front of the first stage of the impeller, the different angle at which they are adjusted allows the creation of a pre whirl, which is the phenomenon of adding a tangential component to the inlet air. Figure 6 represents a graph showing how the different pre-swirls are created to allow the compressor to operate at different conditions.

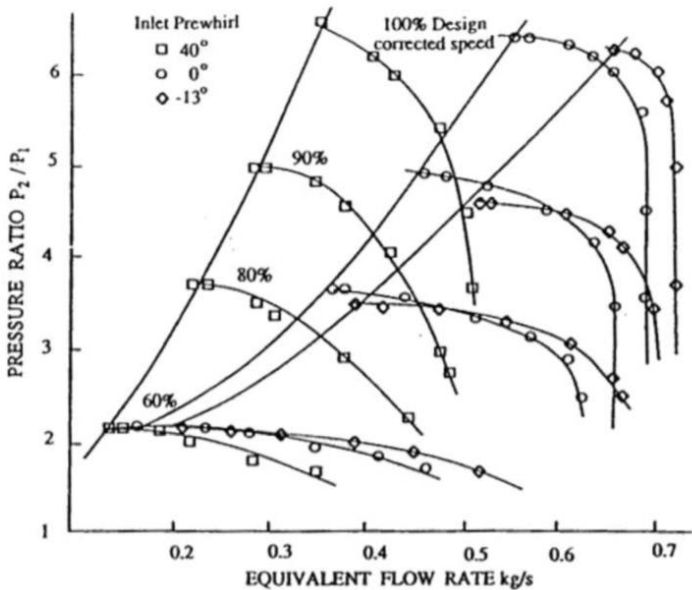


Figure 6: Compressor map representing how the impeller stalling is influenced by IGVs (source: [6])



By using IGVs, the absolute velocity of the fluid at the leading edge of the impeller can deviate angularly. The fluid flow is directed according to the angle of attack of the IGVs. It translates into the most notable effect of using IGVs.

Therefore, it can be concluded that the performance of the compressor stage varies by inducing this pre-swirl for a given rotational speed and mass flow rate [7], as shown in figure 6.

For a better comprehension of the IGV effect, the most fundamental and famous equation in turbomachinery can be seen, the Euler's pump equation:

$$w_{compressor} = \Delta h_t = u_2 c_{u2} - u_1 c_{u1} = \frac{1}{2} ((u_2^2 - u_1^2) + (c_2^2 - c_1^2) + (w_1^2 - w_2^2)) \quad (1)$$

where  $h_t$  represents the enthalpy and the term defined by the quadratic difference of rotational speeds,  $u$ , represents the working input to the fluid by a loss-free centrifugal effect due to the change in rotational speed. In this equation,  $c_1$  and  $c_2$  are the absolute velocities of the fluid at the inlet and outlet respectively.  $w_1$  and  $w_2$  are the relative velocities of the fluid with respect to the blade at the inlet and outlet respectively.  $u_1$  and  $u_2$  are the velocities of the blade at the inlet and outlet respectively. The second and third terms describe the deceleration of the impeller, depending on the blade angles and the angle of the inlet flow.

From this equation and observing figure 7, it is possible to conclude that the creation of a negative pre swirl (with opposite direction to the impeller rotation) results in the creation of higher work by the compressor [8].

Figure 7 shows the effects on the triangle of velocities resulting from the control of the angle of the IGVs and the different pre swirls induced by the use of IGVs.

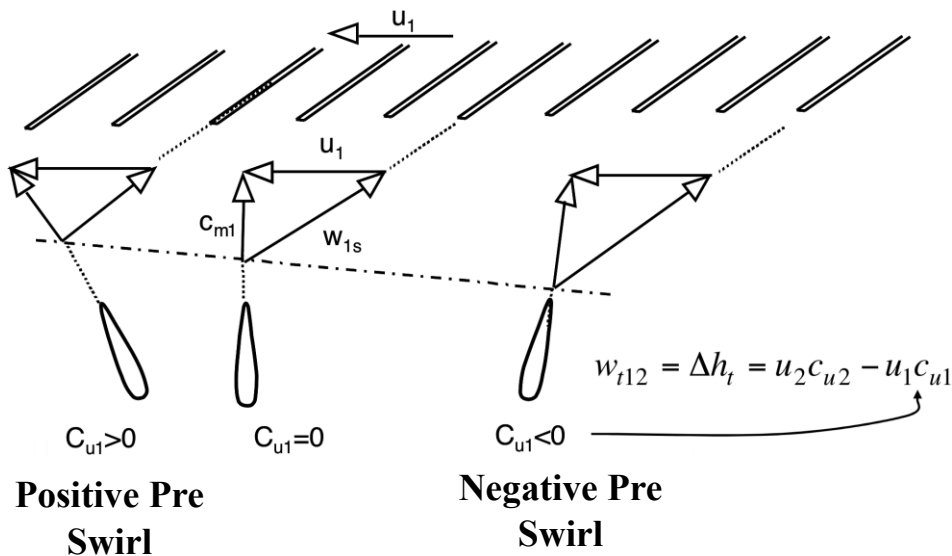


Figure 7: Influence of IGV angle on output work of a centrifugal compressor ( source: ITSM University of Stuttgart)

Lastly, it should be noted that the use of IGVs is only feasible in this type of applications because the benefits of IGVs by improving range are more significant than the performance penalty due to additional loss.

Regarding the use of IGVs it is essential to notice that the direction that gives the fluid is limited by choice of the airfoil profile chosen to shape the blades. If the adjusted angle is higher than the angle of the airfoil for which there is separation, the flow does not follow the blade angle and pressure losses reach significant levels [9].

### 2.3. Guide Vane Mechanisms

About the mechanism used in the control of IGVs, it should be noted that it has the purpose of adjusting the blade angle with the highest possible accuracy. The final goal of a control mechanism is to ensure that the deviation between the operator-adjusted angle and the final blade angle is as low as possible.

According to the dictionary, guide vanes are airfoils that direct air, gas or water to the moving blades of a turbine/ compressor. It is crucial, therefore, to know how the guide vanes are controlled and to perceive the components that compose the control mechanism for it.

The IGV control mechanisms used in the industry consist of: airfoil profile that makes up the vanes, connecting shaft, control unit in the form of levers, actuators (motors) and controllers, as shown in figure 8.

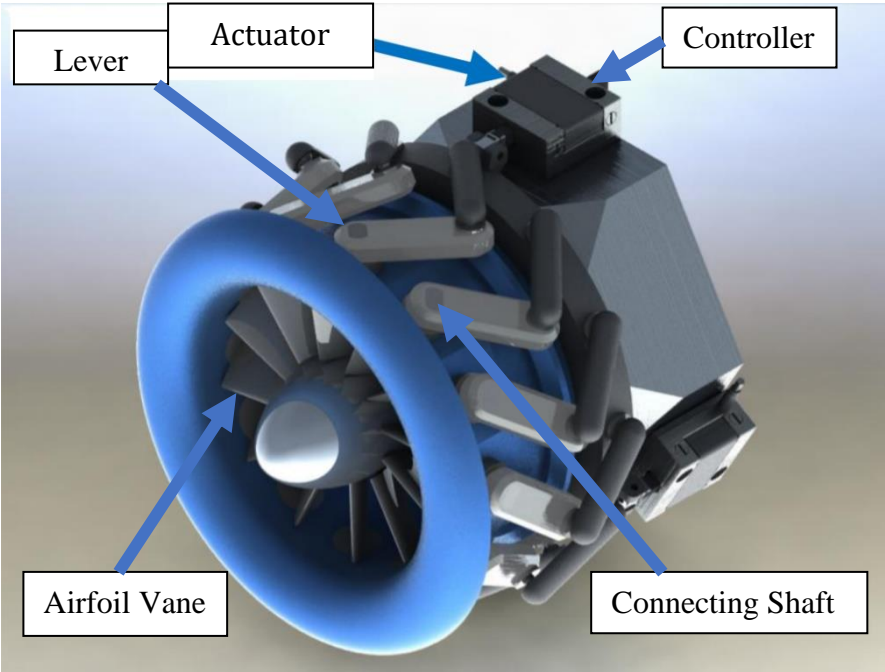


Figure 8: Components of a guide vane lever mechanism (source:[10] )

The items noted in figure 8 are part of the essential elements of a control system for IGVs. The difference between each type of design is the result of the choice of actuator type (linear or rotary) and the mechanical mechanism of motion transmission (with levers or with gears). In section 2.3.2 of this chapter, the different guide vane mechanisms are presented.

### 2.3.1. Guide vane air foils

IGVs have vanes shaped according to the airfoil profile chosen for them. Depending on the Airfoil profile of the vanes, the operating range of the angular adjustment mechanism differs. The maximum possible range of flow angles is determined by the separation angle of the airfoil. Once this angle is passed, the blades no longer direct the fluid, and their use ceases to make sense, due to flow separation. Consequently, the choice of the airfoil is a key factor when designing the blades that compose the control mechanism. Depending on the shape of the vanes chosen, the system losses due to the use of IGVs can be reduced if an airfoil profile with a low drag coefficient is chosen.

In the work of Pillets [9], several NACA airfoils have been examined. For the mechanism subject to this project, a symmetrical NACA 0012 airfoil was chosen (Figure 9). The operating range of this airfoil profile is between  $-16^\circ$  and  $+16^\circ$ , values that will serve as a reference for the operating range of the vanes. When operating outside this range, the blade angle value will differ significantly from the flow value due to the separation of the flow.

The NACA 0012 airfoil has a 12% thickness to chord length ratio: it is 12% as thick as it is long. Due to its symmetry (indicated by 00), it has no curvature, allowing it to work in both directions. It can generate positive and negative pre swirls, serving the  $0^\circ$  of the blades for not creating pre swirl.

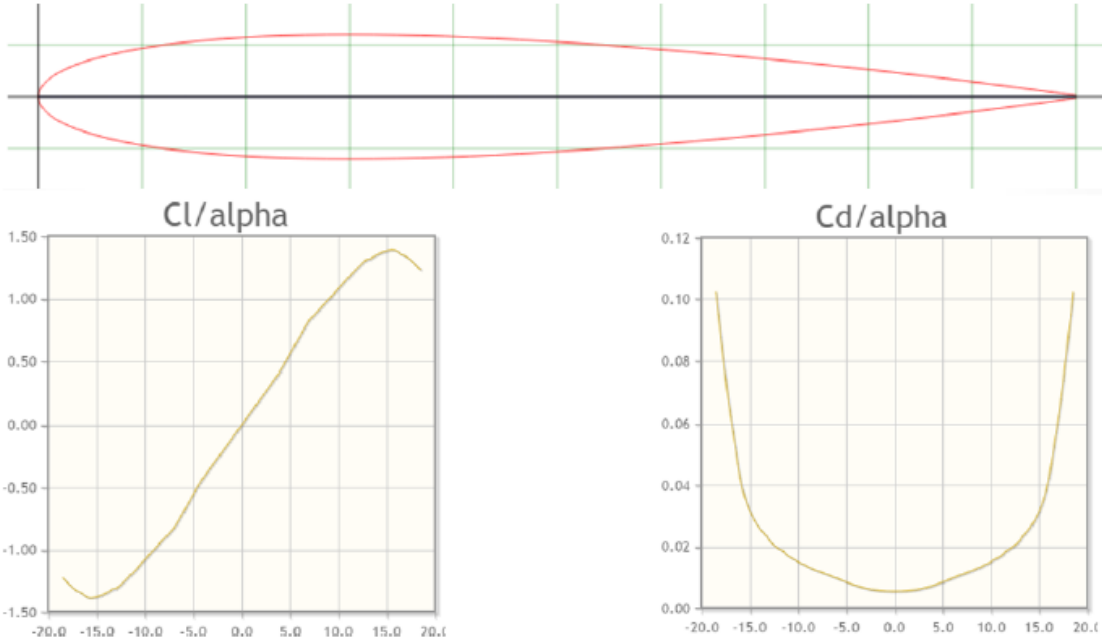


Figure 9:NACA 0012 Airfoil with its lift and drag coefficient curves ( source:[9])

As in the previous design of Pillet [9], it is essential to note the scale of the application. The blade will be 3.5 mm long and 0.4 mm thick at the maximum. All the six vanes will be directly milled on the six shafts.

### **2.3.2. Control mechanism**

The component responsible for angular control is particularly important in IGVs. It is responsible for the angular control of the blades, and therefore, the angle at which the fluid will pass through the impeller. A precise system implies an accurate control mechanism. In this regard, it is important to identify the full range of control mechanisms available in the industry.

This subsection presents the research results of the different mechanisms used to control IGVs. Several types of mechanisms for acting on IGVs were found in the research. However, it should be noted that all examples were presented as variants of four kinds: lever mechanism, geared mechanism, manual mechanism and direct drive mechanism. In this research, only mechanisms involving electric or manual actuation are presented. Hydraulic mechanisms were not taken as relevant research as, in addition to offering themselves as solutions that require much space, since the application involves testing with refrigeration fluids, the use of any oil in the operation of the mechanism is forbidden.

It is to be pointed out that no mechanism has been found, specially designed for small scale applications as is the case for the use of this study.

It is therefore vital to notice which are the characteristics of the mechanisms currently used to ensure they do not lose functionality with the downscaling of the application.

#### **2.3.2.1. Lever Mechanism**

The lever mechanism is the most widely used mechanism in the industry to control IGVs. A variety of patented variants of this type of mechanism can be found. In this design, a rotating ring and lever mechanism to the vanes is used. An actuator turns the ring that is linked to the levers.

This type of design is present in a wide range of variants, as shown in figure [10](#). However, the principle remains the same. Only the type of actuator that controls the levers can be different, namely linear or rotary.

One of the major problems of this type of mechanism, when applied to reduced scale machines, is the loss of precision due to the presence of joints (surrounded by red in figure [10](#)), which reduce accuracy.

By using it in small-scale applications, the effect of the presence of clearance in the joints gains more relevance in the overall adjustment accuracy of the system.

In figure [10](#), different designs using levers are presented, and in all of them, it is possible to observe the presence of the joints. The use of these mechanisms in small scale is only compatible with the suppression of these components. This is only possible using a material capable of resisting the efforts resulting from the adjustment of the angle, and whose deformation is supported only by the elastic domain of the material (linear).

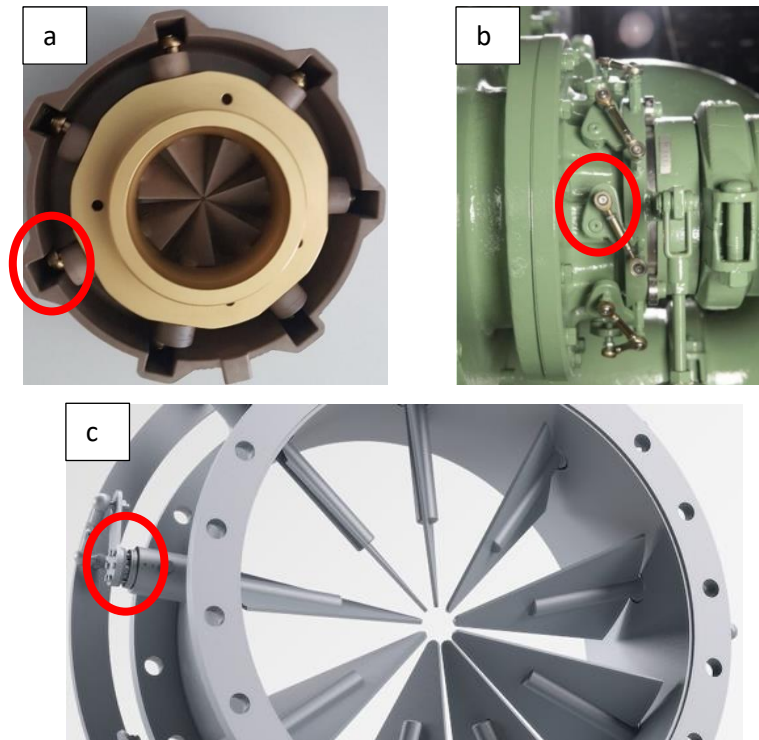


Figure 10: Joints (red mark) present in different lever guide vane mechanisms: a) LAMD b) (source: [11])  
c) Piller Blowers & Compressors (source: [12])

### 2.3.2.2. Geared Mechanism (Used in LAMD)

For the adjustment of IGV angles, a mechanism involving gears can be used. In this type of mechanisms, the presence of a crown gear, responsible for the transmission of movement, is emphasised. Bevel gears are placed on the shafts in which the vanes are manufactured, which are associated with the crown gear that acts as a planetary gear.

In this design, there is only one active shaft (directly connected to the actuator - stepper motor), and all the other vanes are moved from the action of the gears, as shown in figure 11.

Determination of the position is realised using the stepper motor. All researched and patented geared mechanisms present themselves as identical solutions to the mechanism presented, and there are no variants that are distinct enough to be described in this section as can be seen in the patented design of the Ingersoll Rand Company, which can be seen in figure 11. One of the problems with this design, especially when in small-scale applications

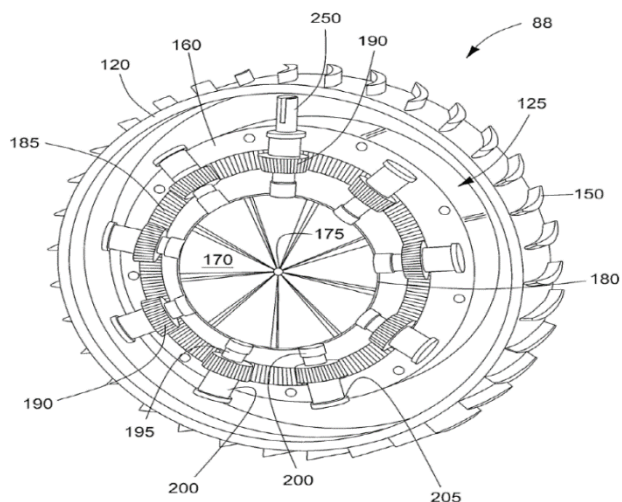


Figure 11: Geared Mechanism (source: [13])

is the angular backlash (i.e. the play that exists in the gear train). This problem is caused by the gap between the gear teeth and the tooth thickness that leads to inaccuracy in the blade angle adjustment movement.

It follows that once dealing with small-scale applications, this factor acquires more relevance, due to the ratio between the adjustment range and the backlash of the gear train.

### 2.3.2.3. Manual Mechanism (Used in LAMD)

The manual mechanism was conceived in order to increase the accuracy of IGV angle adjustment. In this design, each blade is mounted on a shaft with an indicator arm. Consequently, each blade angle can be adjusted directly with a cursor manually by the operator without slack as there are no intermediate mechanisms.

This type of design allows giving accuracy to the adjustment mechanism as the accuracy of the angle is only influenced by the manufacturing tolerances of the parts involved in the control of the same. In this project, the presence of compression springs should be emphasized, as shown in figure 12b). Its use ensures the calibration of the system in the axial axis.

Since it is manual and not automated as the other mechanisms, it is not suitable for performing test cycles. This happens because the repeatability of the tests is very dependent on the adjustment made by the operator.

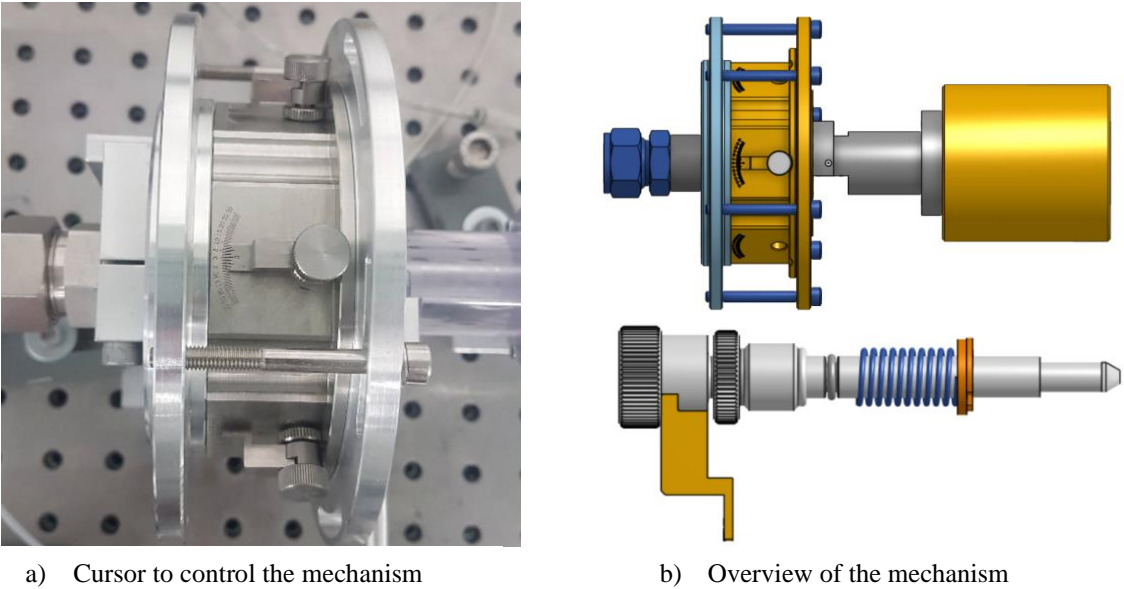


Figure 12: Manual Mechanism to control IGVs present at LAMD

#### 2.3.2.4. Direct Drive Mechanism

Another mechanism used to control IGVs uses multiple actuators, with a direct drive mechanism, as shown in figure 13.

In this design, each vane is directly connected to the actuator and can therefore be controlled independently. As a result, the motion transmission mechanism of the actuator for the vanes that are not directly connected (passive axes) is suppressed.

A further advantage is the rapid response rate of the system and the ease of replacing damaged parts in the system. Such happens due to the lack of interaction between the different moving parts of the system. In this sense, one of the disadvantages of the mechanisms described in the previous sections is solved.

This design, by replacing mechanical elements for the electrical ones, allows having better control of the angle adjusted for each blade, as there are no passive shafts in the system.

It should also be noted that the use of this mechanism is also compatible with small-scale applications, as it does not involve the manufacture of small moving parts in the system. As a result, the manufacturing tolerances of the parts, the resolution and accuracy of the actuator are the factors left to influence the accuracy of the system.

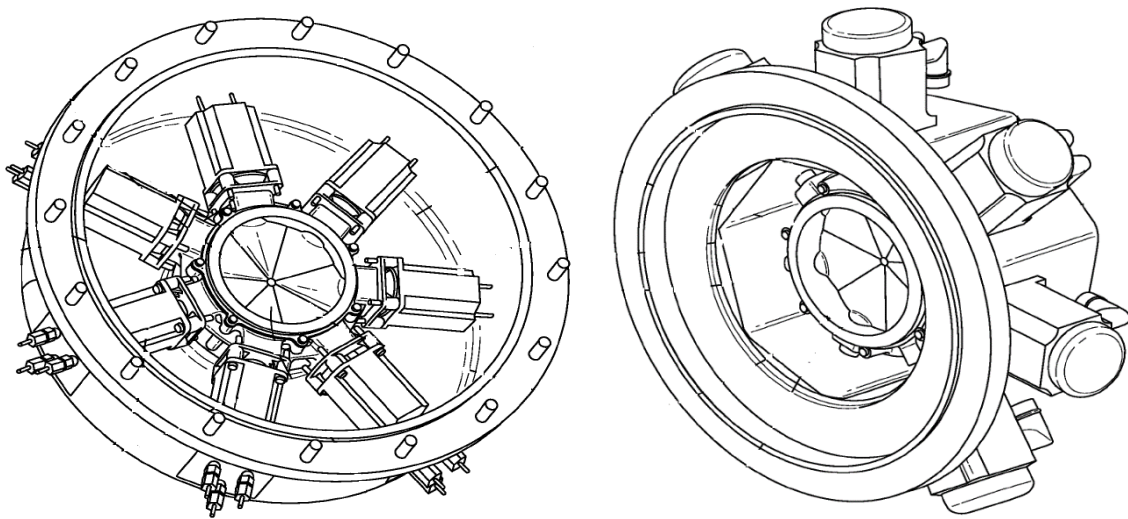


Figure 13: Different variants of multi actuator control mechanisms (source: [14])

### 3. Experimental Investigation

This chapter is concerned with the experimental component involved in the thesis. It consists of three main sections. Firstly, the whole apparatus and test bench present in the laboratory that serves as a basis for the experimental evaluation of the tested mechanisms (manual and automated) is presented.

Section 2 presents the experimental conditions under which the tests are carried out and how it is necessary to calibrate the system to be able to carry out the experiments. How the results of the experiments should be processed and how they allow concluding on the accuracy of the IGV control mechanisms are studied.

The last section of this chapter presents the CFD results obtained from Aeschbacher's work [2], which provide the angular flow values that will be compared to the results obtained after the experimental testing of both mechanisms, which are presented in the sections [4.1.3](#) (automated geared mechanism) and [4.2.3](#) (manual mechanism results). The mean aerodynamic deviation resulting from the difference between the theoretically adjusted angle and the fluid angle resulting from the CFD results is also computed.

#### 3.1. Description of the setup

In this section, the configuration scheme used in the tests is described. As mentioned by Aeschbacher [2], the design of the experimental configuration and the measurements of the IGVs were carried out by Sahin.C [15].

The IGVs are contained within an independent and wholly sealed module (figure [14](#)) being mounted inside the inlet pipe. After the inlet pipe, instead of the rotor, a measuring section is installed. The fluid (air) is conducted through the test configuration by a blower (figure [14](#)) connected to the outlet of the measuring section. The inlet section consists of a bell mouth.

A thin cylindrical pressure probe ( $\varnothing$  0.6mm) with a measuring hole of  $\varnothing$  0.35mm on the side is inserted laterally into the measuring section 2. The probe is rotated around its axis to find the minimum and maximum pressures.

This information is used to calculate the flow angle, as explained in [subsection 3.2](#). The probe is moved in the radial direction to access different positions in the IGV channel. In the same axial position, the static pressure of the wall is registered by a static pressure probe.

Figures [15](#) (a) and (b) show the IGV channel cut view with the dimensions relative to the test plan. All dimensions were decided by Sahin [8]. Due to their dimensions, the IGVs do not allow the total closure of the channel to the fluid passage (figure [15b](#)). In this sense, the fluid that crosses the IGVs in the channel only suffers angular deviation due to the action of the IGVs to  $\frac{r}{R} > 0,45$  channel positions.



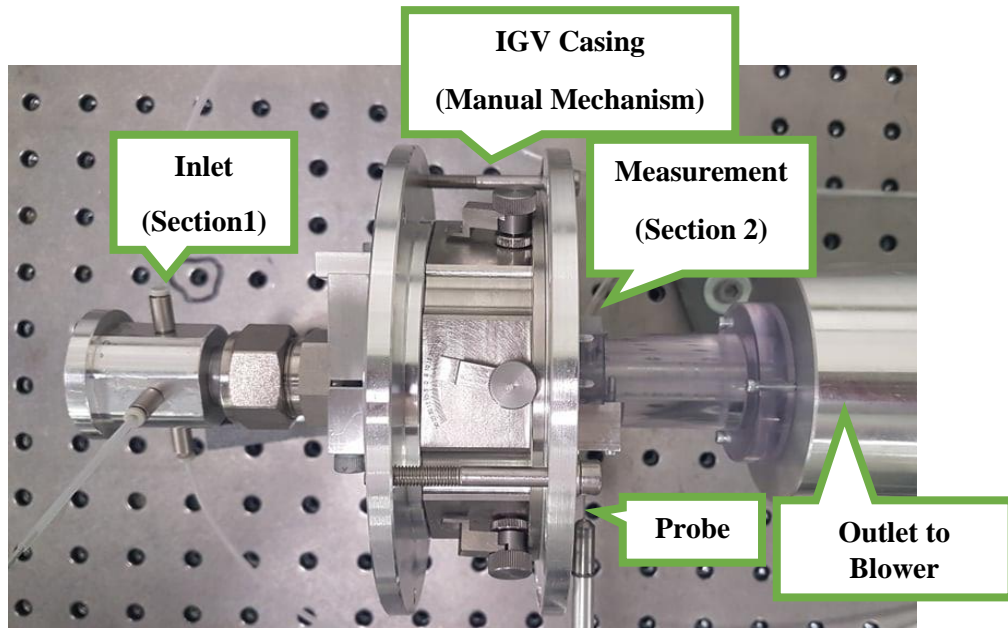
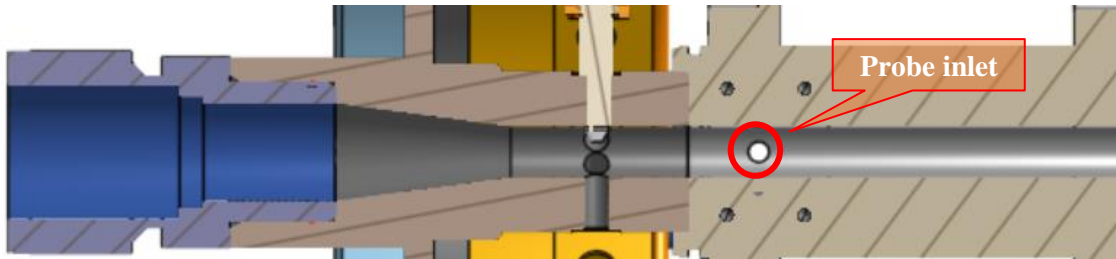
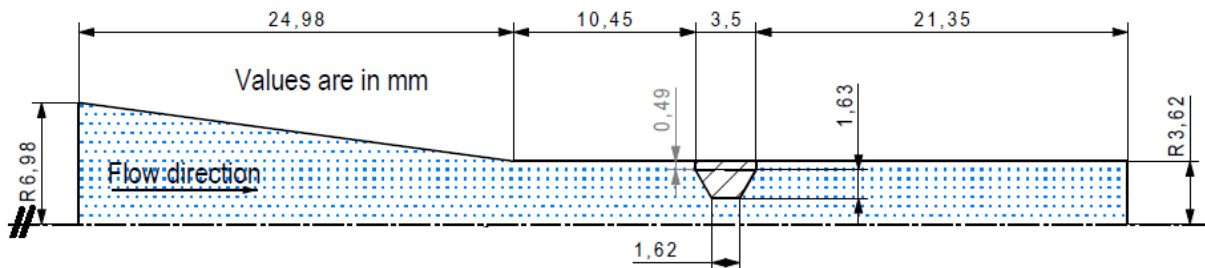


Figure 14: Experimental setup of the IGV with the IGV control manual mechanism



a) Cut view of IGV channel



b) Cut view with dimensions of IGV channel (source: [2])

Figure 15: Overview of IGV channel

### 3.2. Experiment conditions

As the purpose of this test is to measure the deviation between the flow angle and the operator-adjusted angle, it is essential to specify how the test was performed and how the flow angle was calculated. In order to obtain the reference axis for the angle measurement, a first test is performed along the probe axial axis (figure 16), ( $R_p$  axis), to determine the center of the radial position of the tube. The center of the channel is the position where the pressure is highest, and which is less impacted by the use of IGVs. During this test, the position of the probe to the axis  $\alpha$  remained constant. The results are presented in the graph in figure 17.

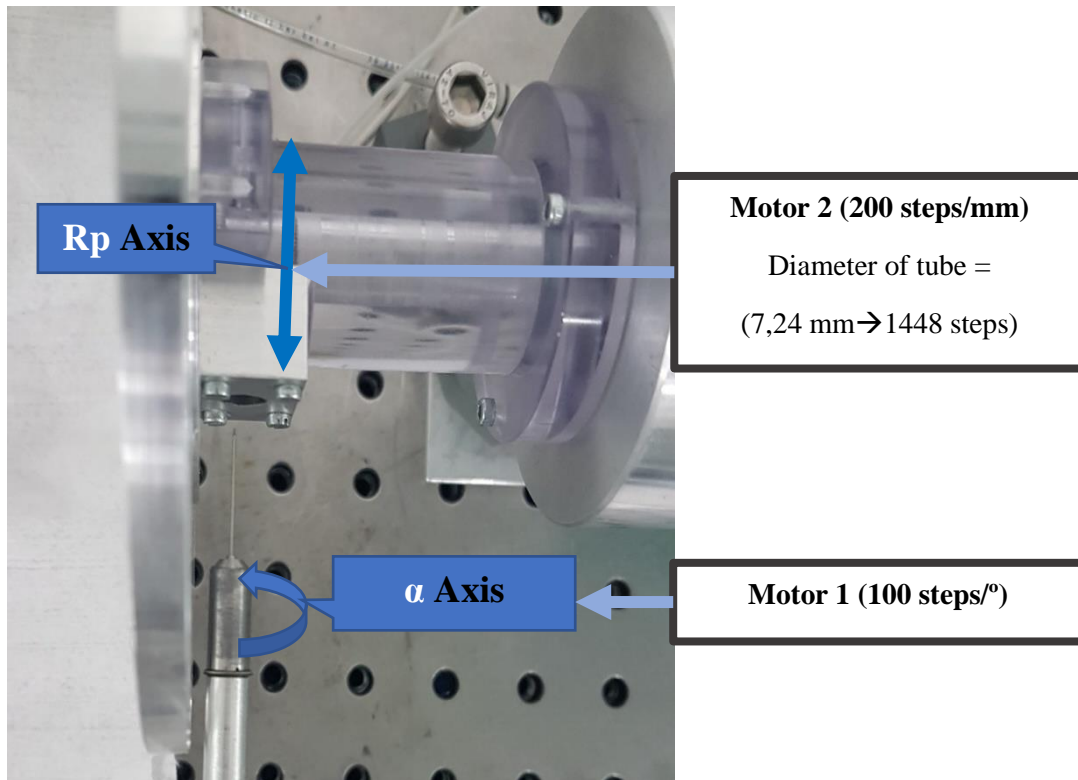


Figure 16: Reference axes in the probe manipulation

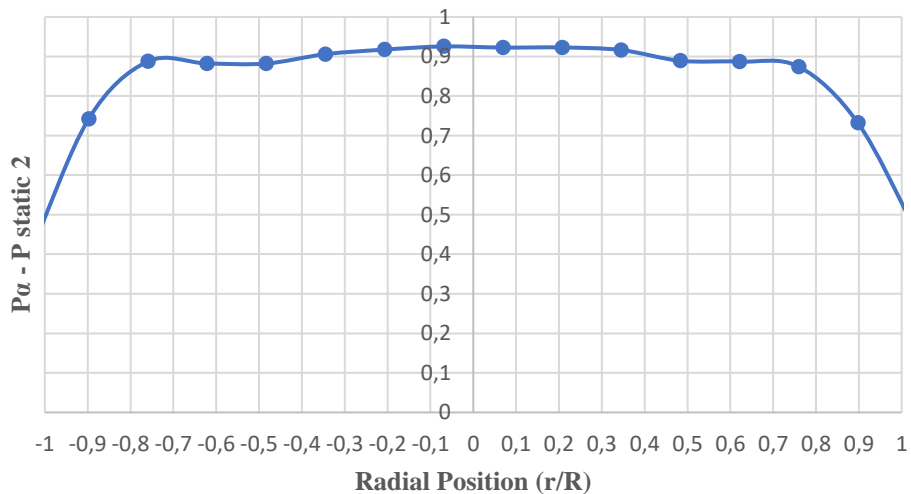


Figure 17: Results to figure out center of the IGV channel

After discovering the centre of the IGV channel, it is then necessary to figure out the center of the  $\alpha$  axis. As mentioned in [section 3.1](#) of this chapter, the probe is characterised by the presence of a small hole with a diameter of  $\varnothing 0.35$  mm, which is located in the position for which the value of the graphic  $P_\alpha - P_{\text{stat}2}$  will be highest. In this test, the position of the probe relative to the Rp axis remained constant at the origin discovered in the previous test.

The probe then rotates along the  $\alpha$  axis, recording the pressure value of the angular position in which it is located. Due to the time-consuming tests, the shaft was rotated with different angular steps. The accuracy of the measurement is related to the way the 2nd order function approximates the results (figure [18](#)).

Tests were performed using a step of 10° and 5° as it was observed that the mean deviation between the two approaches was about 5%, which translated into an absolute error of 0.0105°. As it was the smallest error, using a 5° step, the 5° was adopted as the test measurement resolution. The results of both tests are shown in the graph in figure 18.

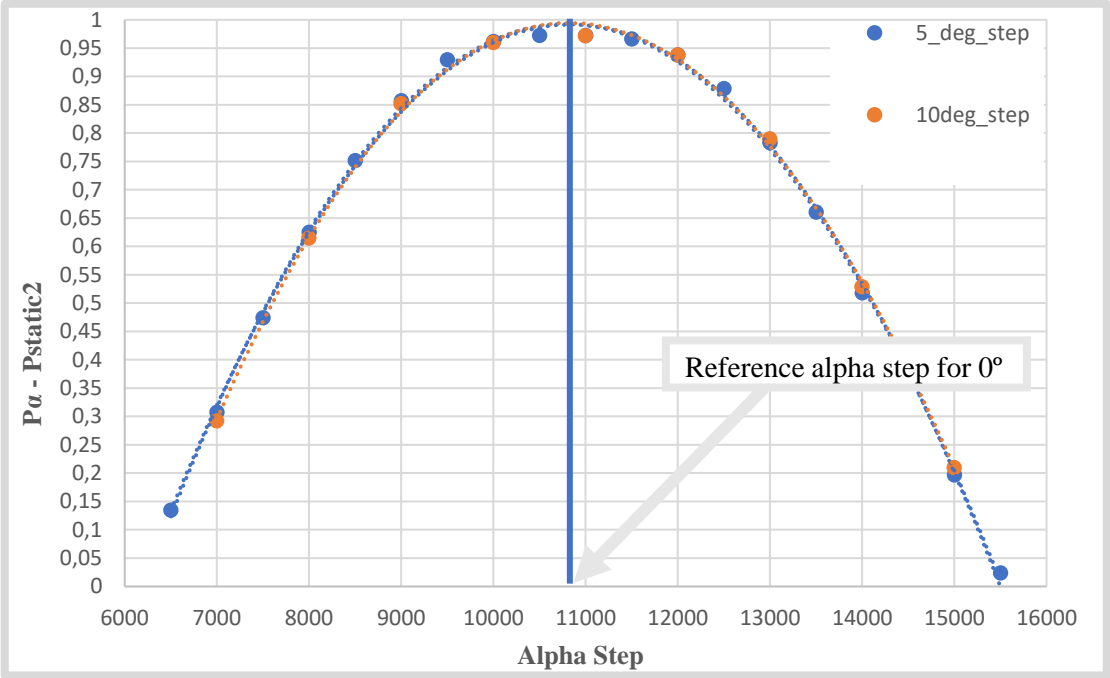


Figure 18: Results to figure out the center hole in the probe

Therefore, the value of the flow angle will be a result of the difference between the reference 0 degree angle and the angle measured by the probe for a specific radial position, as shown in the graph of figure 19.

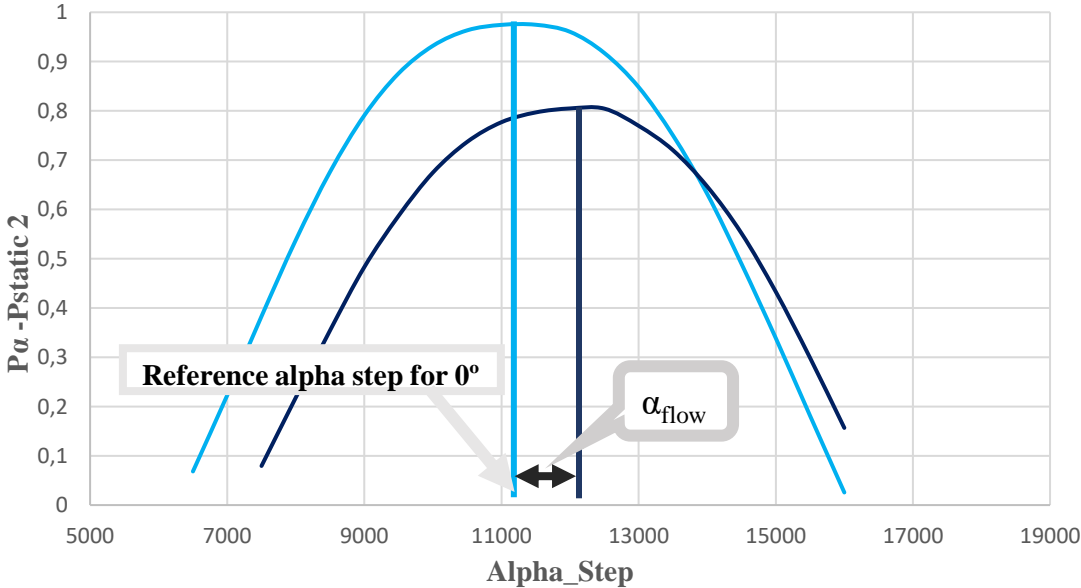


Figure 19: Method to calculate the flow angle for a given radial position

It should be noted that the results from this type of test are independent of Reynolds number insofar as it is present in the subsonic regime (Mach Number  $< 0.3$  , where incompressible equations can be used). Regarding Reynolds, the tests occur for values for which the regime is turbulent ( $Re > 2300$ ) and where the coefficient of friction is approximately constant. For these reasons the results of both tests can be comparable since the variation of the test parameters will have no significant influence on the angle of flow, affecting only the magnitude of pressure values and consequently the speed. The uncertainty in the measured flow angle is indicated with  $0.8^\circ$  by Sahin, C [15]. This value is the result of the inaccuracy of the sensors that make up the test bench (probe and pressure sensors).

In order to obtain a more reliable comparison of results between tests, the value of the variables related to the setup should remain constant. In this regard, the most relevant variable in the results is the relative position of the IGVs to the probe, which is reflected in the  $\beta$  angle illustrated in figure 20. As such, their positions remained constant in the tests performed.

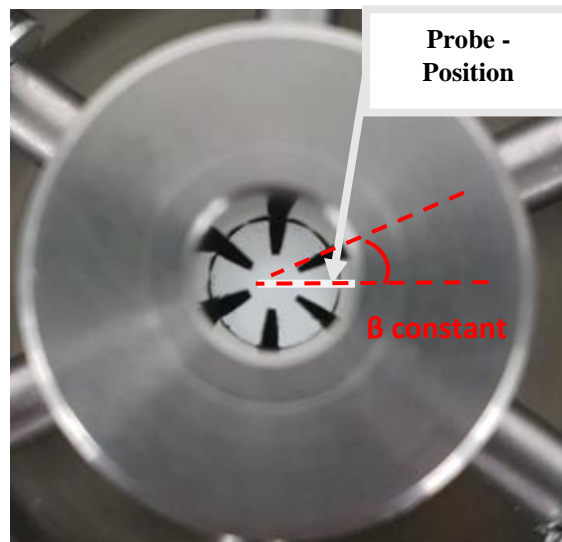


Figure 20: IGVs position relative to the probe position

### 3.3. CFD results

CFD results from the study of Aeschenbacher [2] were used for experimental evaluation of the mechanism presented in LAMD. These simulations were performed to compare and validate the accuracy of CFD with experiments performed with the automated mechanism.

About the parameters used in the simulations performed, the same are related to geometry, mesh and solver adopted by Aeschenbacher and were validated in [2]. The fluid used was air. The dimensions of the IGV channel replicated in the simulation are the same as those presented in figure 15 b).

From an experimental point of view, it is essential to distinguish the sources of the error. Through analysis of the control mechanism and the test bench, two possible sources of errors can be distinguished when comparing the flows angle with the angle theoretically chosen in the adjustment of the IGVs:

- **Aerodynamic absolute error:** the difference between theoretical values and values obtained by numerical simulation, based on numerical calculations, which simulate the fluid flow and its interaction with the defined surfaces through boundary conditions. These values are configuration-dependent of the experimental setup.
- **Mechanism absolute error:** includes the error resulting from the system precision losses in the intermediate mechanisms as well as the loss of precision in the acquisition of data derived from the resolution of equipment such as motors and sensors.

Thus, in order to compute the aerodynamic error, the results of the simulation made by Aeschenbacher [2] in his previous study were used, as shown in the graph in figure 21.

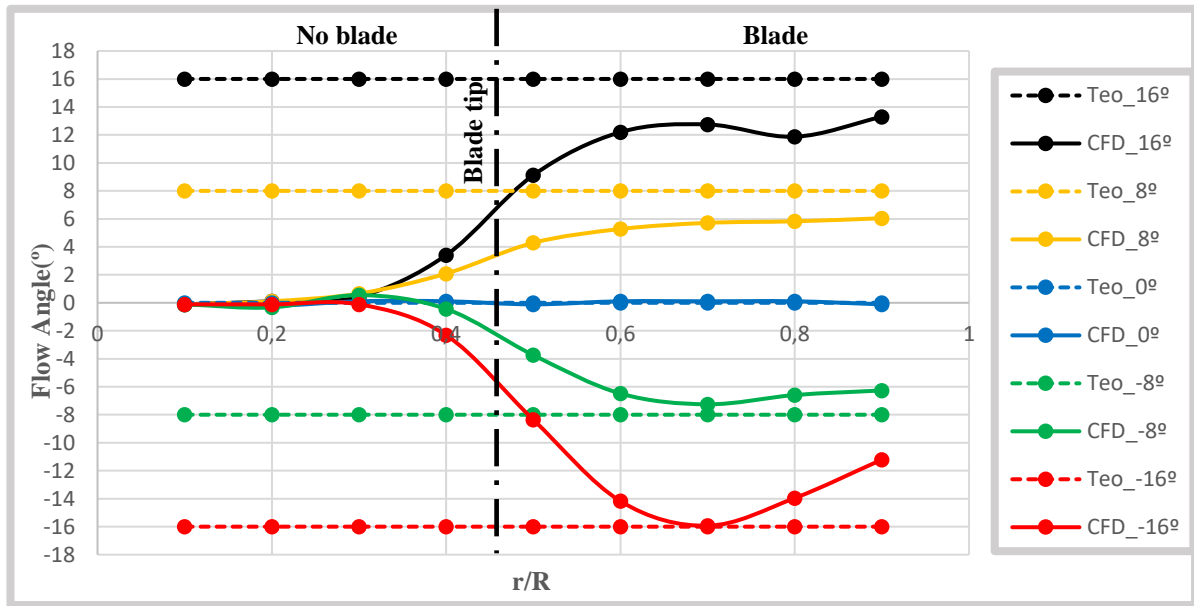


Figure 21: Angle profiles of CFD and theoretical angles adjusted by the operator with error bars

Taking the theoretical values of the angle as a reference,  $\alpha_{Teo}$ , through equation (2) can be calculated the mean absolute deviation,  $dm$ , in the difference between the theoretical values,  $\alpha_{Teo}$ , and the CFD values,  $\alpha_{CFD}$ ,

$$dm_{CFD} = \frac{1}{5} * \sum_{r=0,5}^{0,9} \frac{|\alpha_{Teo}(r) - \alpha_{CFD}(r)|}{\alpha_{Teo}(r)} \quad (2)$$

It should be noted that in the calculation of the CFD deviations from the theoretical value only the radial positions reachable by the IGVs in the flow direction were used because the IGVs do not sufficiently influence central positions (i.e.,  $r/R$  [0;0,45]) in the flow direction. Table 1 shows the average deviations obtained in each test.

Table 1: Absolute error between CFD results of [1] and theoretical values for blade angle

Foils Angle (°)	Error (°)	Error (%)
-16	3,27	20,47
-8	1,93	24,18
0	0,11	-----
8	2,57	32,14
16	4,15	25,96
<b>Mean Absolute Deviation</b>	<b>2,41</b>	<b>25,69</b>

## 4. Mechanisms Analysis

This chapter presents the work done in analysing the problem to be solved. The mechanisms were analysed according to a theoretical and an experimental approach.

In the theoretical analysis, individual problems and sources of error were identified in each mechanism. Quantifying the maximum error caused by each source served to measure the influence of each on the final inaccuracy of the mechanisms. For the experimental analysis of the mechanisms, the tests were performed in the laboratory. Subsequently, their results were compared with the CFD results obtained from Aeschenbacher [2].

In the final section of this chapter, a survey of the failures and advantages of each design is also performed to help in the solution-finding stage.

### 4.1. Automated Mechanism

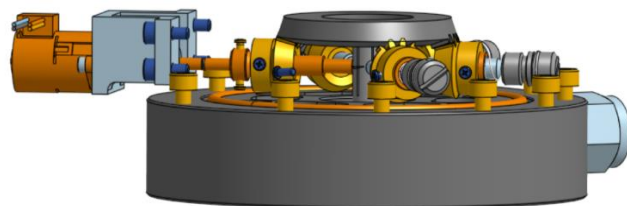
#### 4.1.1. Description of mechanism

The automated version is based on the geared mechanism presented in [section 2.3.2.2.](#)

Blade angle adjustment works via a planetary gear. All six blades are connected via a crown gear that is responsible for the transmission of the movement between the active shaft (shaft directly connected to the stepper motor) and the five passive shafts. One of the satellite gears is connected to a stepper motor, driving the assembly as shown in the figure [22b](#)). Determination of the position is realised using the stepper motor.



a) Crown Gear System



b) Connection between active shaft and passive shafts

Figure 22: Automated control mechanism for IGV present in the LAMD

### 4.1.2. Key elements and error sources

It was found on the automated system that the slack between the gear wheels resulted in large position tolerances, both between blades and in terms of each blade absolute angle. Furthermore, the gear ratio was chosen so that the stepper motor could not operate in its optimum range (below the stepper motor torque vs speed curve - figure 25).

An analysis of the current automated system detected some problems that contributed to the system's failure to comply with its requirements. The analysis is presented below.

In figure 23, a cut view of the automated system is presented for better identification of its inaccuracy sources. In the subsequent subsections, each source is analysed individually, and the maximum deviation that the sources could cause was quantified in terms of angular error.

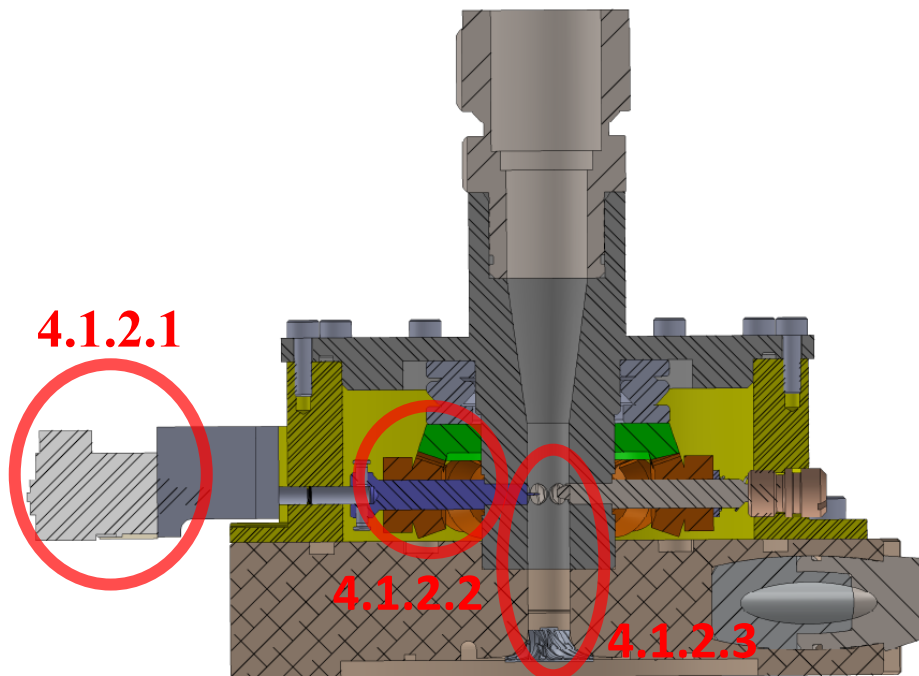


Figure 23: Sources of inaccuracy in the automated geared system

#### 4.1.2.1. Stepper motor

Regarding the choice of a stepper motor, four features must be taken into account: the step angle, positioning accuracy, high torque-to-inertia ratio and stepping rate, also known as speed.

Taking into account that the application is based only on the pre-test positioning of the IGV angle, speed is not particularly important when choosing the stepper motor. The stepper motor used to control the automated system was the 2-phase stepper motors *SPG1518M0504-102* from *Nanotec*. In figure 24, the features of the same one are presented.

Type	Step Resolution °	Current per winding A/winding	Voltage per winding V/winding	Holding torque N cm	Resistance per winding Ohm/winding	Inductance per winding mH/winding	Rotor inertia torque g cm <sup>2</sup>	Weight kg	Dia meter (mm)
SPG1518M0504-102	0.176°	0.50	5.0	20.000	10.0	2.30	1.000	0.012	15
CONNECTION		BIPOLAR							
SPECIFICATION									
VOLTAGE (VDC)		5							
AMPS/PHASE		0.5							
RESISTANCE/PHASE (Ohms)@25°C		10±7%							
INDUCTANCE/PHASE (mH) @1KHz		2.3±20%							
HOLDING TORQUE (Nm) [lb-in]		0.2 [1.76]							
GEAR RATIO		1:102.5							
STEP ANGLE (°)		18/102.5							
STEP ACCURACY (NON-ACCUM)		±7%							
ROTOR INERTIA (Kg-m <sup>2</sup> ) [lb-in <sup>2</sup> ]		1.0x10 <sup>-7</sup> [3.416X10 <sup>-4</sup> ]							




Figure 24:SPG1518M0504-102 stepper motor datasheet (source:[16])

From these technical data about the motor, there are some conclusions to be drawn:

- the reduction of 102.5 allows that for every 102.5 turns the end shaft of the gearbox will do one turn;
- The minimum angle possible to control in this stepper motor is 0,176°;
- Step accuracy reflects a possible deviation of  $\pm 0,01232^\circ$  (7%);
- The torque required by the system should not exceed the holding torque (torque needed to move the motor one full step when the windings are energized, but the rotor is stationary) otherwise the stepper motor will not be able to run efficiently and could overpass some steps.

Another necessary parameter to evaluate when analysing if the stepper motor will achieve the performance required by the application is the torque-speed chart of it. It allows knowing the torque provided by the motor as a function of the speed used and the selected electrical parameters (voltage) [17].

The Torque speed chart, for SPG1518M0504-102 stepper motor, could not be found, even after contacting Nanotec, so the only information possible to obtain regarding torque, from the datasheet was the holding torque value. Figure 25 shows a typical curve of the operation of the stepper motors [18].

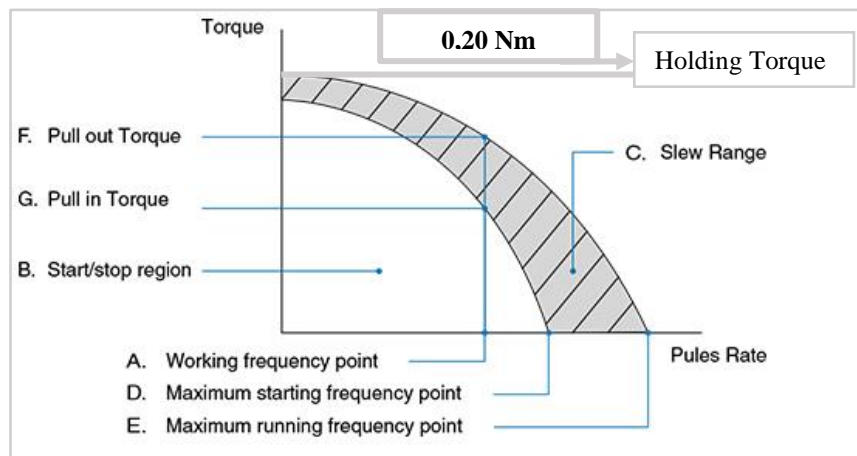


Figure 25: Generic example of a Nema stepper motor torque vs speed chart (source: [18])



It should be noted that the stepper motor needs to operate below the rotation range so that the accuracy of the step is preserved. Since the operating speed is not a requirement of the design (blade angle adjustment), it can be assumed that the stepper motor can operate in the start/stop region (see figure 25).

Thus, the only inaccuracy introduced into the mechanism due to the presence of the stepper motor is the one associated with the step angle, as shown in table 2, which shows the number of steps required to complete one full turn of the output shaft.

Table 2: Match between the number of steps and the angle adjusted in stepper motor

Step Number	Angle of the Stepper motor (°)
1	0,176 ±0,01232
2	0,352 ±0,01232
...	...
2045	359,92 ±0,01232

This way, it can be defined as the **maximum error** that can arise from the adjustment of the blade angle as:

$$\varepsilon_{\text{StepperMotor}} = \frac{\text{Step Angle}}{2} \pm 0,01232 \quad (3)$$

Thus, *equation (3)* represents the maximum angular distance from the desired angular position, an example of which is shown below.

**Ex: Place the IGV at 1° relative to the initial reference of 0°**

In this case, to know the number of steps, N, it is necessary to go through *equation (4)*.

$$1^\circ = 0,176^\circ * N \quad (4)$$

$$\Leftrightarrow N = 5,68 \text{ (steps)}$$

This way, the operator has to decide if he wants to order the stepper motor to travel 5 or 6 steps. In this case, the best option is to go through 6 steps because it is closer to the calculated value.

Thus the final error in the angle adjustment will be of:

$$\varepsilon = (6 - 5,68) * 0,176^\circ \quad (5)$$

$$\Leftrightarrow \varepsilon = 0,05632^\circ \pm 0,01232^\circ$$

With this and using *equation (3)* that reflects the most extreme case, the final error will be of **0,10032°** in the adjustment of the blade, assuming that the stepper motor operates in the start/stop region.

**Conclusion:** With an analysis of the technical datasheet of the model used (figure 24), it is possible to conclude that the chosen stepper motor is accurate concerning its resolution in the angle adjustment. The fact that the system does not require an operating torque higher than the holding torque of the stepping motor contributes to the preservation of this factor. Otherwise, if more torque is required by the system than can be obtained from the stepper motor, it will lose its synchronisation and consequently accuracy in its operation.

#### 4.1.2.2. Geartrain- (Angular Backlash)

As previously mentioned when presenting the automated system in subsection 4.1.1, the system consists of a gear train that transmits the rotational movement to control the blade angle of the active shaft (the shaft that is directly connected to the stepper motor) to the remaining five passive shafts.

However, this transmission of motion does not occur with the desired efficiency. The backlash between the gear wheels results in large position tolerances, both between the blades and in terms of the absolute angle of each blade, when used on a small scale.

##### 4.1.2.2.1. Backlash in Gear Train - Background

The backlash of a gear train, sometimes also called lash or play, can be defined as the maximum distance or angle through which any part of a mechanism may be moved in one direction without applying appreciable force or motion to the next part in mechanical sequence.

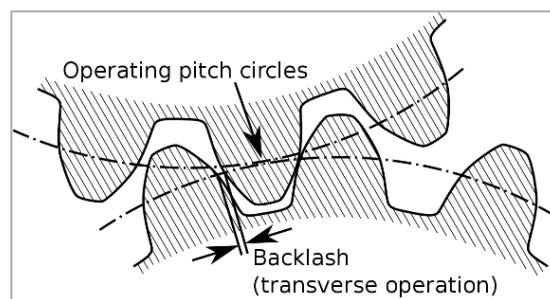


Figure 26: Backlash on a gear train (source: [19] )

Based on figure 26, the backlash in a gear train can be defined as:

$$\text{Backlash} = \text{Tooth Space} - \text{Tooth Thickness} \quad (6)$$

It should be measured from the pitch circle line.

However, this is a reductive way of analysing this concept since this expression is the general one when it comes to the backlash of a gear train. According to the type gears that compose the geartrain, different types of backlash can be identified: circumferential, normal, angular, radial and axial.

All are measured in mm except the angular backlash which is measured in °. In figure 27, there are different types of backlash that exist in the different gear trains.

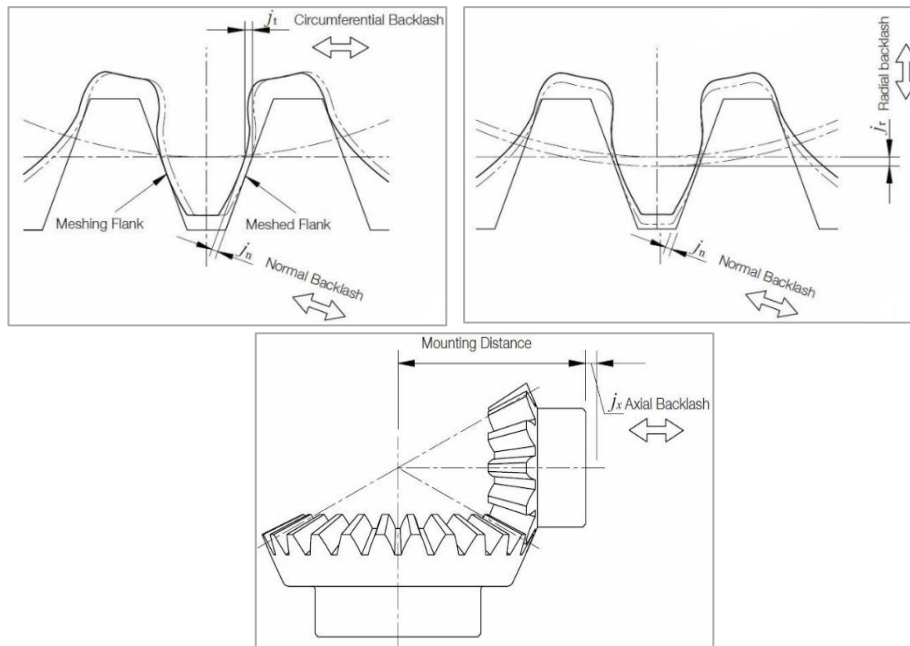


Figure 27: Different types of backlash in a gear train (source: [20] )

To assess the accuracy of the current mechanism, the factor that matters is the angular backlash, since it is the one that will quantify the angular error of the system coming from the current crown gear system [21].

#### 4.1.2.2.2. Backlash Measurement

In assessing the capabilities of the current system about the backlash, it is necessary to know the gear mesh that is currently being used in this system. From the manufacturer drawings, the data regarding the mesh of the gear system used that can be accessed is presented in figure 28 (The supplier of the gear train is Nozag).

The play of the gear train was theoretically evaluated using KISSsoft, a software for the analysis and sizing of gear trains. Also, a more practical way was used, having been measured the backlash experimentally.

In this subsection are described the steps performed in both cases.

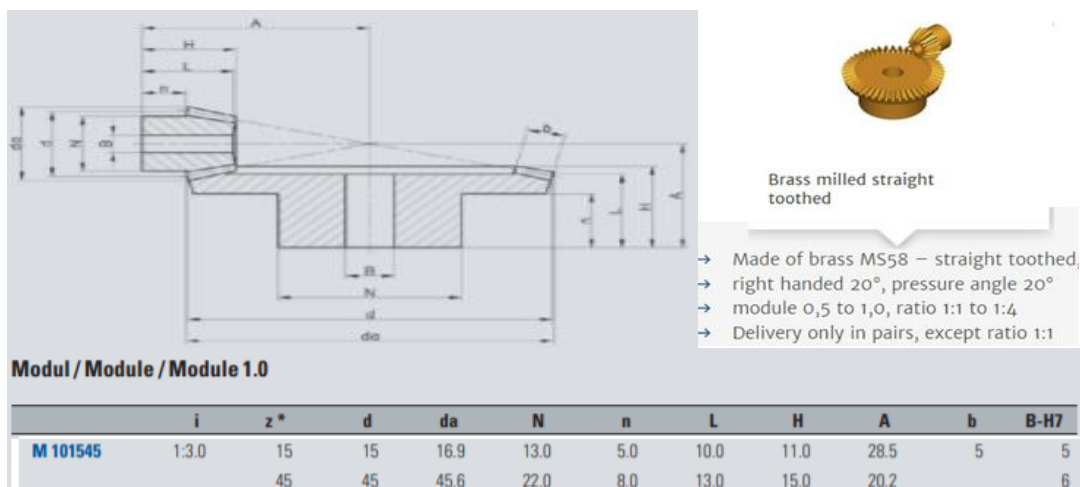


Figure 28: Gear train used in automated mechanism (Gears from Nozag) (source: [22])

### A. KISSsoft Simulation

The majority of systems involving gear associations are designed with some slack. In some cases the same is minimal, just to avoid the system blockage, also called jamming.

Currently, only systems involving cycloid or harmonic gears trains, which are based on a large number of contact teeth during gearing, allow zero backlash.

KISSsoft is a software that is useful when there is a need to design or evaluate the system of machine elements, like a gearbox or a power train. In the case of this application, it was used to reproduce as similarly as possible the gear train of the real automated system. This gives a forecast of the possible backlash to be achieved by using the selected gear train in the simulation and how the KISSsoft software is to be used in the analysis [23].

Annex [A.1](#) contains the steps performed in the simulation and how the KISSsoft software is to be used in the analysis. The results are presented in figure [29](#).

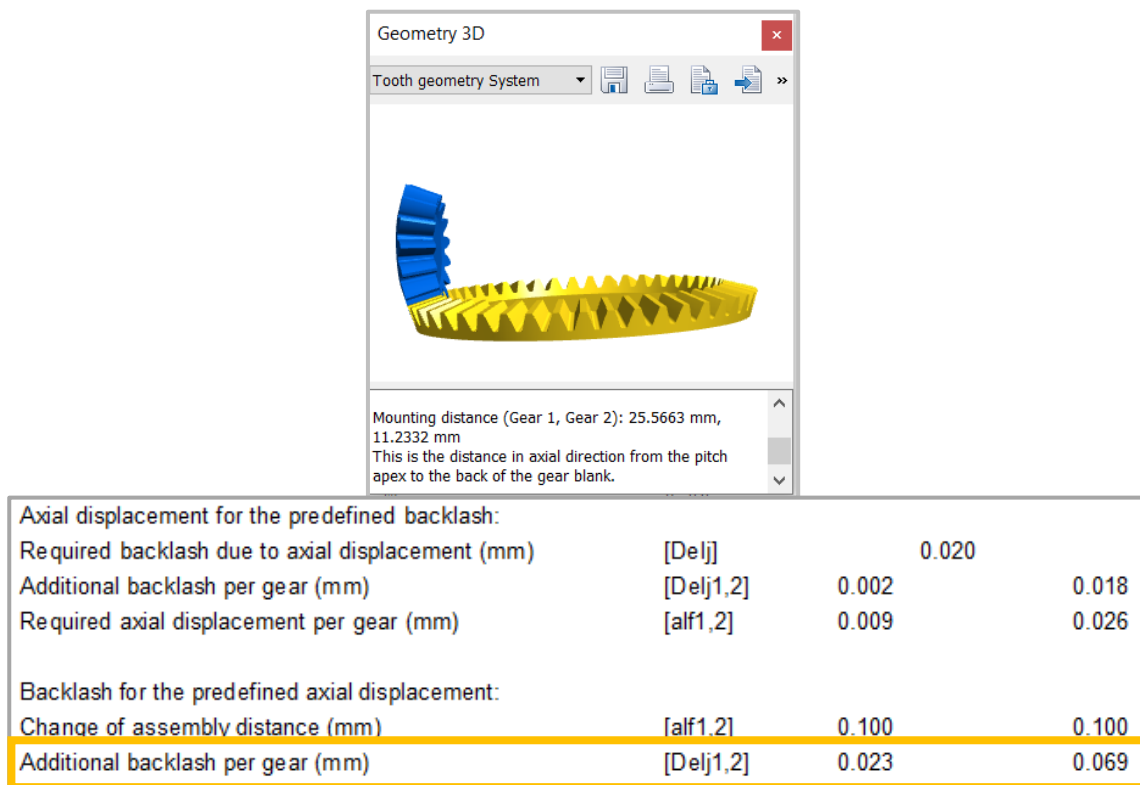


Figure 29: Results from KISSsoft analysis

Based on these results, a forecast can be made of the maximum backlash of the system, taking into account the predefined mounting distance of both gears of the system, recommended by the program. As it is possible to see in figures [29](#) and [30](#), the system backlash will be the result of *equation 7*.

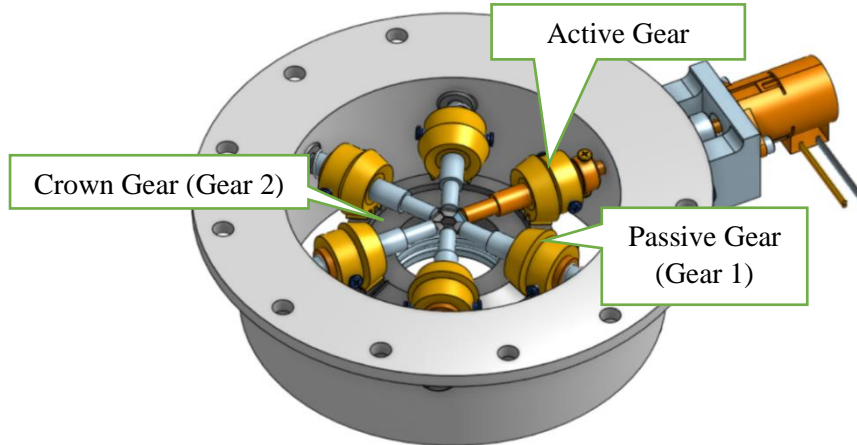


Figure 30: Components contributing to the backlash of the gear train

$$\text{Max Gear Train Backlash} = (\text{Active Gear Backlash} + \text{Passive Gear Backlash} + \text{Crown Gear Backlash}) \quad (7)$$

$$\Leftrightarrow \text{Max Gear Train Backlash} = 0,023 + 0,023 + 0,069 = \pm \mathbf{0,115 \text{ (mm)}}$$

The value is relative to the circumferential backlash.

## B. Manual Backlash Measurement

In order to have a more reliable value and more compatible with the real case, in which possible errors of the operator in the assembly are accounted for, an experimental measurement was carried out and is presented below.

### Procedure to measure the backlash experimentally in a gear train [24]:

1. Position the system securely in a table in a way the operator can access the gears with his own hands;
2. Fix one of the gears in the train (preferably the crown gear instead bevel gear);
3. Mount the dial indicator in a fix position in contact with the tooth of the non-fixed gear;
4. Turn the adjustment knob on the side of the dial indicator gauge until the gauge needle points to the "0" setting (in case of using an analogic dial indicator instead of a digital one);
5. Rock the gear back and forth with the hand while monitoring the gauge needle. The distance indicated on the gauge is the circumferential gear backlash.

In order to obtain the value of the backlash tests with 2 different configurations of the automated system were carried out. In the 1st test, the backlash measurement of the system was performed without the use of springs to preload the model. This configuration was used by [1] and as such the previously observed results are influenced by this fact. In the second configuration the springs were used to compress the gear train and in this way the observed values for the circumferential backlash were reduced.

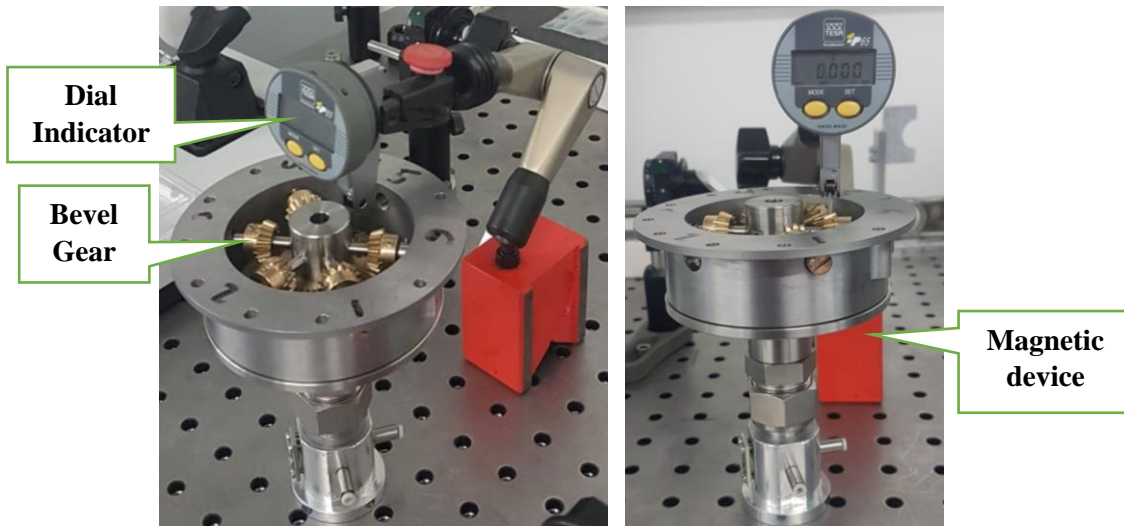


Figure 31: Scheme of the test setup used to measure the backlash of the gear train

It is also relevant to mention that the use of springs has led to a large increase in the torque required to move the system, making it impossible to control with the stepper motor used. So this spring design will require an actuator with much more power than the stepper motor used. This would have a significant increase in the costs of the drive mechanism of the system and was not realised.



Figure 32: Results obtained for circumferential backlash using a system: without springs (left) and with springs (right)

Table 3 presents the values obtained for the backlash in both tests for the two configurations. The values obtained in both cases (experimentally and in KISSsoft simulation), are relative to the circumferential backlash. For the final measurement of the error coming from the gear train, the resulting angular error in the passive bevel gear must be computed. Thus the value obtained for the circumferential backlash must be converted to angular backlash through the equation 8.

$$\text{Angular Backlash} = \frac{360 \times \text{Circumferential Backlash}}{\pi \times d_{\text{passive gear}}} \quad (8)$$

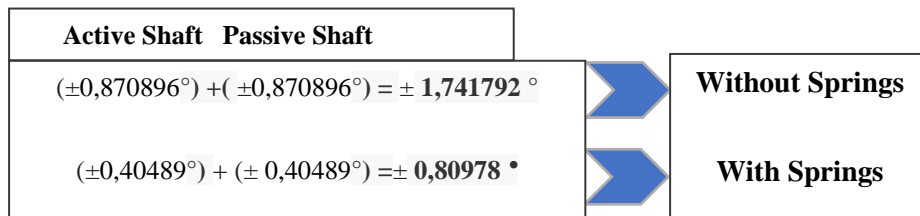
Table 3: Experimentally and theoretical obtained results for the backlash of the gear train (crown gear)

Type of Backlash	Without Springs	With Springs	KISSsoft (without Springs)
Circumferential (mm)	± 0,114	± 0,053	±0,069
Normal(mm)	0,046521	0,021628	
Axial (mm)	0,077548	-----	
Angular (°)	± 0,870896	± 0,40489	

From table 3, It is possible to notice that the circumferential values measured experimentally without springs and those obtained by KISSsoft simulation are somewhat distant. This is because most probably the actual system assembly was deficient and the distances between gear centres used in the simulation are challenging to replicate experimentally. As they provide the real values about the backlash of the gear train, the experimentally measured values were taken for analysis and quantification of the system error.

**Conclusion of the gear train analysis:**

- The results obtained refer to the backlash of an active bevel gear. Since the gear train is responsible for transmitting the movement of the active shaft to the passive shaft, in the worst case, the total backlash sums up to:



- The accuracy of the results can be improved if springs for system pre-loading are used;
- Design with springs:
  - The system becomes more stiff. This fact is related to the presence of springs leading to more intense contact between the teeth of the gears, creating more friction in the interaction between the gears;
  - More prone to jamming (system lock);
  - Mounting is most error-prone as the operator will need more assembly instructions for the operator (details such as the number of turns needed to tighten the bushing become very important for the operation of the system);
  - Larger stepper motor needed, which is reflected in a more expensive solution.

**4.1.2.3. Calibration of automated mechanism**

The calibrator plays a significant role in the functioning of the current automated mechanism as it allows fixing the initial position of the IGVs. It is responsible for ensuring that the initial position of the vanes is situated at 0° of the referential.

However, because of the tolerances required to leave in the material for machining and manufacture thereof (figure 33), the calibrator becomes a source of error in the adjustment of the vanes, failing to ensure that the initial position of the vanes is 0 degrees.

In a study by Schreiber [25], the uncertainty adjacent to the use of this part in the calibration of the automated mechanism was quantified. The results of the analysis are shown in figure 35.

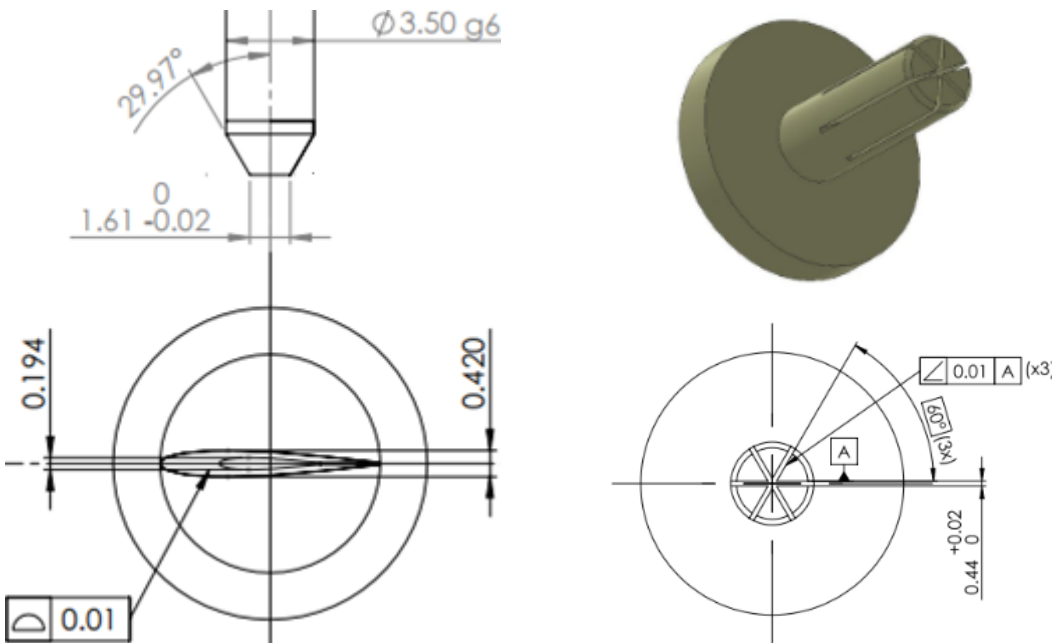


Figure 33: Dimensional and Geometrical Tolerances of the part used to calibrate the Initial position of the system

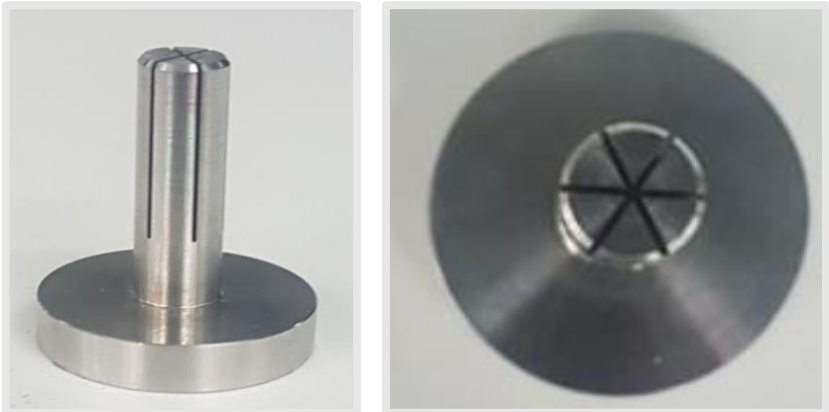


Figure 34: Calibrator used in automated system



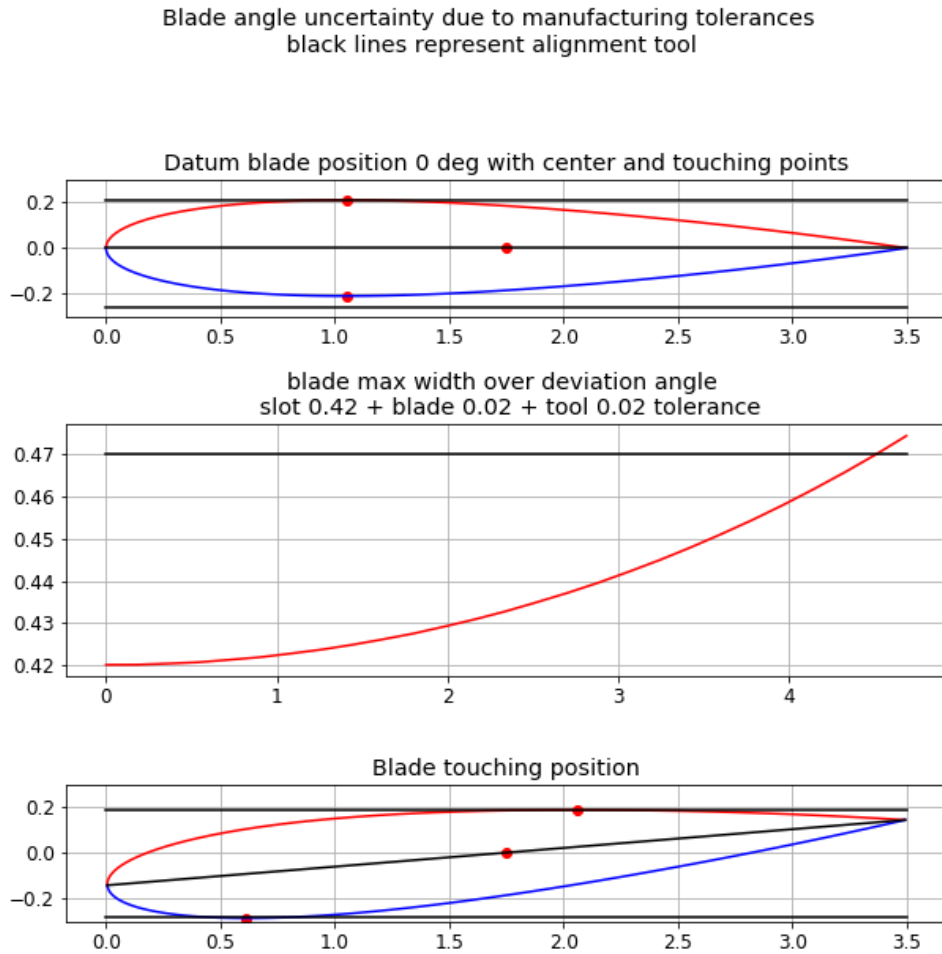


Figure 35: Deviation in blade adjustment caused by the calibrator and manufacturing tolerances

From these results, it can be seen that the calibrator plays a vital role in the accuracy of the system. The worst-case scenario can lead to an initial blade deviation of  $4.5^\circ$  from the 0 degrees taken as a reference for the initial blade position. Thus, the calibration part translates into the primary source of error for the entire system, and by solving this problem, the accuracy of the system can be significantly increased.

### 4.1.3. Experiment testing with the mechanism

In the experimental evaluation of the automated geared mechanism, the results of Aeschenbacher [1] were used. In order to evaluate its accuracy, the mean absolute deviation of the mechanism between the adjusted angle and the fluid flow angle was calculated. The results of the automated system are presented below in the graph of figure [36](#).

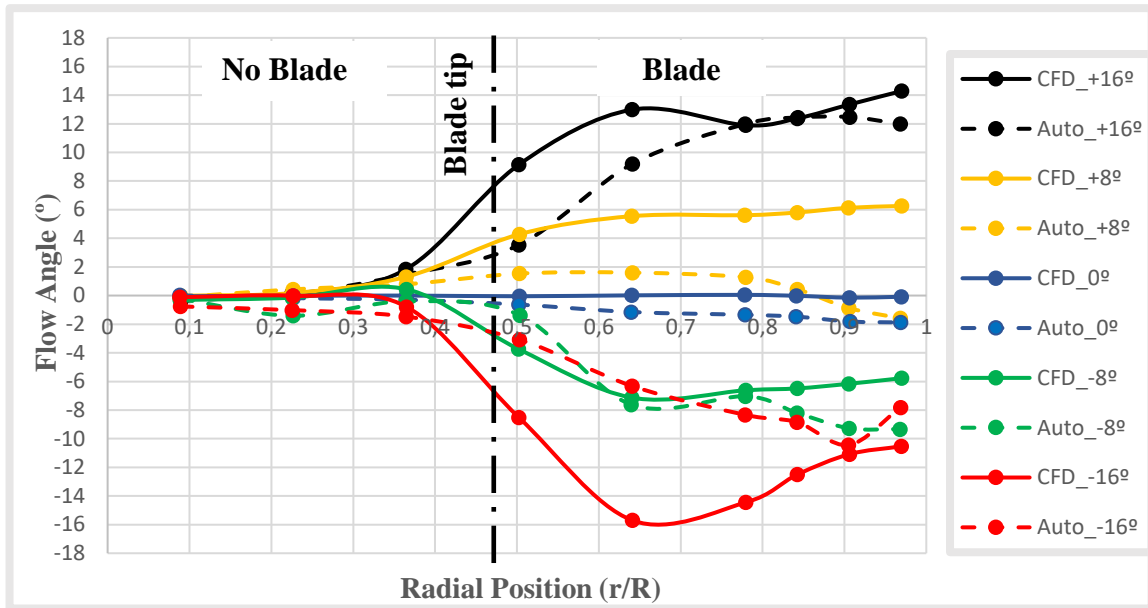


Figure 36: Deviation between automated mechanism and CFD angle profiles

Taking the CFD results of the angle as a reference,  $\alpha_{CFD}$ , through *equation 9* can be calculated the mean deviation,  $dm$ , in the difference between the automated mechanism and CFD.

$$dm_{Automated\ mechanism} = \frac{1}{6} * \sum_{r=0,5}^1 \frac{|\alpha_{CFD}(r) - \alpha_{aut}(r)|}{\alpha_{CFD}(r)} \quad (9)$$

The results regarding the error of the automated system are presented in table 4. From the data, it can be seen that the current automated mechanism cannot accurately control the angle of the blades.

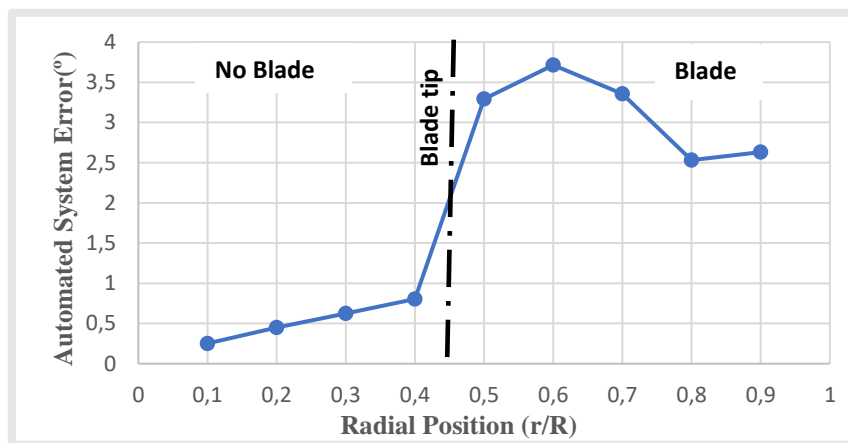


Figure 37: Error in the adjustment of the blades angle with the automated system function of radial position

Table 4: Error between the experimental data from Automated Mechanism and CFD results

Foils Angle (°)	Error (°)	Error (%)
<b>-16</b>	4,66	37,78
<b>-8</b>	1,94	35,80
<b>0</b>	1,34	-----
<b>+8</b>	5,21	90,77
<b>+16</b>	2,12	19,06

With these values, it is possible to define a mean absolute deviation of the system in relation to the correct adjustment of the vane angle that will serve as the precision gauge of the system. In this way, a result of **3.05°** is achieved.

#### 4.1.4. Analysis Conclusions

As can be seen, all these factors listed in this section lead to the final position of the blades to be inaccurate against what is intended. Factors related to poor system assembly can lead to increased system inertia leading to higher torque being required for system operation:

- Which can lead to the stepper motor leaving the range where it works correctly without "missing" steps.

Table 5 presents a summary of the possible angular deviations in the flow adjustment, coming from different sources that were described above.

Table 5: Summary of the error quantification of the sources in the automated system

Source	Max Error Angle (°)	% of Total Error
<b>Manufacturing Tolerances</b>	Included in calibrator calculation	----
<b>Backlash Gear Train</b>	±1,742	43,10
<b>Calibrator</b>	+4,5	55,66
<b>Actuator Accuracy</b>	+0,10032	1,24

#### Conclusions:

- Most of the system error comes from the gear train and the system calibration tool;
- In the new design, the use of gear systems that are very sensitive to poor assembly can lead to abrupt increases in blade angle adjustment and should be avoided;
- The way to calibrate the system needs to be rethought. The manufacture of a single tool for this purpose leads to significant errors in the accuracy of the mechanism due to manufacturing tolerances;
- The deviation between the theoretical and experimental results is explained by the increase of the error in the theoretical analysis, through the quantification of the maximum theoretical error. The maximum possible error caused by each source of error was calculated. Thus, the final result of the accuracy of the system should not be the sum of all the theoretical contributions of the sources of error, but the result obtained experimentally. In this sense, it is normal that the theoretical results are always higher than the values measured experimentally.

## 4.2. Manual Mechanism

### 4.2.1. Description of mechanism

This mechanism has been designed to replace the automated mechanism (presented in [section 4.1.1.](#)) in order to comply with the quality criteria regarding the accuracy on blades angle adjustment.

As described and detailed in [section 2.3.2.3.](#) each blade is mounted on a shaft with an indicator arm. Like this, each blade angle can be adjusted directly with a cursor manually by the operator.

Figures [12](#) (a) and (b) in [section 2.3.2.3](#) show the manual mechanism currently available in the LAMD.

### 4.2.2. Key elements and error sources

In the manual mechanism, the accuracy of blade adjustment operations depends on manufacturing tolerances and operator accuracy.

#### 4.2.2.1. Manufacturing Tolerances

Figure [38](#) identifies possible sources of error in the final blade angle adjustment. Thus, in this subsection, the exercise of calculating the possible effect of manufacturing tolerances was done in order to compute the final error in the adjustment of the angle of the blade.

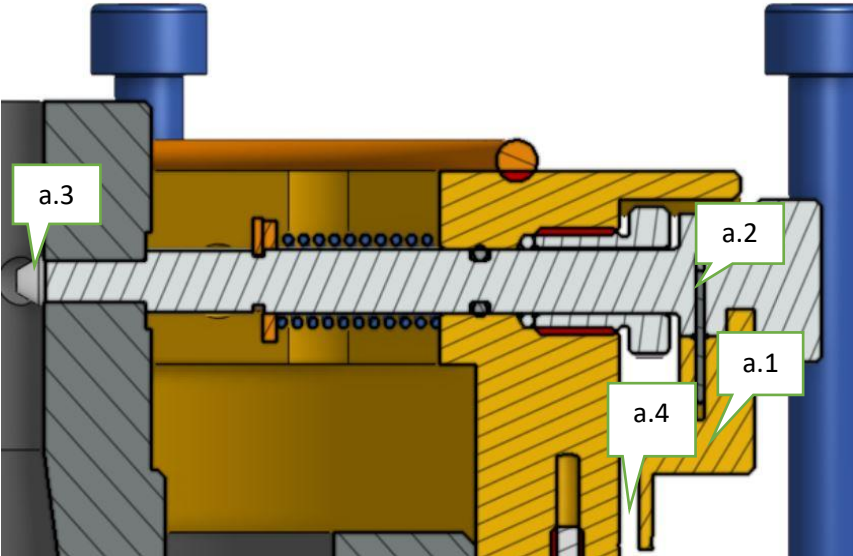


Figure 38: Sources of innaccuracy due the manufacturing tolerances in manual system

#### 4.2.2.1.1. Cursor

The cursor is one of the parts involved in adjusting the angle. The present recordings serve as a reference for the operator when the manual adjustment of the vane angle is performed, and as such, this is a part that must be done with good precision.

From here, the possible error resulting from the scale tolerance can be quantified. As 1° and the initial mark spaces each mark has a position tolerance of 0.01 mm, this may reflect, in the worst case, an angle adjustment error of 0.02938° due to the scale.

$$\tan(\text{Error}_{\text{Angle}_1}) = \frac{0,01}{19,5} \Rightarrow \text{Error}_{\text{Angle}_1} = \pm 0,02938^\circ$$



Figure 39- Angle scale present on cursor

#### 4.2.2.1.2. Cursor + Pin 8734 + 0012 Naca Shaft

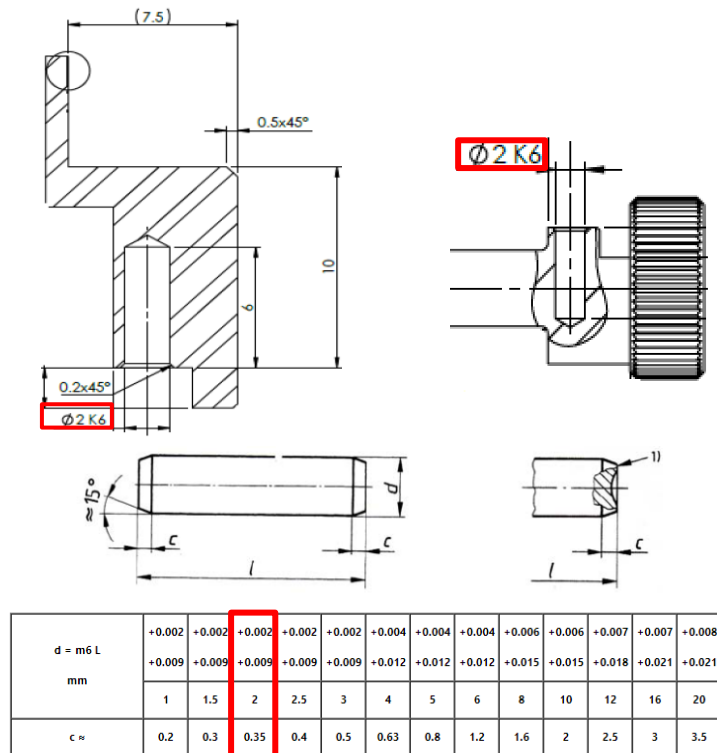


Figure 40: Dimensional tolerances of parts involved in blade adjustment (source: [26])

Assuming the dimensions of the parts that provide the highest error when adjusting the final angle in order to increase the error, one obtains the following:

$$\tan(\text{Error}_{\text{Angle}_2}) = \frac{2,006 - 2,002}{5}$$

$$\Rightarrow \text{Error}_{\text{Angle}_2} = \pm 0,04584^\circ$$

$$\begin{array}{l} \text{Ø 2 K6} \quad \left\{ \begin{array}{l} 2,006 \text{ mm} \\ 2,002 \text{ mm} \end{array} \right. \end{array}$$



Figure 41: Scheme used in error calculation

#### 4.2.2.1.3. Blade Position in Naca Shaft

Due to the small scale of the system, the foil present in IGVs also needs to be small scale. As this is a complex geometry and has to be manufactured with extreme precision, it is clear that it is a source of error. However, as can be seen in figure 42, in technical drawings it only has geometric tolerance and is not related to curvature, so it is difficult to quantify the error that can arise from this in angular terms.

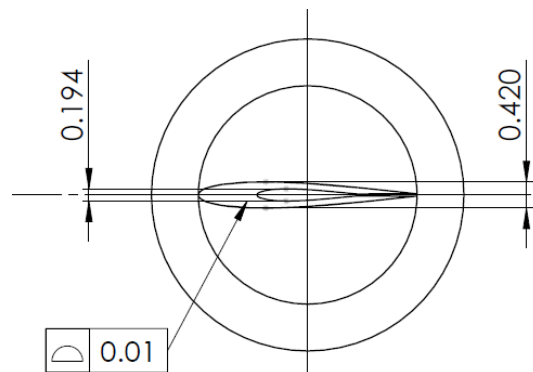


Figure 42: Dimensional and geometric tolerances presents in blade manufacturing

#### 4.2.2.1.4. Distance between Cursor and Casing grade

Since there is a distance between the cursor used by the operator to adjust the angle and the scale present in the casing, it leads to a possible error by the operator in adjusting the blade angle.

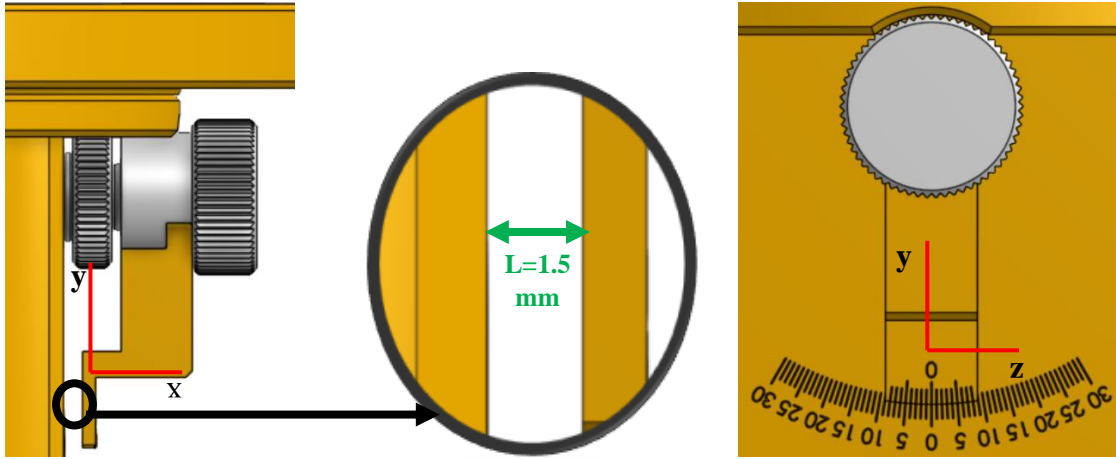


Figure 43: Reference axis used to compute the error coming from the distance between cursor and casing grade

Therefore, in this case, the error in the setting will depend on:

- Distance in the x-axis at which the operator is from the cursor, X;
- The distance on the z-axis at which the operator is from the centre of the scale, W.

The graph presented in figure 44 shows the possible error depending on the variables described. The graph presented in figure 44 shows the possible error depending on the variables described. Through the graph it can be observed that an error of  $\pm 1.6^\circ$  can be reached.

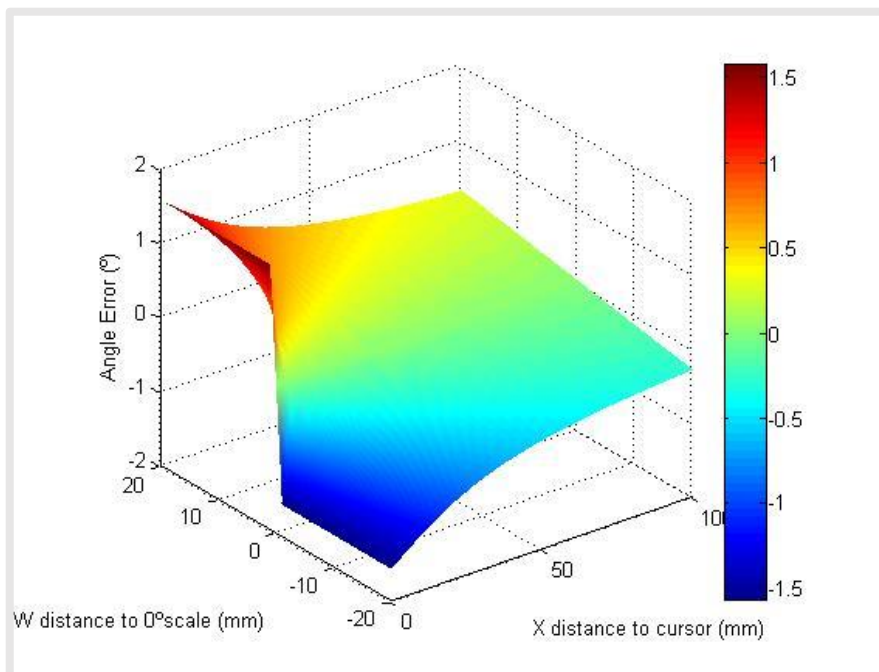


Figure 44: Possible error coming from operator precision to perform the task of adjust blades angle

#### 4.2.2.2.Operator Dependent

A manual adjustment mechanism, will always depend heavily on the operator's precision. Due to the angle gauge is small scale, most of the system error will likely be sourced from the operator. This factor is crucial because if an automatic mechanism is designed, it can suppress this contribution in the final error of the new system.

Thus it is seen that the manual system is not efficient when repeatability is intended in the process.

Possible operator errors in adjusting the vane angle:

- Operator accuracy in the correct placement of the vane angle;
- Operator repeatability for placing all blades at the same angle;
- The operator must be at 90 degrees from the cursor's degree scale;
- Difficult to adjust correctly due to the small scale, even with magnifying glasses.

Table 6:Summary of the error quantification of the sources in the manual system

Source	Max Error Angle (°)	% of Total Error
Manufacturing Tolerances	±0,075	4,48
Operator Dependent	± 1,6	95,52

#### 4.2.3. Experiment testing with the mechanism

As had been done by Aeschenbacher [2] with the automated mechanism, tests were performed in the laboratory with the manual mechanism. The tests were used to assess the capabilities regarding the accuracy of the manual mechanism. The results are presented in the graph in figure 45. The conditions under which all the tests occurred are present in table 7.

Table 7:Inlet and Outlet pressures of the experiment with manual mechanism

Fluid: Air				
Angle Adjusted	Total Pressure(Pa)	P <sub>t</sub> - P <sub>static1</sub> (Pa)	P <sub>t</sub> - P <sub>static2</sub> (Pa)	Temperature(°C)
-16°	963400	0,0803	9,3608	23,9
-8°	968900	0,0859	9,3605	24,5
0°	971900	0,0881	9,3847	24,9
+8°	966300	0,0853	9,3726	24,9
+16°	965700	0,0806	9,3176	24,4

Through these values and using the *equations 10 and 11*, presented below, it is possible to calculate flow velocity profiles and from there, a set of parameters that generally characterize the fluid flow. Since they are not relevant to the objective of this thesis, the same are not presented.

$$P_{total} = P_{static} + P_{dynamic} \quad (10)$$



$$P_{dynamic} = \rho * \frac{v^2}{2 * g} \quad (11)$$

where  $\rho$  is the specific mass of the fluid,  $v$  is the fluid absolute velocity and  $g$  is the standard acceleration due to gravity.

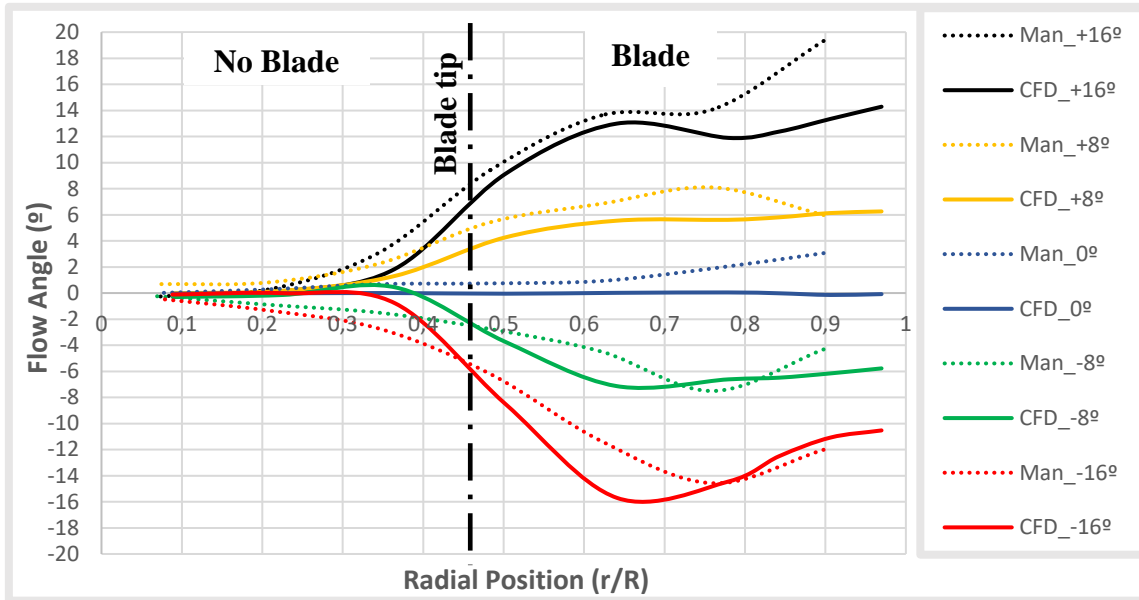


Figure 45: Deviation between manual mechanism and CFD angle profile

**Observations:**

- The manual mechanism does not still allow to control with total accuracy the angle of the foils;
- Although the use of the manual system in most cases causes the flow angle to be higher than initially adjusted, the variation does not follow a linear pattern, so that the values obtained are the result of a set of factors explained below in this section.

The graph presented in figure 46 shows the average error in angle adjustment as a function of the radial position.

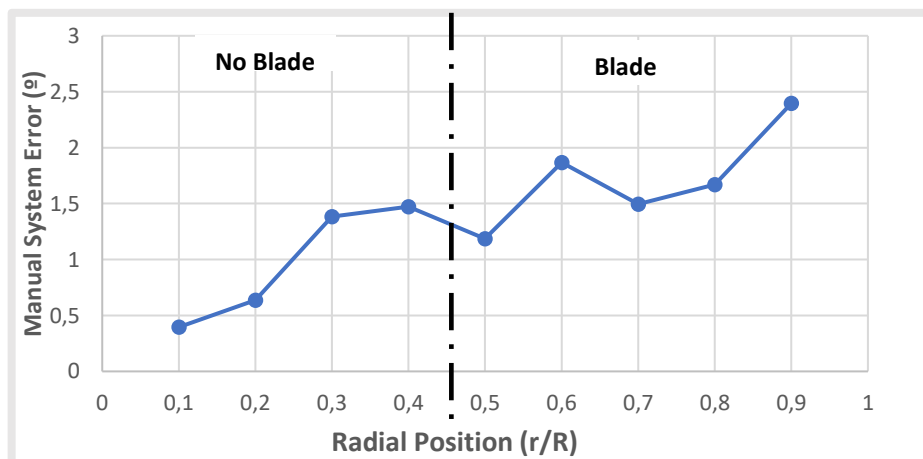


Figure 46: Angle error function of the radial position

Taking the CFD results of the angle as a reference,  $\alpha_{CFD}$ , through *equation 12* the mean deviation,  $dm$ , can be calculated as the difference between the manual mechanism results,  $\alpha_{man}$ , and CFD.

$$dm_{Manual\ mechanism} = \frac{1}{4} * \sum_{r=0,5}^{0,9} \frac{|\alpha_{CFD}(r) - \alpha_{man}(r)|}{\alpha_{CFD}(r)} \quad (12)$$

Table 8: Error between the experimental data from Manual Mechanism and CFD results

Foils Angle (°)	Error (°)	Error (%)	Previous Results Automated Mechanism (°)
-16	1,94	16,07	4,66
-8	1,59	26,62	1,94
0	1,69	3311,97	1,34
+8	1,27	24,175	5,21
+16	2,27	17,75	2,12

With these values, an average system error can be set to the correct adjustment of the vane angle that will serve as the precision gauge of the system manual. This gives a result of **1,75°**. This value reflects an improvement in the task of adjusting the blade angle since it obtained a **reduction in mean absolute deviation of 43 %** compared to the automated system.

#### 4.2.4. Conclusion of the analysis

Once both systems were analysed and evaluated, the advantages and disadvantages of each system could be summarised. The main conclusions of this analysis are presented in table 9.

Table 9: Summary of pros and cons of manual and automated system

Mechanism	Positive	Negative
<b>Manual</b>	<ul style="list-style-type: none"> <li>✓ No calibrator tool</li> <li>✓ Mechanical Accuracy (just dependent of small manufacturing tolerances)</li> </ul>	<ul style="list-style-type: none"> <li>✓ Operator dependent</li> <li>✓ Bad repeatability</li> <li>✓ No remote control</li> <li>✓ No usage in test cycles</li> </ul>
<b>Automated</b>	<ul style="list-style-type: none"> <li>✓ Repeatability</li> <li>✓ Remote Control</li> <li>✓ Stepper Motor</li> </ul>	<ul style="list-style-type: none"> <li>✓ Calibrator</li> <li>✓ Mechanical Accuracy</li> <li>✓ Precise Assembly (Stepper motor can't have enough accuracy because the torque required by the gear train is too high)</li> </ul>

Since the characteristics of each of the mechanisms used to adjust the IGVs have already been collected, it remains to know the requirements and constraints of the project. After that, the new mechanism can be designed. In the next subsections of this chapter, the topics mentioned are presented.

## 5. Solution Finding

Once the problem has been analysed, and the need to design a new design has been identified, it is necessary to go through the next steps to the final design of the mechanism. In this sense, this chapter presents itself as an intermediate step in the conclusion of this objective.

This fifth chapter deals with the methodology used in the search for a final design solution. The first sections present the specifications of the project (requirements and constraints).

The methodology involved in the choice of the final design concept is presented below. Two final designs were considered, which were analysed, taking into account the criteria selected for the project. At the end, it was chosen the solution that best meets the criteria considered.

### 5.1. Requirements

The requirements are part of the specifics of the project. They are a set of guidelines that the project must respect in order to be fully functional and meet the needs for which it is designed.

Regarding the requirements of the project, it can be collected from Pillet's work [9]:

- I. The IGV mechanism must be an independent module that will be fixed on the volute of the compressor;**
- II. The mechanism must allow controlling the blades angle between  $-16^\circ$  and  $+16^\circ$  (range of angles in which the airfoil chosen for the vanes does not stall);**
- III. The mechanism must be completely sealed;**
- IV. The step angle of the vanes must be lower than  $0.5^\circ$  to have precise control of the compressor map;**
- V. The module must work oil-free on any component (may not be used when in contact with R-134a).**

Another requirement necessary for the correct functioning of the mechanism is related to the **manufacture of IGVs**. As it is a small scale part with complex geometry, it must be manufactured with high precision from high-quality material. The manufacture **in stainless steel** can be considered a design requirement insofar as it is the best option in this case because of its high resistance to corrosion and heat.

### 5.2. Constraints

Regarding project constraints, these concern limits or boundaries that cannot be crossed in the design. Thus, they are mostly related to the costs of the mechanism and adjacent parts.

To reduce cost, one of the constraints is designing a system where some parts of previous designs (connection parts of the module) that have been expensive can be reused.

The volute and the inlet pipe must be kept in the new design due to its compatibility and connection to the test bench. The distance  $L = 31.2\text{mm}$  must be kept under penalty of having to manufacture a part that connects the volute to the inlet pipe and prevents the flow out of the channel formed by the two parts. The SS\_1210 part that is a Swagelok must also be maintained because it connects to the inlet of the setup to the test bench.

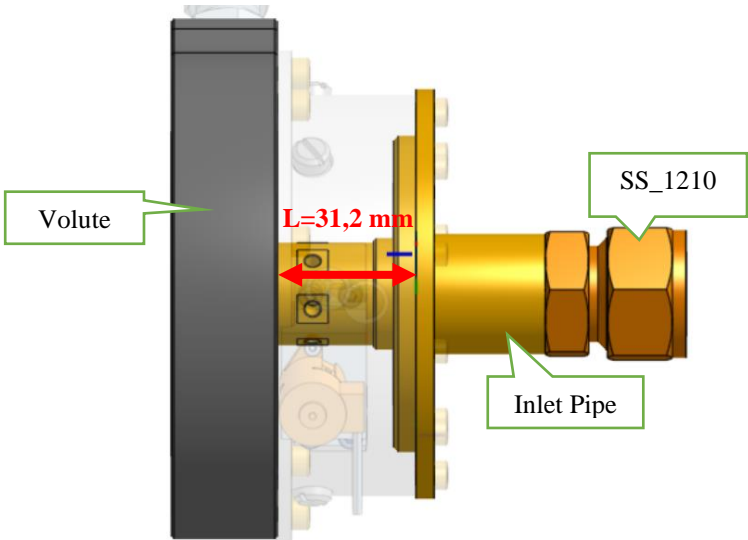


Figure 47: Adjacent parts of the assembly constraining IGV build space

### 5.3. Methodology in design choice

Once the existing problem with the mechanisms used in the laboratory was identified, it was essential to develop a method that would allow a solution to be found that could overcome the flaws of the previous mechanism. It should be noted that the problem is small scale and it is not possible to quantify in a real way the influence of each of the variables on the final error of the system. The required step with the new mechanism is to reduce the number of variables (sources of error) to reduce uncertainty in the sources of system error. Figure 48 shows a schematic of the steps required to solve the problem.

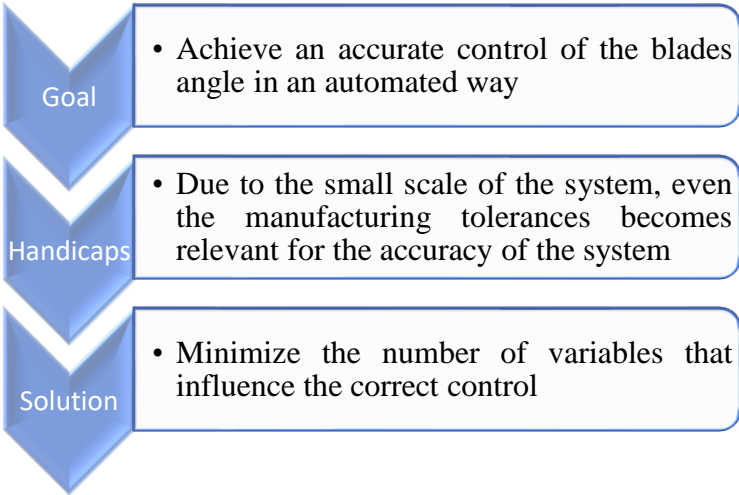


Figure 48: Schematic summary of the steps required to solve the problem

The starting point for the development of the new mechanism was the solutions resulting from the research presented in [section 2.3.2](#). From the existing design types, the conceptual design is generated. The next step is to investigate the feasibility of the mechanism to be made and produced. It is then checked whether the design can meet the specificities of the project. The search for standard materials and parts that may need to be acquired for the system design takes place next. With the collected material, details are then investigated that serves as a factor in the choice of the final design: theoretical calculation of the accuracy of the mechanism in adjusting the IGV, the relationship between the blade angle and the angle of the actuator and estimated costs in the mechanism's design. Once the final design is chosen, the details of the modelling are completed in CAD software and sent to a workshop to be produced. The diagram shown in figure 49 summarises the iterative process described.

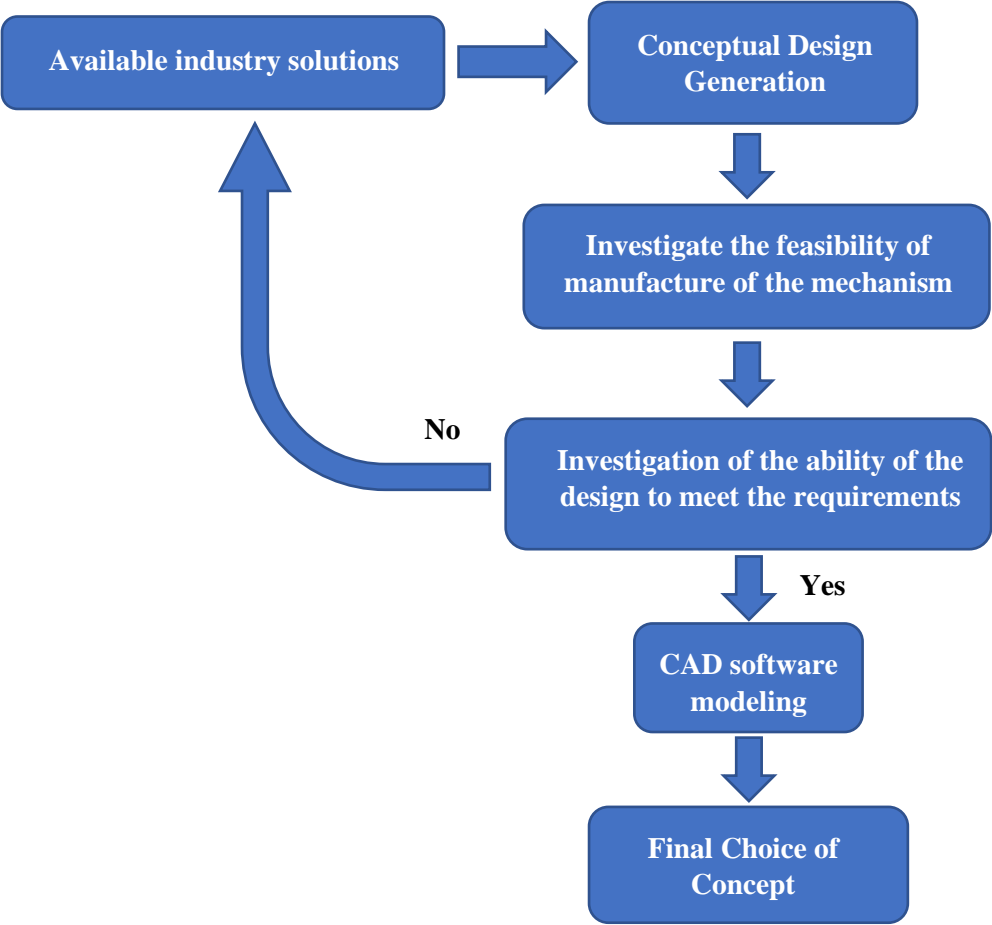


Figure 49: Steps involved in solution finding stage

After several iterations in this process, several concepts were developed. In its design, the main concern was to understand which of the concepts would allow better accuracy and at the same time be easier to manufacture and assemble, also taking into account the costs. This process has shown that the design of the mechanism results from the choice of combinations of three main characteristics transversal to all solutions:

- Type of Actuator:
  - Stepper Motor
  - Linear Motor
- Type of calibration:
  - Grades inscribed in parts
  - Specific Tool
- Mechanical Transmisson:
  - Levers
  - Direct Drive
  - Gear Train

Following this step in the finding of concepts, the next step is the choice of the final concept which is considered in section [5.4](#). For those concepts that have fulfilled the requirements, details of the concepts are given below:

**Levers Mechanism:** Several alternatives within this concept have been considered. All involved the use of a ring to transmit the movement of the active lever to the other levers. Regarding the actuator, to obtain a higher precision to the mechanism, a linear actuator was chosen. In stepper motors, the accuracy is provided in angular terms ( $^{\circ}$ ), and therefore, the accuracy in the control of IGVs will always be greather or equal than the stepper motor accuracy.

For linear stepper motors, the accuracy is given in terms of  $\mu\text{m}$ , which makes it possible to control the accuracy in the control of IGVs by the diameter chosen for the ring used. Regarding the type of calibrator of the system, due to the existence of small moving parts and in order not to make the system more prone to error, it was decided to inscribe markings on the mechanism to ensure the  $0^{\circ}$  of the initial position of the IGVs.

**Geared Mechanism:** Due to the project requiring precision in the movement of IGVs, the feasibility of using cycloid and harmonic gears (used in watchmaking applications) was first investigated. It was found that their use is not applicable when there are intersecting shafts (as is the case of this application) [15]. These gear trains allow zero backlashes in the system in applications where the transmission occurs as parallel shafts (figure [50](#)).

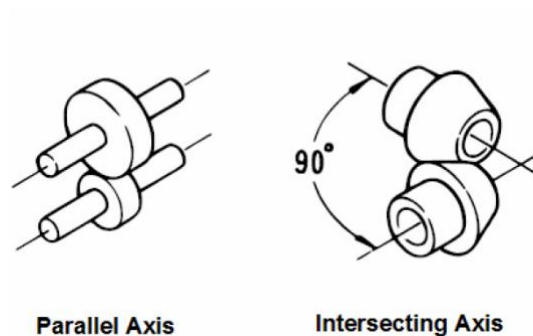


Figure 50: Gears classification according to the position of shaft axes (source: [27])

Aiming to reduce the backlash that was the main problem identified in the designs involving gears, the solution considered includes a split gearing system (figure 51). This type of design provides the effective tooth thickness increases so that it fills the tooth space of the mating gear, thereby eliminating backlash. The calibration in this type of design would be done through marks inscribed in the mechanism and the actuator used would be a stepper motor.

However, designs involving gears, requires extreme accuracy in assembly, particularly concerning the correct mounting of the center distance from the gears. A poor assembly will lead to a loss of precision or even to the locking of the gear system, called jamming. For these reasons, the design of these designs is not practical even because of the difficulty of obtaining accurate results. Therefore, designs with gears were not considered in the final choice of the concept.

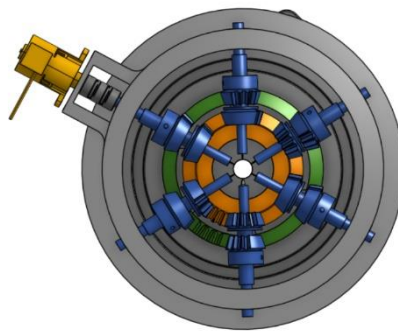


Figure 51: Split gearing solution considered

**Direct Drive Mechanism:** The design involving direct drive mechanism presents itself as a more expensive solution from an electronic point of view, as it requires more actuators, and consequently, more controllers for the mechanism's operation.

In this design, most of the mechanical error is replaced by the electronic error resulting from the accuracy of the actuators and controllers. The actuator type chosen was a stepper motor, and the system is calibrated using a specific tool for this purpose. Due to the existence of a few small scale moving parts, the assembly of the mechanism becomes more straightforward and less error-prone compared to the other two types of design.

## 5.4. Choice of Final Concept

In the choice of the final concept the last 2 concepts considered for the control of the IGVs angle are presented. The design of these solutions was the ultimate step in the choice of the final concept.

In the final choice of the concept, the two most suitable designs for manufacturing and assembly were analysed. As mentioned in [section 5.3](#), geared mechanisms were not considered at this stage of the design due to the need of meticulous assembly to correctly pair the gears.

Therefore, a concept involving levers and another involving a direct drive were considered. This subsection presents the description and theoretical calculation of the accuracy of these mechanisms. A decision matrix was also created to choose the final concept.

### 5.4.1. Lever mechanism

The solution that meets the requirements and is most feasible concerning the use of levers includes a linear motor for IGV angle control. Below are some characteristics of the mechanism.

In applications where the direction of the actuator is not collinear with the direction of motion transmission to other shafts (case of this design), using a linear motor instead of a stepper motor is more advantageous. This is because the backlash of the linear motor is translated by the distance in mm instead of an angular quantity in °.

#### 5.4.1.1. Description of the mechanism

- A system consisting of 2 Levers per NACA shaft;
- Linear stepper motor responsible for controlling the angular position of the vane;
- Rotating ring responsible for the transmission of motion to the passive shafts (shafts that are not directly connected to the linear stepper motor);
- Based on the movement of sliding of the lever 2 in lever 1.

One cut of the design of the IGV control mechanism is presented in figure 52. The external view of the mechanism is presented in figure 53.

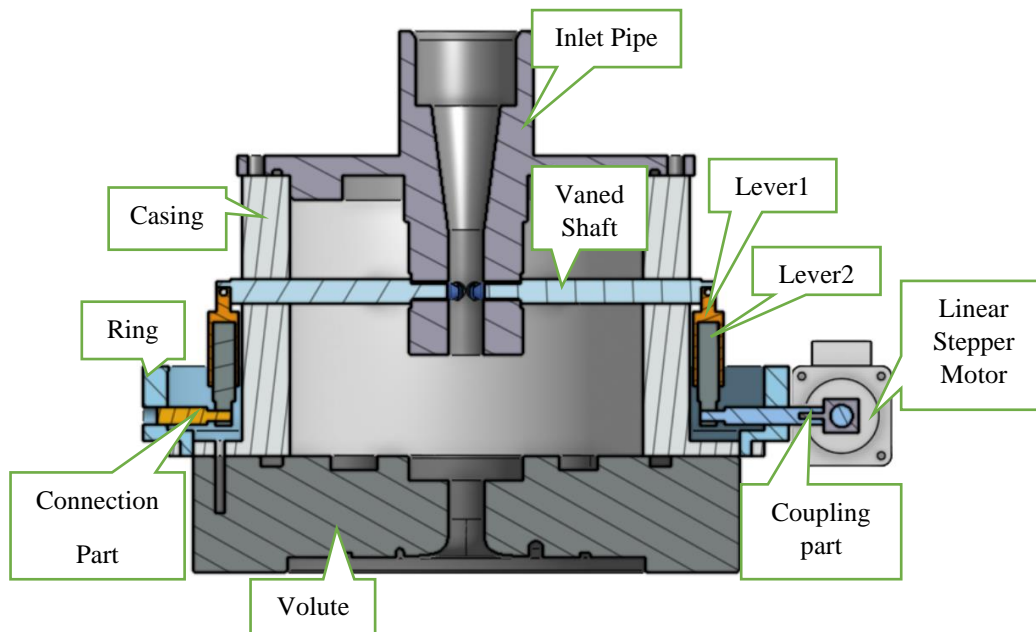


Figure 52: Lever Solution Design- Cut View



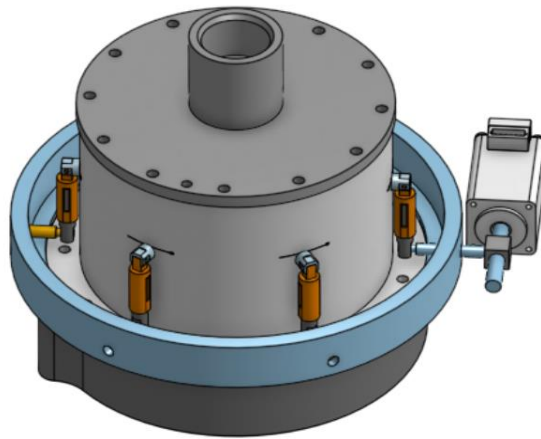


Figure 53: Solution with Levers and Linear Stepper Motor- External View

### 5.4.1.2. Mechanism Accuracy

There is no need for a calibration tool in this solution. As seen, the tool used for calibration played an vital role in the loss of accuracy of the automated system (subsection [4.1.2.3.](#)). Thus, it will be explained below how the calibration works in this new solution.

The accuracy of this project depends on two factors:

- Manufacturing tolerances of the parts that connect the linear actuator to the blades (critical in the calibration task);
- Actuator accuracy.

#### 5.4.1.2.1. Calibration

The calibration task is performed to ensure that the initial blade angle is  $0^\circ$ . Therefore, it is vital in achieving the lowest loss of blade angle accuracy for the linear actuator with this design. The following figures show the relationships designed to reduce the error in the system calibration task.

##### a.1) Blade and 0012\_Naca Shaft

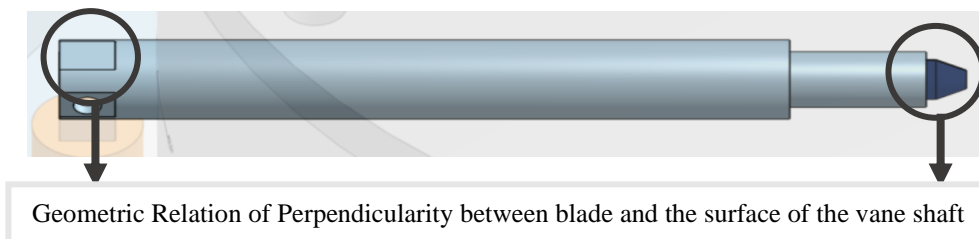
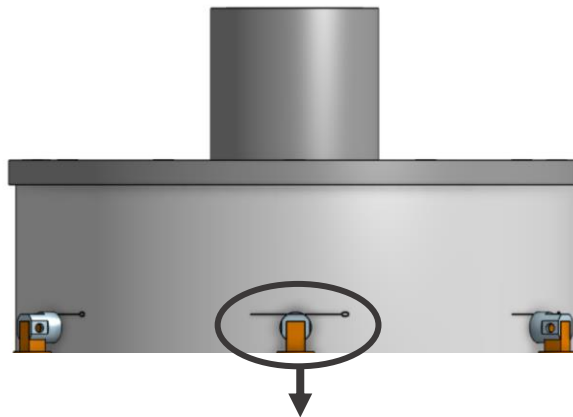


Figure 54: 0012 NACA Shaft

**a.2) 0012\_NacaShaft and Casing**



Grade inscribed in the casing that allows to know which should be the Initial position of Lever 1

Figure 55: Grade inscribed in the external surface of the casing

**a.3) Lever1 and Lever 2**

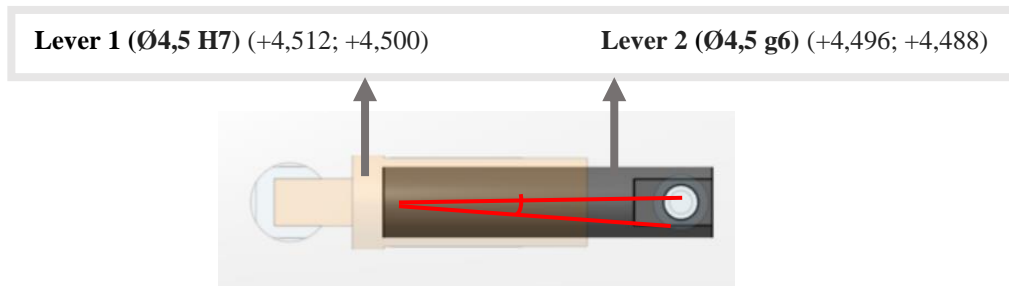


Figure 56: Relation between lever 1 and Lever 2

$$\tan(Error_1) = \frac{4,512 - 4,488}{13} \Rightarrow Error_1 = \pm 0,1058^\circ \quad (12)$$

**a.4.1) Lever 2 + Ring (for the passive shafts)**

In this case, it should be noted that the maximum error will depend on where the blade is located. Thus the maximum error will occur for the initial position of the blade, in this case, 0°, cause the contact length between the casing and the shaft 1 changes.

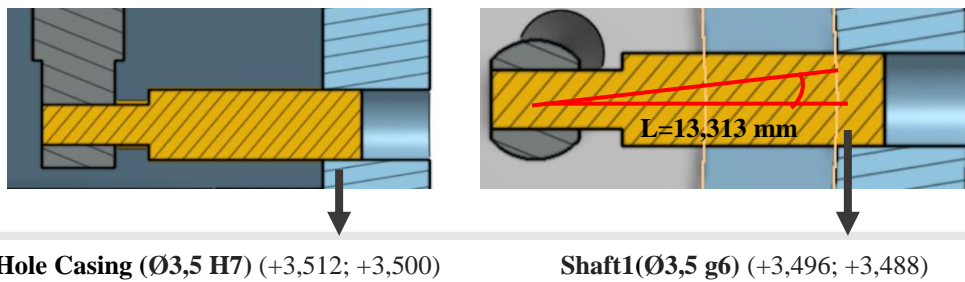


Figure 57: Inaccuracy in connection between ring and lever 2

$$\tan(Error_2) = \frac{3,512 - 3,488}{13,313} \Rightarrow Error_2 = \pm 0,1033^\circ \quad (13)$$

**a.4.2) Lever 2 + Linear Actuator (for the active shaft)**

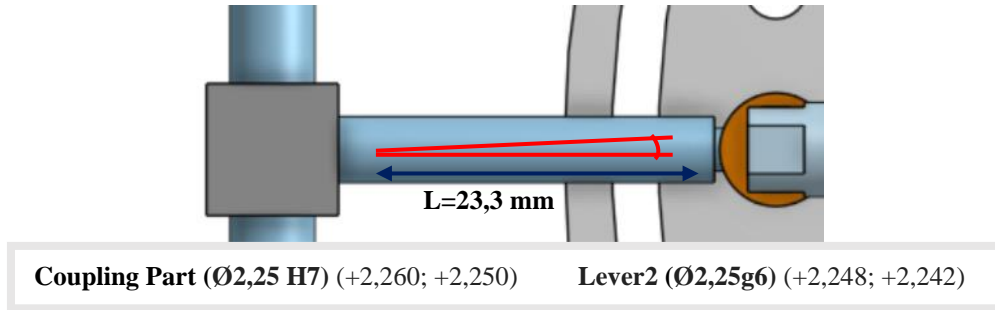


Figure 58: Connection part between linear actuator and lever 2

$$\tan(Error_3) = \frac{2,260 - 2,242}{23,3} \Rightarrow Error_3 = \pm 0,0443^\circ \quad (14)$$

**a.5) Ring and Casing**

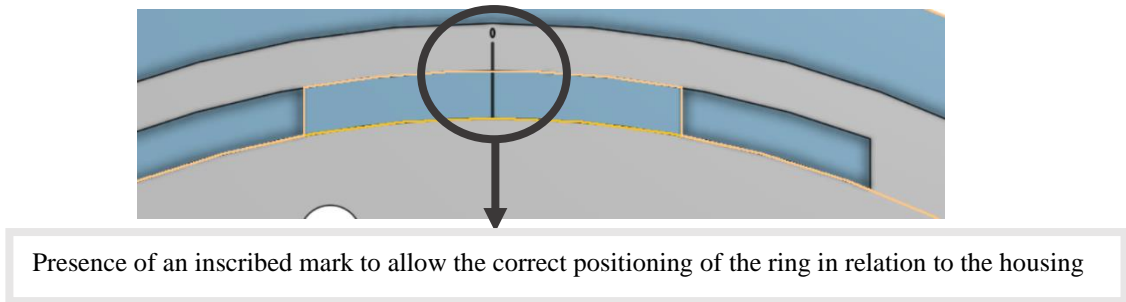


Figure 59: Absence of gap between the casing and the scale inscribed in the ring reduces the error in the system calibration.

Table 10: Error quantification due to manufacturing tolerances in the system calibration task

	Active Shaft(°)	Passive Shaft(°)	Total(°)
<b>Manufacturing Tolerances Error</b>	±0,1501°	±0,2091°	±0,3592°

**5.4.1.2.2. Linear Actuator**

In order to quantify and make a possible evaluation of the system before choosing the final solution, different types of linear actuators that could serve the application were researched.



Figure 60: Different types of linear motors (source:[28])

Regarding this, there are three different types of linear motors: external, non-captive and captive. It should be noted that there are no design requirements in terms of space. System response time is also not a requirement, only the accuracy with which it responds.

Therefore, the type of linear stepper motor that best adapts to this application is the **non-captive one**. Figure 61 shows the technical data of the actuator chosen to drive this system from Nanotec.

LA281M15-A-THCA – NON-CAPTIVE LINEAR ACTUATOR - NEMA 11  
 TECHNICAL DATA

Size	28 mm	NEMA	11
shaft end	single	Force	152.1 N
Speed	35 mm/s	Current per Winding	1.5 A
Thread Diameter	5 mm	Thread Lead	2 mm
Resolution	10 µm/step	Resistance per Winding	1.45 Ohm
Inductance per Winding	1.25 mH	Socket Length "L"	15 mm
Max. Axial Play	±0.05 mm	Length "A"	41 mm
Weight	0.14 kg		

Figure 61: Technical data of linear actuator necessary to compute systems accuracy from Nanotec (source: [28])

With the axial backlash value (the one of interest in this case), the prediction of the maximum error coming from actuator can be made. The graph in figure 62 shows the error coming from the actuator as a function of the position of lever 2.

It is possible to observe that the higher the displacement of lever 2, the smaller the error will be in the adjustment of the final angle of the blade. This is one of the advantages that make a linear actuator a better solution for this type of ring drive systems than a stepper motor.

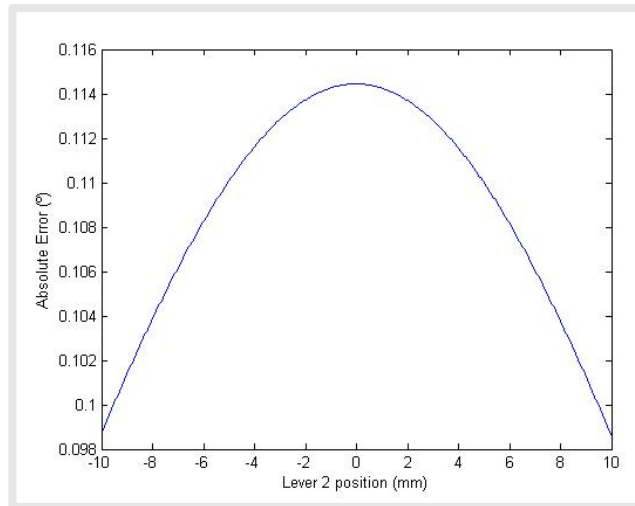


Figure 62: Error in blade adjustment coming from the linear actuator

Table 11: Summary of inaccuracy sources of the levers mechanism designed

<i>Source</i>	<b>Max Error Angle (°)</b>	<b>% of Total Error</b>
<b>Manufacturing Tolerances</b>	$\pm 0,3142^\circ$	73,26
<b>Linear Actuator Accuracy</b>	$\pm 0,1147^\circ$	26,74
<b>Total</b>	$\pm 0,4289^\circ \leq 0,5^\circ$ (Requirement)	100

### 5.4.1.3. Relation between blades angle and linear actuator step

The lever mechanism features one handicap. It does not allow the complete rotation of the blade. In this case, it is essential to know the relationship between actuator control and blade angle control. The relation between a blade angle and the linear actuator step will not be precisely linear and can be defined as:

$$\text{Vanes Angle} = \pm \text{tg}^{-1} \left( \frac{\text{Linear Actuator Step}}{48} \right)$$

Distance of the lever 1 to the center

$$\Leftrightarrow \text{MaxAngle} = \pm \text{atan} \left( \frac{20}{48} \right) = \pm 22,6 > |16|^\circ \text{ (requirement)}$$

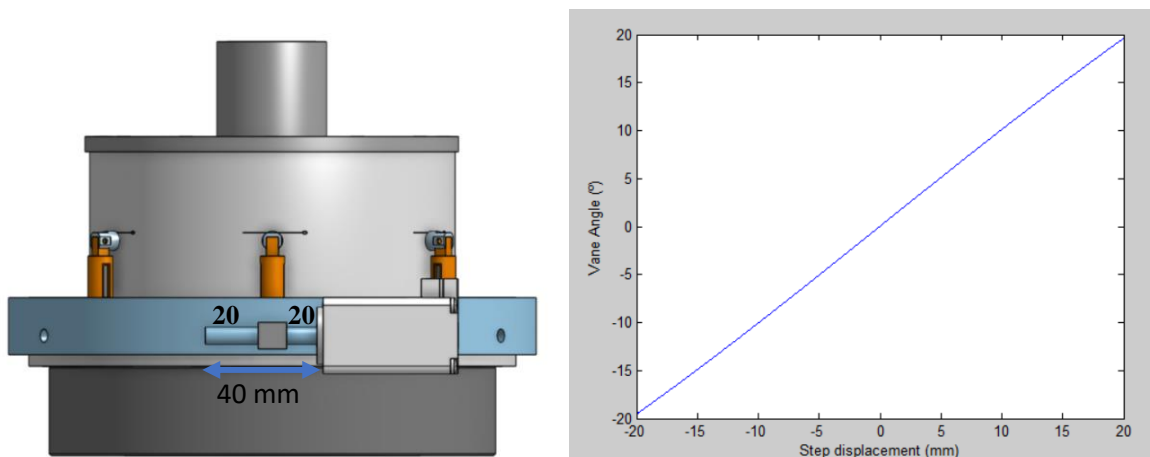


Figure 63: Relation between linear actuator step and blades angle

#### 5.4.1.4. Expected Costs

The choice of the final solution is a compromise between the accuracy and the cost of the system. The expected costs of the design of the explained system are presented in table 12. The costs are presented according to the currency used in Switzerland, the Swiss Franc (CHF - 1CHF =0.905766 Euros on 26.10.2019). The suppliers' material values can be found on the companies' websites [17]. The values for the manufacturing of parts were estimated based on values from previous LAMD projects with the workshops indicated.

Table 12: Expected Cost involved in levers mechanism design

Parts	Supplier	Price (CHF)
<b>Inlet Pipe, Volute</b>		
<b>Controller</b>	Nanotec	92,30
<b>Linear Stepper Motor</b>	Nanotec	62,72
<b>Casing</b>	ATME	400
<b>Ring</b>	ATME	200
<b>6x Shafts_Assembly</b>	ATPR	1200
<b>O-Rings</b>	123 Roulement	20
<b>Screws, Couplings</b>	Misumi	60
		<b>2035,02</b>

#### 5.4.2. Direct Drive mechanism

In the case of this solution, better precision can be obtained by replacing most of the mechanical parts with an electronic mechanism. The great advantage is that it allows a smaller amount of "information" between the actuator and the blades. Due to these facts, the error associated with manufacturing tolerances can be reduced compared to levers mechanism solutions.

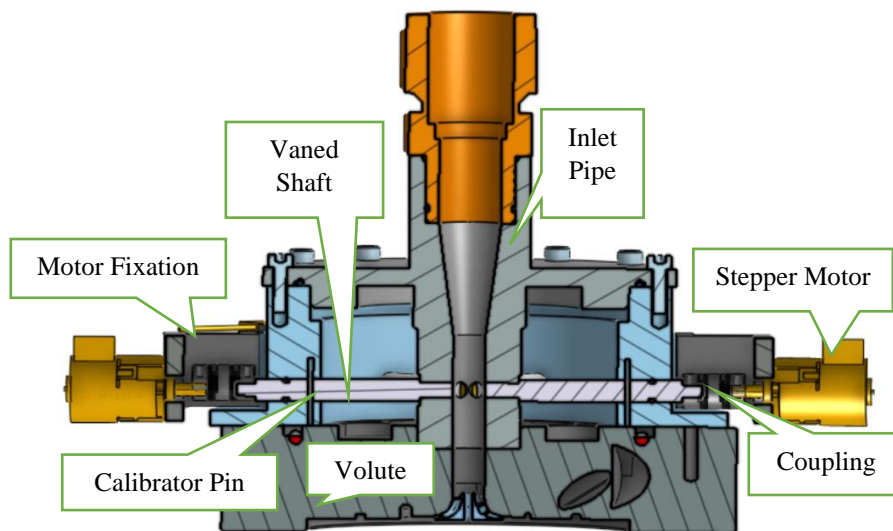


Figure 64: Direct Drive Solution Design- Cut View

**5.4.2.1. Description of the mechanism**

The direct drive mechanism is based on six vanned shafts, directly connected to the stepper motors through couplings. In this system, there are six steppers motors responsible for controlling the position of the blades. There is also a calibrator tool for each vanned shaft to ensure that the initial position of the blade is 0°.

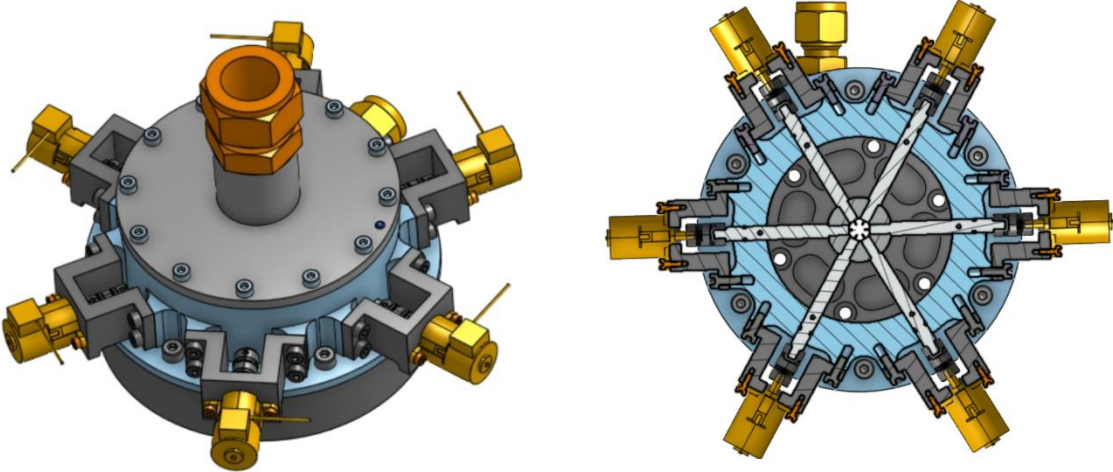


Figure 65: Final design of the VIGV direct drive mechanism: External view (left) and Cut View (right)

**5.4.2.2. Mechanism Accuracy**

The accuracy of this solution depends on two factors:

- Manufacturing tolerances of the parts involved in calibration task
- Accuracy of the actuator.

**5.4.2.2.1. Calibration**

In this case, the calibration mode is similar to the automated geared mechanism used in the LAMD, done through a specific tool, although it is different from the one currently used. The following figures show the relationships designed to reduce the error in the system calibration task.

**b.1) Blade and Vanned Shaft**

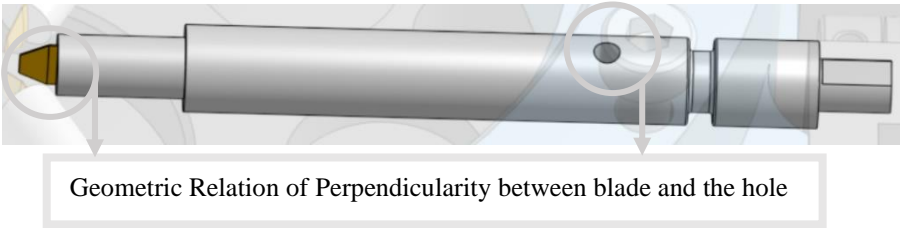


Figure 66: 0012 NACA Shaft of Direct Drive system

## b.2) Calibrator pin and Casing

As the top surface of the casing will always be perpendicular to the direction of fluid flow in the setup tests, this surface can be used as a reference for calibration of the correct initial blades angle.

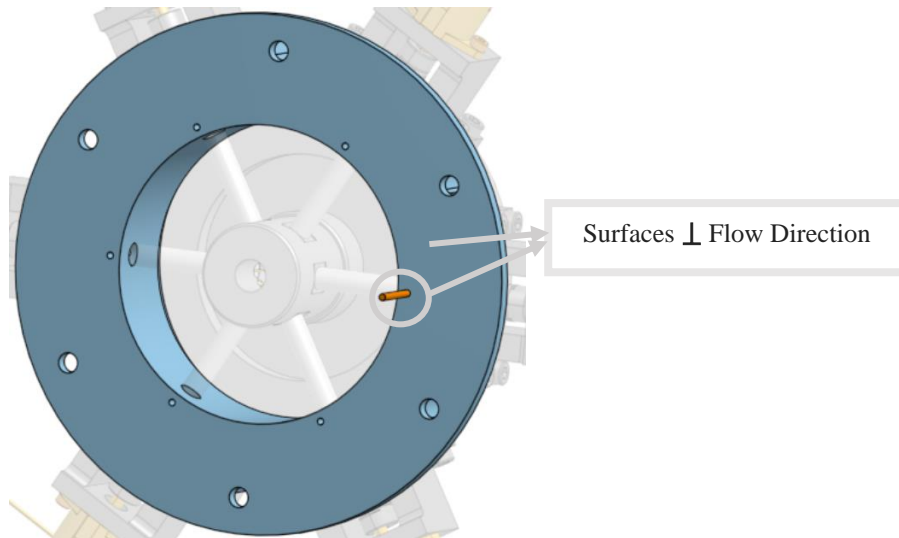


Figure 67: Casing of Direct Drive system

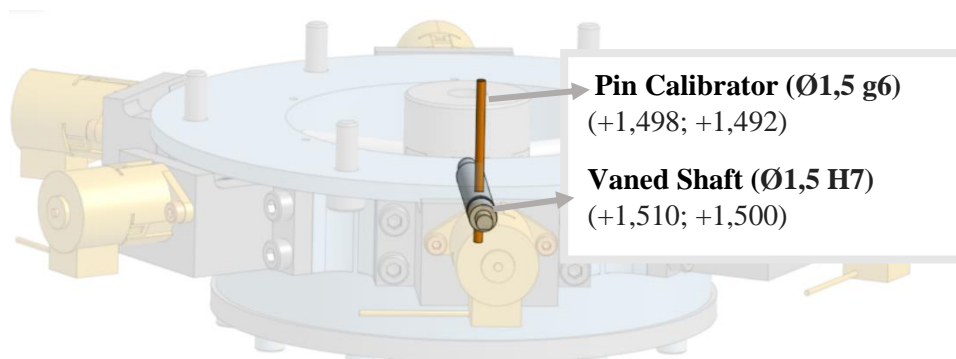


Figure 68: Calibration of the system with Direct Drive System

$$\tan(Error_1) = \frac{1,510 - 1,492}{15 \text{ (Pin length)}} \Rightarrow Error_1 = \pm 0,0688^\circ \quad (16)$$

### 5.4.2.2.2. Actuator Accuracy

The chosen stepper motor is a *SPG1518M0504-102* biphasic stepper motor, already discussed in section [4.1.2.1](#). This way, the maximum error in the accuracy of the mechanism in the adjustment of the blade angle is 0,10032°.



Table 13: Summary of inaccuracy sources of the designed Direct Drive mechanism

Source	Max Error Angle (°)	% of Total Error
Manufacturing Tolerances	±0,0688	40,69
Stepper Motor Accuracy	±0,1003	59,31
<b>Total</b>	$\pm 0,1691^\circ \leq 0,5$ (Requirement)	100

#### 5.4.2.3. Relation between blades angle and linear actuator step

Opposite to the design that used levers, in this design, the relation is almost linear (exclude the error from calibration operation), given that the shaft is directly connected to the stepper motor. Thus, there is no need to develop a scale to use as a reference for the operator. Regarding the range of rotation of IGVs, it is equal to the actuator, being allowed a rotation higher than 16° for each side considered as a project requirement.

#### 5.4.2.4. Expected Costs

In order to predict the costs associated with this mechanism, the table 14 shows all the suppliers of the parts needed for the IGV mechanism. The costs are presented according to the currency used in Switzerland, the Swiss Franc (CHF - 1CHF =0.905766 Euros on 26.10.2019). The suppliers' material values can be found on the companies' websites [17]. The values for the manufacturing of parts were estimated based on values from previous LAMD projects with the workshops indicated.

Table 14:Expected Cost involved in Direct Drive mechanism design

Parts	Supplier	Price (CHF)
<b>Inlet Pipe, volute</b>		
<b>6x steppers Motors</b>	Nanotec	6 x 29,69 = 148,45
<b>Controler</b>	Nanotec	207,95
<b>Arduíno</b>	Teil 3	50
<b>Casing</b>	ATME	800
<b>6x motor attachment</b>	ATME	250
<b>6x Vanned 1</b>	ATPR	600
<b>1 Calibrator</b>	ATPR	20
<b>6 Couplings)</b>	Misumi	50
<b>6 Pin connections or Screws</b>	Misumi/ATPR	50
<b>Orings</b>	123 Roulement	60
		<b>2236,4</b>

### 5.4.3. Conclusion

In order to make the best decision, in choosing the final design, a summary of all the variables present in the analysed designs was made (table 15). Finally, a metric decision (table 16) was made to compare the most important characteristics that the final design should have. As a result the Direct Drive Mechanism design was chosen.

Table 15: Summary of the variables involved in the accuracy of the analysed systems

Manual System	Automated System	Lever Mechanism	Direct Drive Mechanism
<b>Accuracy of the blades adjustment depends on:</b>			
<b>1.Manufacturing Tolerances</b> (Cursor and between pin and Naca Shaft)  <b>2.Operator precision and repeatability</b> in correctly placing the blades angle	<b>1.Manufacturing Tolerances</b> (Naca Shaft, Coupling Axis, Fixation of the motor)  <b>2.Backlash</b> (Angular) between crown gear and bevel gear  <b>3.Accuracy of Stepper Motor</b>  <b>4.Calibrator tool</b> to fix initial position	<b>1.Manufacturing Tolerances</b> (External ring, ConnectionShaft, Lever2, Lever1, Blades shaft)  <b>2.Accuracy of the linear actuator</b>	<b>1.Manufacturing Tolerances</b> (Naca Shaft, Coupling Axis, Fixation of the motor)  <b>2.Accuracy of the stepper motor</b>  <b>3. Calibrator</b>

Table 16: Metric Decision Table

Criteria	Importance (0 to 10)	Lever Mechanism	Best Option
			Direct Drive Mechanism
Manufacture ease	7	4	6
Control ease	6	5	4
Control of the blades angle	7	4	7
Cost	8	7	5
Assembly ease	8	5	7
Accuracy	9	7	8
Stages/Possible sources of play	5	3	4
<b>Final Score</b>	<b>50</b>	<b>35</b>	<b>41</b>

**Manufacture ease:** Directly related to the manufacturing cost. The lever mechanism due to the presence of small mobile levers and the need for them to connect and interact with each other presents itself as a more complicated solution to achieve without errors. At this point, the Direct Drive Mechanism presents itself as a better solution.

**Control ease:** This criterion refers to the complexity of the control system of the mechanism. Since the Lever mechanism only requires one actuator connected to a driver, it is easier to control than the Direct Drive mechanism, which will require an Arduino to control all six stepper motors simultaneously.

**Control of the blade angle:** At this point, the Direct Drive mechanism allows the blade angle control to be linear with the motor steps control. On the other hand, in the lever mechanism, the blade angle control varies with the step defined in the linear actuator according to the arctan function. In this sense, the direct drive mechanism is a better option.

**Cost:** Essential criteria in the choice of the mechanism in the sense that, as in all companies, it is necessary to establish a threshold from which the investment does not compensate the return that comes from design. In this sense, both designs have similar cost values, although due to the higher presence of electronic components, the final cost of the actuator mechanism may increase.

**Assembly ease:** This criterion emerges in the sense that the mechanism can be assembled by anyone who wishes to use it. Thus, due to the larger number of elements of small moving parts, the lever mechanism presents itself as a solution of more difficult assembly. This presents itself as a focus of possible inaccuracy if the system is not correctly assembled.

**Accuracy:** Most relevant criteria, insofar as the more precise the system is, the more reliable the task of optimisation and design of future compressors. Thus, the Direct Drive mechanism by replacing many of the mechanical parts with electronic components, and by having fewer stages, translates into a solution that can lead to a better result.

**Stages/Possible sources of play:** When assessing the results, and detecting sources of error, it is crucial that the mechanism not to have many degrees of freedom between the actuator (which processes the operator command) and the blade (main goal to be controlled by the operator). In this regard, the existence of only a coupling part between the stepper motor and the blade has an advantage from the Direct Drive mechanism. On the other hand, the lever mechanism has small moving parts between the actuator and the blades, as well as a ring responsible for transmitting the movement from the active to the passive axis.

## 6. New IGV Mechanism Design

This sixth chapter deals with the steps involved in the design and manufacture of the mechanism, after the final choice of concept. The elements involved in the mechanical design of the parts that make up the mechanism are analysed. The procedure involved in the manufacturing of the components and the assembly of the mechanism is also presented.

The last section concerns the electronics of the system and how it has been designed and chosen. Also, the controlling part of the mechanism and the adjustment and control of the IGV angle is described.

### 6.1. Mechanical Design

Once the final concept had been chosen and designed, it was necessary at this stage to develop the entire mechanism so that it complied with the project requirements stated in section [5.1](#). The requirements related to the accuracy and range of operation in the adjustment of IGVs had already been checked in section [5.4.2](#).

The next step was to design the parts that make up the mechanism. In this task, it is essential to identify the loads that the parts will be subjected to during operation and then calculate the stresses in the material. Subsequently, the choice of the O-rings essential in the task of sealing the mechanism was also analysed.

Lastly, to guarantee the correct choice of the actuators that make up the system, the stepper motor was sized to ensure that the torque supplied by it is sufficient for the correct adjustment of the blade angle.

#### 6.1.1. Structural analysis to the vanes

The IGV's in this project are only subject to loads from the flow. Since IGVs can plague the functioning of the entire compressor, it requires high accuracy in the handling and manufacture.

The parts of the system that are subject to the highest stresses are also those that require the highest manufacturing accuracy (e.g., NACA 0012 shaft blades). As such, parts need to be manufactured from a high yield stress material that can be easily machined. For these reasons, the components of the mechanism will be made of stainless steel. The chosen material was the same as the previous design, the stainless steel 1.4305, also known as 303 stainless steel, the most readily machineable of all the austenitic grades of stainless steel.

Since the blades that make up the IGVs are the only part of the mechanism subject to stress resulting from interaction with the fluid during operation, they were analysed. This analysis was performed to predict failures in the static design as well as in the fatigue design.

To facilitate the assembly of the mechanism, the vanes are directly milled on their shafts. Each section of the vane is a NACA 0012 airfoil (figure [69](#)). At the edge of the blade, a rounding of 0.03 mm has been created to facilitate the milling of the part. The shafts will be manufactured with a turning machine and the blade with a 5-axis milling machine [9].



Figure 69: 0012 NACA blade analysed

### 6.1.1.1. Project safety factor

When designing or checking a component, the safety coefficient of the design must first be defined. Thus, regarding its calculation, it was considered that:

- The material that makes up the blades is of very good quality;
- The accuracy of the stress analysis and the experimental data collected is good (the value of the total pressure of the channel is known);
- The danger associated with the operation of the equipment is moderate;
- In case of manufacturing defects, the economic impact is considerable insofar as it affects the design of centrifugal compressors.

With this in mind, the Pugsley method [29] can be applied, from which it is obtained:

$$n_{project} = n_{px} \times n_{py} = 1,6 \times 1,3 = \mathbf{2,08} \quad (17)$$

where the design safety factor,  $n_{project}$ , is the result of multiplying the safety dependent on the variables related to the material and loads applied,  $n_{px}$ , with the safety attributed relative to the operator's experience and economic impact of the application,  $n_{py}$ .

It is with this value that the safety coefficients obtained later in the static and fatigue design are compared.

### 6.1.1.2. Static Project

Regarding the static verification of the project, the most critical loading during operation must first be defined. In Pillet's work [9] a structural simulation for the blades has been carried out. A uniform load of 6 bar was applied, double what the blades are subjected to during the tests. It was observed that the stresses on the blades with profile 0012 were low (77MPa) compared to the yield stress of the material (415MPa). Since this design uses the same NACA 0012 profiles, there is no need to perform the structural analysis for the system, since there are no relevant loads on the other parts of the mechanism.

Conditions of the structural simulation performed with CATIA V5 are present in table [17](#). In this simulation were used elements of the linear type tetrahedron (TE4 - four-nodes iso-parametric solid element) [30]. After several iterations and decreasing the size of the elements, the stresses in the vane converged to the values presented in table [17](#).

Table 17: Conditions used in Catia V5

<b>Data</b>		
	<b>Blades Material</b>	Stainless Steel 1.4305 [31]
	<b>Yield Stress (MPa)</b>	415
	<b>Ultimate Tensile Strength (MPa)</b>	690
<b>Applied Loads</b>	<b>Pressure in the inlet pipe(bar)</b>	3
	<b>Pressure applied to the blade(bar)</b>	6
<b>Results</b>		
	<b>Max Von Mises Stress(MPa)</b>	72
	<b>Safety Coefficient</b>	5,76 [32]

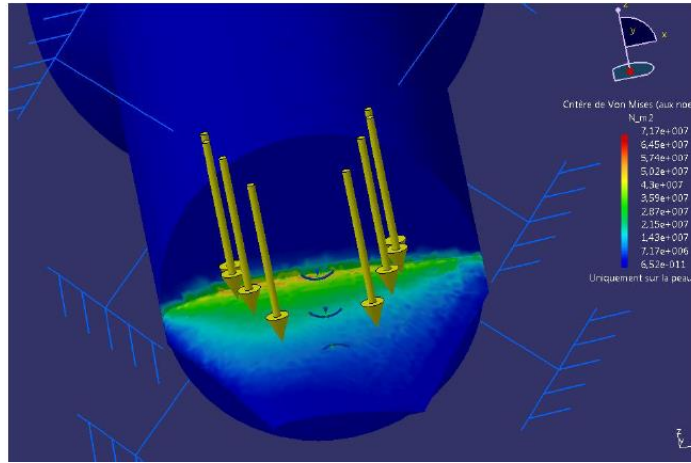


Figure 70: Stress in the vane (source: [9])

To complete the static design, it is sufficient to verify that the safety coefficient for the static stresses,  $n_{static}$ , obtained is higher than the safety coefficient defined in the blade design.

$$n_{static} = \frac{S_y}{\sigma_{applied}} = \frac{415}{72} = 5,76 > n_{project} \quad (18)$$

In (18),  $S_y$  represents the yield stress of the material used, and  $\sigma_{applied}$  is the stress present in the material for this application. It is therefore concluded that the static safety coefficient is checked.

### 6.1.1.3. Fatigue Project

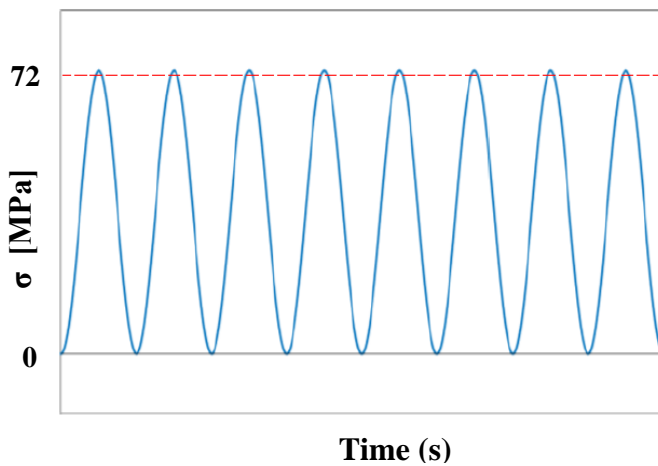
In this subsection, the dynamic analysis of the blade was performed, with the main objective of verifying its fatigue and yield strength.

Due to the complex and non-uniform shape of the Airfoil Naca 0012 profile and to simplify the calculation, the profile was approximated to a parallelepiped so that the stresses suffered by the blade are of axial origin only, as shown in figure 70. Due to the complexity of the blade geometry and the non-applicability of the

geometry in some parameters, many of the correction parameter values were taken in order to increase only the values resulting from the stresses. In this way, a conservative approach is being taken to the design of the blades.

Thus, in the dynamic analysis, it is necessary to define two situations that allow a stress variation in the part being projected. In this regard, it is valid to consider an oscillation between a minimum zero stress, (corresponding to the situation in which the blower is switched off and the blade is not subject to any load), and a maximum stress (corresponds to the positioning of the blade at a 90° angle), as in section 6.1.1.2 in the static design.

In order to simplify the dynamics of the blade, it was considered that it would be subjected to a sinusoidal loading (figure 71). In order to be conservative, it was deemed that the blade, in all operating cycles, would be subject to the maximum stress obtained from static analysis. Figure 72 represents the load considered in this analysis.



$$\sigma_m = \frac{\sigma_{max} + \sigma_{min}}{2} = 36(MPa) \quad (19)$$

$$\sigma_a = \frac{\sigma_{max} - \sigma_{min}}{2} = 36(MPa) \quad (20)$$

In (19-20),  $\sigma_m$  is the mean stress applied and  $\sigma_a$  is the alternating stress.

Figure 71: Graph of applied stress over time

### 6.1.1.3.1. Corrected Stress

For the corrected mean and alternating stresses, it is necessary to apply the fatigue stress concentration factor ( $K_f$ ) to the previously calculated stresses. Where is given by:

$$K_f = q \times (K_t - 1) + 1 \quad (21)$$

Table 18: Parameters involved in fatigue stress concentration factor computation [32]

Parameter	Value	Explanation
$K_t$ (Stress concentration factor )	1,9	Shoulder fillet—well rounded and axial stress (Table 7-1 from Shigleys)
q (Notch sensitivity)	0,85	Maximum value for axial loads for steels with $S_{ut} = 0,7$ GPa
$K_f$ (Fatigue -stress concentration factor )	1,765	

With the  $K_f$  value, it is possible to obtain the value of the corrected stresses:

$$\sigma_m^+ = K_f \times \sigma_m = 63,54 \text{ MPa} \quad (22)$$

$$\sigma_a^+ = K_f \times \sigma_a = 63,54 \text{ MPa} \quad (23)$$

### 6.1.1.3.2. Fatigue limit stress

Stainless Steel 1.4305 has a tensile strength ( $S_{ut}$ ) of 690 MPa. Therefore, the theoretical fatigue limit stress is given by:

$$S_e' = 0,5 \times S_{ut} = 0,5 \times 690 = 345 \text{ MPa} \quad (24)$$

For a real component, it is necessary to apply some modifying factors of the resistance limit. The effective fatigue strength limit is then given by:

$$S_e = K_a K_b K_c K_d K_e K_f S_e' \quad (25)$$

The following table shows the values considered for each factor, which are deducted from the tables in Shigley's book [18].

Table 19: Corrective parameters for fatigue limit strength [32]

Parameter	Value	Explanation
$K_a$	0,797	Material is machined $k_a = aS_{ut}^b = 4,51(690)^{-0,265} = 0,798$
$K_b$	1	Axial loading, no size effect
$K_c$	0,85	Axial loading
$K_d$	1	Work in laboratory with $T \approx 20(^{\circ}\text{C})$
$K_e$	0,814	Reliability of 99% (in order to be conservative)
$K_f$	1	No effects

Once the factors for correction have been calculated, the fatigue limit stress,  $S_e$ , is given by:

$$S_e = 0,797 \times 1 \times 0,85 \times 1 \times 0,814 \times 1 \times 345 = 190,25 \text{ MPa} \quad (26)$$

### 6.1.1.3.3. Safety coefficient check

The parameters calculated above can be used to calculate the fatigue safety factor using the Goodman criterion, where the fatigue safety factor,  $n_{fatigue}$ , is given by :

$$\frac{\bar{\sigma}_a}{S_e} + \frac{\bar{\sigma}_m}{S_{ut}} = \frac{1}{n_{fatigue}} \quad (27)$$



As there is only axial loading and this has already been corrected by the load factor  $K_f$ , by the von Mises criterion, the following equivalent stresses are obtained:  $\bar{\sigma}_a = 63,54 \text{ (MPa)}$  and  $\bar{\sigma}_m = 63,54 \text{ (MPa)}$ . The fatigue safety coefficient is therefore given by:

$$\frac{\bar{\sigma}_a}{S_e} + \frac{\bar{\sigma}_m}{S_{ut}} = \frac{1}{n_{fatigue}} \Leftrightarrow n_{fatigue} = 2,35 > n_{project} \quad (28)$$

It is concluded that the fatigue safety coefficient verifies the desired condition. The safety coefficient has also been calculated through the yield criterion:

$$\frac{\bar{\sigma}_a + \bar{\sigma}_m}{S_y} = \frac{1}{n_{yield}} \Leftrightarrow n_{yield} = 3,26 > n_{project} \quad (29)$$

It is concluded that the safety coefficient to yield is verified and that fatigue controls the design since  $n_{fatigue} < n_{yielding}$ .

### 6.1.2. O-ring choice

In the design of the chosen solution, one of the main requirements is that the module has to be gas tight. In the task of sealing the designed module, it is important to know how tight the O-ring will be squeezed by the different parts in order to create an effective seal of the entire module.

The tightness is reflected in the proportion of the amount of deformation applied to the ring. It is quantified by the percentage of the cross-section thickness at the free state. As the ring is made of a material with high elasticity, this inherent elasticity of the materials leads to the appearance of a compression force against the components. This contact force will be responsible for the blockage in the passage of fluids to the outside.

However, this does not mean that the O-rings should always be designed for maximum tightening. The type of application (static or dynamic) is essential in the choice of the percentage of deformation intended in the O-Ring (see graphs of figure [73](#)).

In Table [20](#), there are some of the features involved in choosing the o-rings that seal the designed mechanism. Note that all O-Rings will perform a static type seal, except for the O-Rings present in the shafts (3.5\_1) which will be controlled from the motors. The shafts will be subject to rotational movements to adjust the blade angle during the pre-test. During this period, O-rings must ensure the sealing of the system, which is why the type of sealing, in this case, cannot be considered fully static.

Table 20: Data concerning the existing seal types in the mechanism

O-Ring	Type of seal	Sealing Effect	O ring Type of Stress	Percentage of Flatenning (%)
18.5_1	Static	Piston	Radial	25
14.5_1	Static	Piston	Radial	20
74_3	Static	Flange	Axial	26,67
74_1.5	Static	Flange	Axial	30
3.5_1	Almost Static	Piston	Radial	25

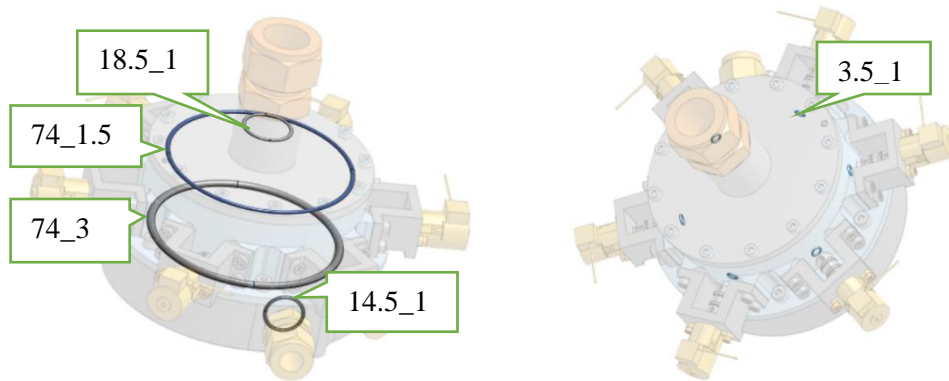


Figure 72: Different types of seal in the mechanism: static (left) and dynamic / almost static (right)

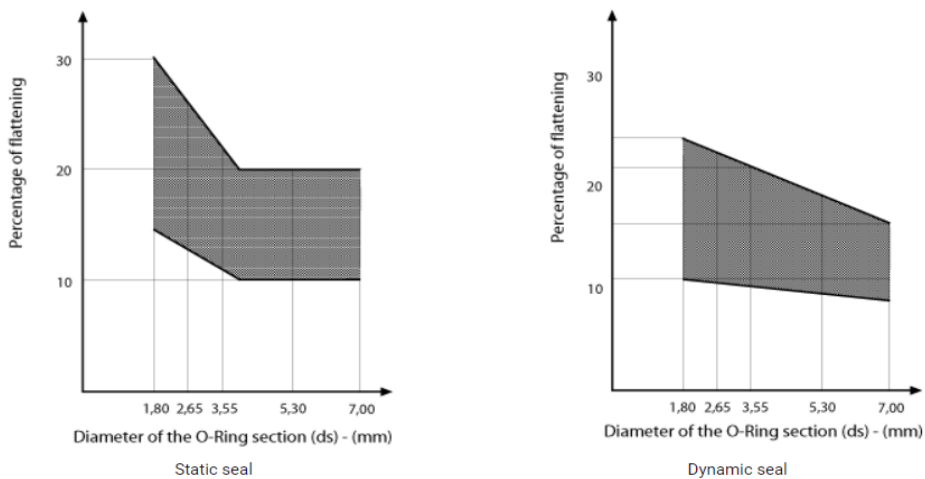
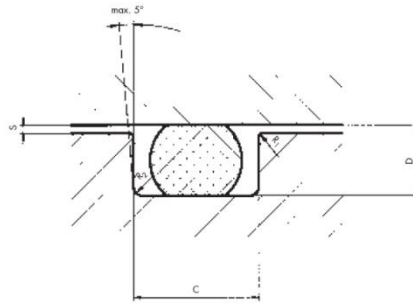


Figure 73: Percentage of O-ring deformation depending on the type of application (source: [33])

In choosing the O-ring material, it was taken into account not only the cost and the excellent elastic properties of the material, but also the possible presence of the refrigerant R-134a in the tests. In this sense, the material chosen could not suddenly change its permeation resistance properties due to the presence of a refrigerant gas as R-134a. Therefore, NBR (nitrile butadiene rubber) was chosen, which meets the requirements previously listed [34]. Also related to this design element, it was necessary to use the table in figure 74, for the design of the housings to place the O-rings to obtain an efficient sealing of the mechanism. The selected dimensions can be observed in the drawing of the NACA Shaft presented in Annex A.2.



Bestimmung der Aufnahme		Conception des gorges						Radien	
Schnurdurchmesser Diamètre de corde	Dynamischer Einsatz radial Utilisation dynamique radiale			Statischer Einsatz axial/radial Utilisation statique axial/radiale			R <sub>1</sub>	R <sub>2</sub>	
	Nutttiefe Hydr. Profondeur de gorge hydr.	Nutbreite Largeur de gorge		Nutttiefe Profondeur de gorge	Nutbreite Largeur de gorge				
d <sub>2</sub>	D <sup>0</sup>	%	c	D <sup>+0.1</sup>	%	C	mm	mm	
1,00	--	--	--	0,70	30	1,5 ± 0,1	0,1	0,25	
1,02	--	--	--	0,70	30	1,5 ± 0,1	0,1	0,25	
1,27	--	--	--	0,90	28	1,8 ± 0,1	0,1	0,25	
1,30	--	--	--	1,10	26	2,2 ± 0,1	0,1	0,25	
1,52	--	--	--	1,10	26	2,3 ± 0,1	0,1	0,25	
1,60	--	--	--	1,20	25	2,3 ± 0,1	0,1	0,25	
1,78	1,45	19	2,5 ± 0,1	1,30	26	2,5 ± 0,1	0,1	0,25	
1,80	1,50	17	2,5 ± 0,1	1,30	27	2,5 ± 0,1	0,1	0,25	
1,90	1,60	16	2,5 ± 0,1	1,50	21	2,5 ± 0,1	0,1	0,25	
2,00	1,70	15	2,6 ± 0,1	1,60	20	2,6 ± 0,1	0,1	0,25	
2,40	2,00	16	3,2 ± 0,1	1,80	25	3,2 ± 0,1	0,1	0,25	
2,50	2,15	14	3,3 ± 0,1	1,90	24	3,3 ± 0,1	0,1	0,25	
2,62	2,20	16	3,5 ± 0,1	2,05	22	3,5 ± 0,1	0,1	0,25	
2,65	2,20	17	3,5 ± 0,1	2,05	23	3,5 ± 0,1	0,1	0,25	
2,70	2,25	16	3,6 ± 0,1	2,15	20	3,6 ± 0,1	0,1	0,25	
3,00	2,60	13	4,0 ± 0,1	2,40	20	4,0 ± 0,1	0,1	0,25	
3,50	3,05	13	4,5 ± 0,2	2,90	17	4,5 ± 0,2	0,2	0,75	
3,53	3,05	13	4,5 ± 0,2	2,90	18	4,5 ± 0,2	0,2	0,75	
3,55	3,05	14	4,5 ± 0,2	2,90	18	4,5 ± 0,2	0,2	0,75	
3,60	3,10	14	4,6 ± 0,2	3,00	17	4,6 ± 0,2	0,2	0,75	
4,00	3,50	12	5,0 ± 0,2	3,30	17	5,0 ± 0,2	0,2	0,75	
5,00	4,40	12	6,5 ± 0,2	4,10	18	6,5 ± 0,2	0,2	0,75	
5,30	4,70	12	7,0 ± 0,2	4,50	15	7,0 ± 0,2	0,2	0,75	
5,34	4,70	12	7,0 ± 0,2	4,50	16	7,0 ± 0,2	0,2	0,75	
5,70	5,00	12	7,5 ± 0,2	4,85	15	7,5 ± 0,2	0,2	0,75	
6,99	6,20	11	9,5 ± 0,2	6,00	14	9,5 ± 0,2	0,2	0,75	
7,00	6,20	11	9,5 ± 0,2	6,00	14	9,5 ± 0,2	0,2	0,75	
8,40	7,50	10	11,0 ± 0,2	7,25	13	11,0 ± 0,2	0,2	0,75	

Figure 74: Dimensions table provided by Normatec regarding the elaboration of enclosures for allocation of O-Rings (source: [35])

### 6.1.3. Sizing of the stepper motor

In this stage, the strategy of checking the capacities of the stepper motor was used, taking into account the torque required for the proper and accurate functioning of the mechanism. As previously mentioned in the section, the SPG1518M0504-102 (see datasheet in subsection 4.1.2.1 and in annex A.2) with 0.176° step angle, planetary reduction gear with a ratio of 1:102,5 and a holding torque of 0.2 N.m. was selected.

Whenever a component is designed, the actuation phase where it is subjected to the highest effort should be identified. In the case of the stepper motor, the situation will occur when it is intended to adjust the blade angle with the fluid flow caused by the blower.

The necessary condition to check is:

$$\text{Torque supplied by the motor} > \text{torque required by the system during operations}$$

Regarding the torque supplied by the engine, due to the impossibility of obtaining the torque vs speed chart by the manufacturer of Nanotec, it was assumed that it would have similar behaviour to engines of the same manufacturer of the same type Nema 11 (figure 75). Thus, by using a low pulse rate can be assumed the torque provided by the engine is the same as the holding torque. For safety reasons in the design, it was assumed that the stepper motor in dynamic conditions only provides a torque with a value of half the holding torque (0.1 Nm).

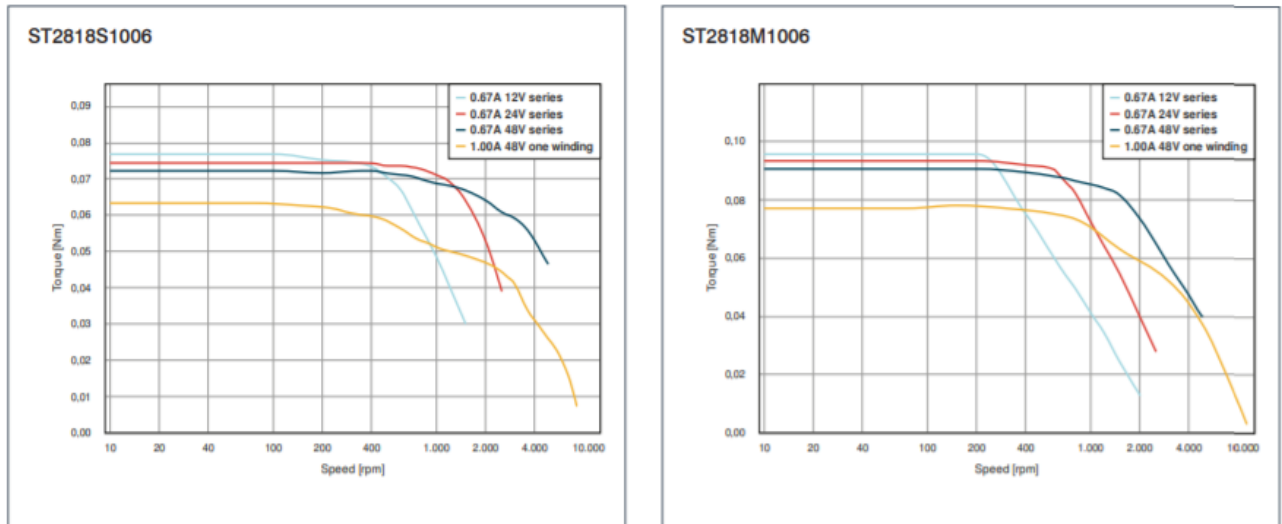


Figure 75: Torque vs Speed Charts of stepper motors with the same size and brand as the chosen one (source:[16] )

Regarding the torque required by the mechanism during the blade angle adjustment operation, it will depend on three factors [36]:

- 1.System inertia
- 2.External forces
- 3.Friction between the different parts of the system

### 6.1.3.1. System inertia

As shown in figure 76, the system driven by the stepper motor will consist of the vanned shaft, the coupling part, and the motor rotor. Table 21 shows the inertia of the components that constitute the new mechanism.

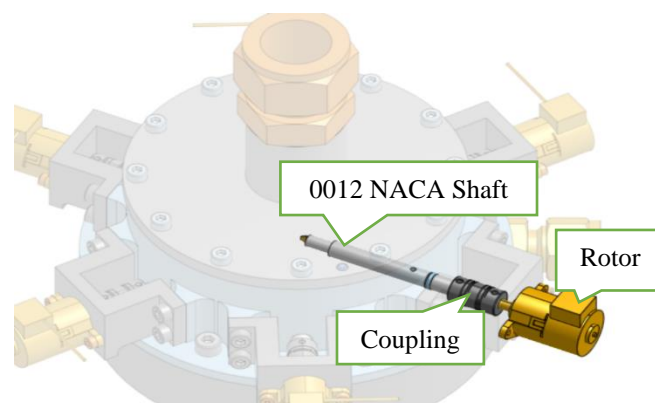


Figure 76:Parts involved in transmitting the movement of the motor stepper to the vane

Table 21: System inertia for specific axis

Part	Material	Specific mass(Kg/m <sup>3</sup> )	Volume(m <sup>3</sup> )	Mass(kg)	Inertia (Kg *m <sup>2</sup> )
0012 Naca Shaft	Stainless Steel 1.4305	8000	7,94 x 10 <sup>-7</sup>	6,36 x 10 <sup>-3</sup>	1,36 x 10 <sup>-6</sup>
Coupling	Provided by Misumi				1,2 x 10 <sup>-8</sup>
Rotor Inertia	Provided by Nanotec				1 x 10 <sup>-7</sup>
					<b>1,472x10<sup>-6</sup></b>

In Naca Shaft's case, the same was approximated to a cylinder in the calculation of its inertia, having been used *equation 30*

$$I = \frac{m \times r_{shaft}^2}{2} \quad (30)$$

From the inertia, the torque required to rotate the system can be reached using the *equation 31*

$$T = I \times \alpha' \quad (31)$$

where,  $\alpha'$  is the angular acceleration and is described by the expression:

$$\alpha' = \frac{w}{t} = \frac{\pi * n(rpm)}{t(s) * 30} \quad (32)$$

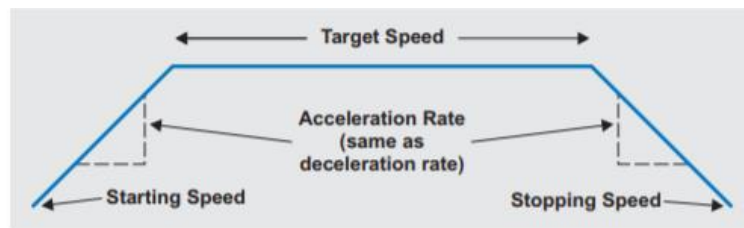


Figure 77: Typical acceleration profile in Stepper motors (source: [36])

Thus, since response time is not a specified requirement of this project, there a value of  $n=200\text{rpm}$  and  $t=1\text{s}$  was used.

$$T=30 \mu\text{Nm}$$

### 6.1.3.2. External forces

For the calculation of the required system torque due to external forces, it is essential to consider the force generated in the Naca profile by the fluid flow along the pipe. This is shown in table [22](#). The setup will be assembled, and two types of fluids will be used in future tests: air and R134a.

Table 22: Data concerning the fluids that can be used for testing the system

Feature /Gas	Air	R134 a
$\rho$ (kg/m <sup>3</sup> )	1,225	4,25
v (m/s)	50	50
A (mm <sup>2</sup> ) Blades Surface Area	12,634	12,634
C <sub>L</sub> (caracteristic of 0012 Naca profile- Lift coefficient)	<1,5	<1,5

Thus and in order to compute the lift torque generated in the vanned shafts [9]:

$$F_L = 0.5\rho v^2 A C_L \Leftrightarrow F_L = 0,101 \text{ N} \quad (33)$$

The lever with which the lift force,  $F_L$ , is applied on the blade is lower than half the length of the blade ( $R_{\max} = 1.75 \text{ mm}$ ) so in the end, the torque created by this lift force is lower than

$$T_{\max} = F_L \times R_{\max} = 177 \mu\text{Nm} \quad (34)$$

### 6.1.3.3. Friction between the different parts of the system

For the final calculation of the torque required by the system for each stepper motor, it is necessary to evaluate the frictional resistance between the moving parts of the mechanism. In this case, the friction torque ( $C_f$ ) that will exist between each of the components will be the result of radial friction and can be calculated using the expression:

$$C_f = F_L \times \mu \times R \quad (35)$$

Where,  $\mu$  represents the coefficient of friction between the materials of the parts that are interacting, and  $R$  represents the radius of interaction, relative to the central axis of the shaft, between both parts. Thus, in table 23, there is shown the different friction coefficients used in the calculations, resulting from the interactions existing in the mechanism (figure 76).

Table 23: Torque required by different system components due to friction [37]

Interaction	$\mu$ , friction coefficient	Friction torque (Nm)
Stepper Motor- Coupling	0,4 (plastic -metal)	0,00012
Coupling - Shaft	0,6 (steel -steel)	0,00018
Oring- Casing	0,7 (rubber -steel)	0,00354

The result of the sizing of the stepper motor is shown in table 24. It can be seen that the torque required by the system for each motor is low compared to the torque that can be provided by the stepper motor. This is an advantage over the previous design in which the stepper motor was also responsible for moving the passive shafts as well as the gear system used.

Table 24: Summary of torque required by the system to work properly

	Torque Required (Nm)	Remaining Torque (Nm)
Motor's Torque	---	0,10
Inertia System	0,00003	0,09997
Friction		
<b>Stepper Motor- Coupling</b>	0,00012	0,09985
<b>Coupling - Shaft</b>	0,00018	0,09967
<b>O ring- Casing</b>	0,00354	0,09613
External Forces		
<b>Lift</b>	0,000177	<b>0,0960</b>

## 6.2. Mechanism manufacturing

After the choice and mechanical design of the direct drive mechanism, the latest version of the mechanism was modelled. The CAD software used in the modelling of the mechanism was Onshape [15]. This software has several advantages: it brings together modelling tools and project data management in a secure workspace in the cloud that is accessible on any device, never loses data and eliminates project congestion.

The drawings of the mechanism were sent to the ATME workshop (EPFL-Lausanne). After being analysed, some modifications were suggested and subjected to corrections. A schematic of the procedure that was carried out is shown in figure 78.

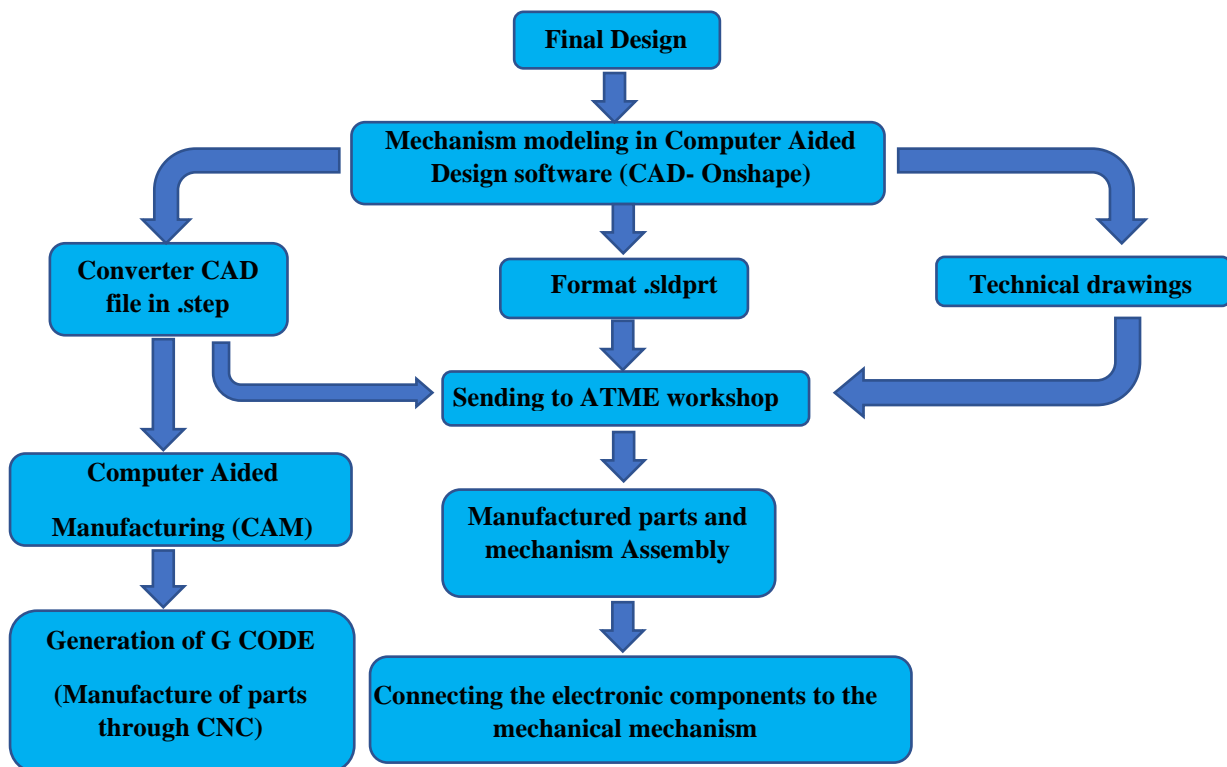


Figure 78: Steps involved in the manufacturing process of the mechanism

The design chosen was, as already mentioned, the mechanism involving the direct drive. The operating mode will be the same as described in subsection [5.4.2](#). However, some modifications were made after contacting the responsible workshop. The calibrator is placed in an inner region in relation to the O-Ring74\_3 to ensure better sealing of the system. A coupling connects the motor to the blade shaft and is connected by using small M2 headless screws. 2D drawings of all parts that needed be manufactured are available in annex [A.2](#).

Figure [79](#) shows physical images of the mechanical part of the mechanism. It is possible to observe the pins that are responsible for calibrating the angle of the IGVs in the initial position of 0°.

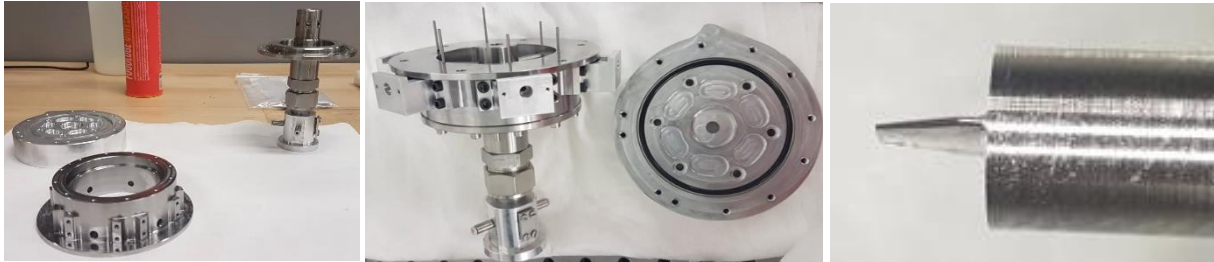


Figure 79: Constituent parts of the new mechanism: Clean parts after ultrasound (left), calibrators mounted on the mechanism (center) and magnified image of an IGV (right)

### 6.3. Assembly of the mechanism

This section describes the assembly process of the designed mechanism. The exploded view (figure [80](#)) can be useful to understand the process better.

#### Assembly Steps:

1. Screw SS\_1210 onto the inlet tube;
2. Place the 74-1.5 O-ring in the milled groove in the inlet tube;
3. Center the casing on the inlet tube and place the pin into its hole;
4. Screw the casing onto the inlet tube (12x M3\_10mm);
5. Place the six O-ring 3.5 \_1 on the six vaned shafts;
6. Place all vaned shafts in their borings;
7. Place the six couplings on the six vaned shafts and screw tight;
8. Screw all the six motor attachments on the casing (24x M3\_8mm);
9. Calibrate the system by setting the calibrator on all the six casing holes passing through the vaned shafts;
10. Screw the motor to its attachment (12xM2\_6mm);
11. The motor on the coupling;
12. Remove the calibrator;
13. Apply a small axial force, from the outside to the inside, with a small piece of plastic in the coupling in order to calibrate the system axially;
14. Screw the volute on the assembled compressor;



15. Screw the VIGV mechanism on the volute after having placed the 74-3 O-ring in its groove.

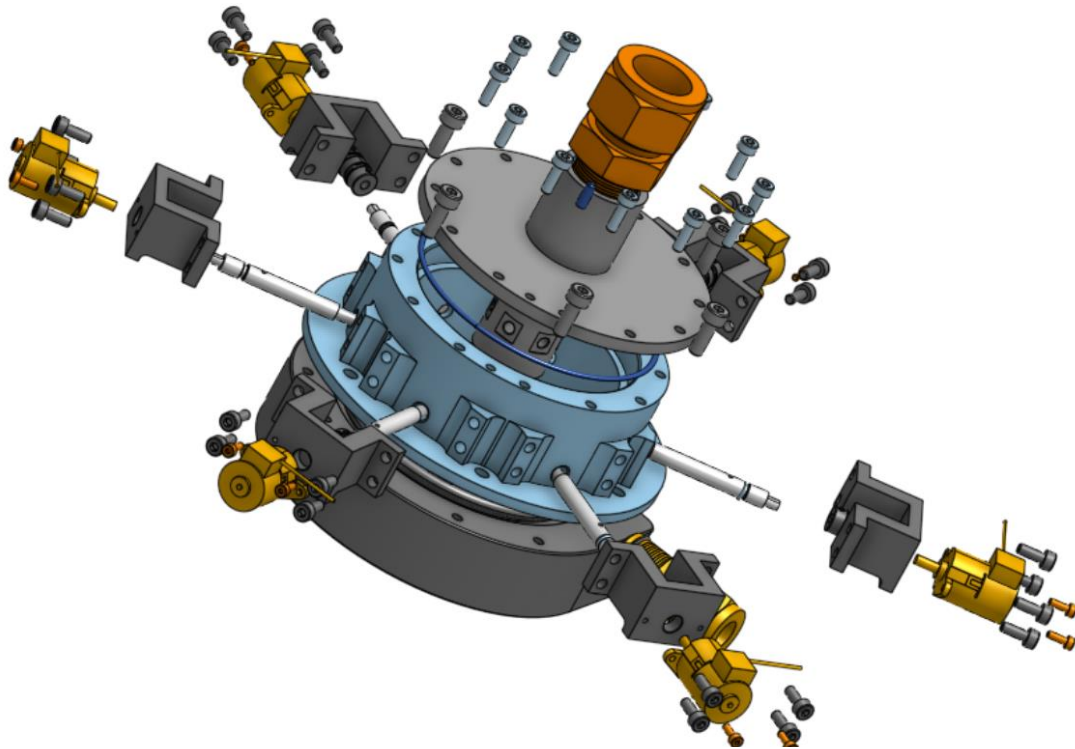


Figure 80:Exploded view of the VIGV mechanism

## 6.4. Control of the mechanism

Once the mechanical design of the mechanism was completed, it was necessary to decide on the electronic configuration of the system to make the entire mechanism functional.

At the time of choosing the final concept, the use of 6 SPG1518M0504-102 type stepper motors was previously selected (section [5.4.2.2.2](#)). The manufacturer Nanotec was contacted and informed of the end of the application for which the stepper motors were intended. After research and dialogue with Nanotec it was suggested the final version used to control the 6 stepper motors simultaneously.

The six stepper motors are controlled via the SMC11-2 controllers (datasheet in Annex [A.3](#)). Each of these controllers is connected directly to an Arduino Mega2560 (the Arduino Uno did not fit due to an insufficient number of ports for the six controllers). The Arduino acts as the master, and the input signals [38] (clock, release, direction) are sent to the motor control.

The diagrams in figure [81](#) and [82](#) shows the configuration of the connections and apparatus of the new mechanism. The technical data of the arduino is presented in Annex [A.3](#).

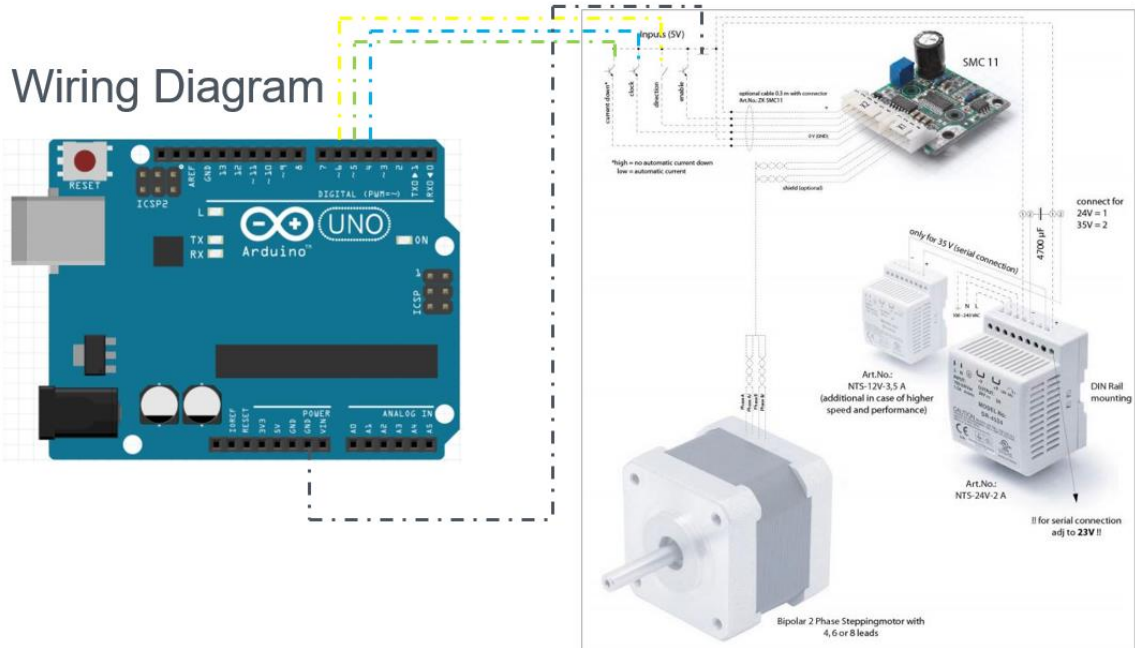


Figure 81: Connection diagram of the control system

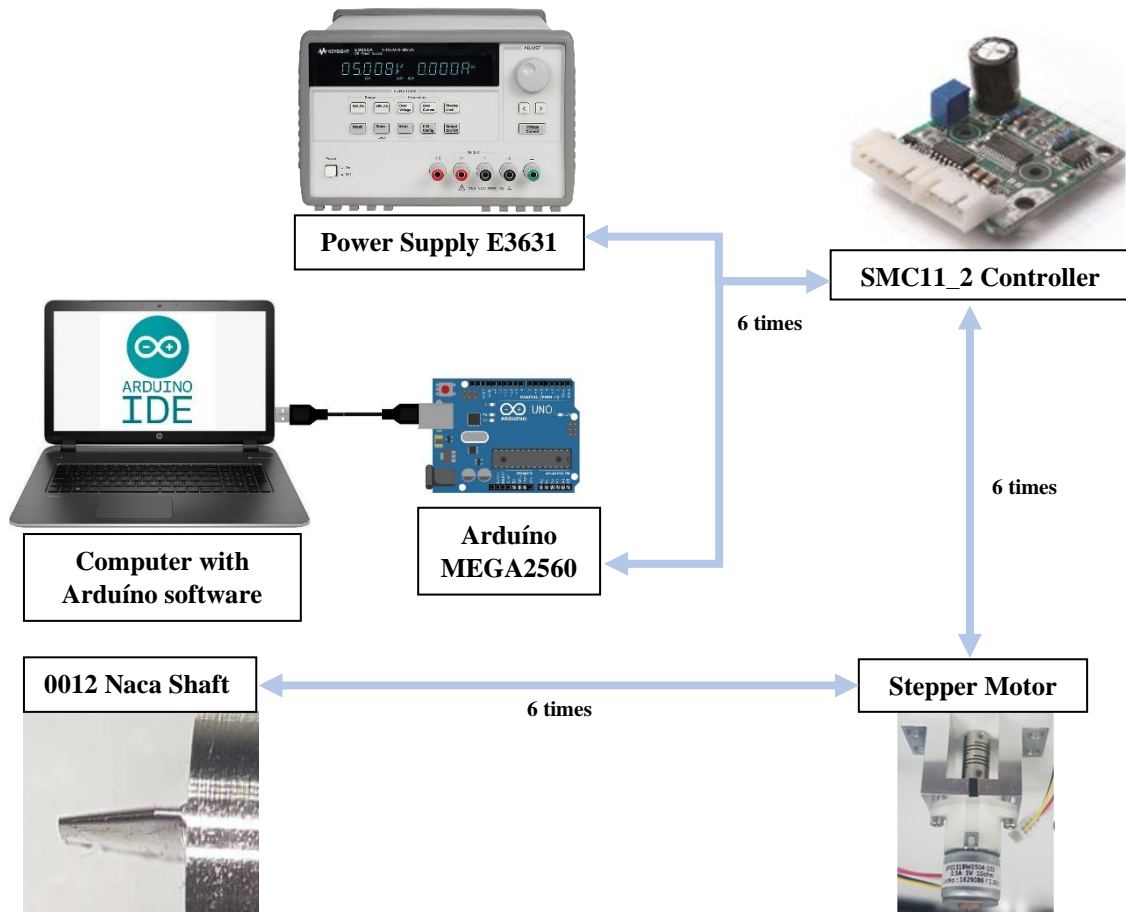
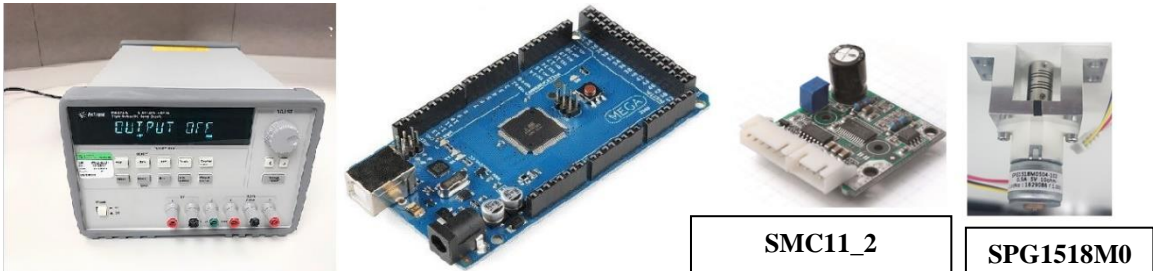


Figure 82: Interaction between electronic components in the functioning of the new mechanism

The performance of the electronic components of the mechanism is dependent on the chosen operating parameters. Therefore, it is important to choose the voltage and current that will be provided to the controllers and stepper motors so that they operate accurately and there is no risk of being damaged due to their inefficient use.

Figure 83 shows the electronic components that make up the entire mechanism, as well as the parameters at which they can operate.



<p><b>Power Supply E3631</b></p> <ul style="list-style-type: none"> <li>➤ Controls the voltage at which the controller operates</li> </ul>	<p><b>Arduino MEGA2560</b></p> <ul style="list-style-type: none"> <li>➤ Operates at 5V (supplied by computer)</li> </ul>	<p><b>SMC11_2 Controller</b></p> <ul style="list-style-type: none"> <li>➤ 12- 35VDC</li> <li>➤ Rated Current=1.4(A)</li> <li>➤ Peak current =2.4(A)</li> </ul>	<p><b>SPG1518M0 504-102</b></p> <ul style="list-style-type: none"> <li>➤ 5 VDC</li> <li>➤ I=0,5 (A)</li> </ul>
--	--	--	--

Figure 83:Electronic components constituting the new design

Annex A.3 shows the routine developed in Arduino for controlling the blade angles using the stepper motors. Annex A.4 contains the necessary user procedure to test the mechanism.

**Important notes about the electronic part of the mechanism:**

- Operate at 24 V preferably, but the system can operate at 12 V if less torque is required from the system;
- Do not set the controller potentiometer (blue part) to a value above level 3 in order to supply no more current than the 0.5 Amperes supported by the stepper motors.

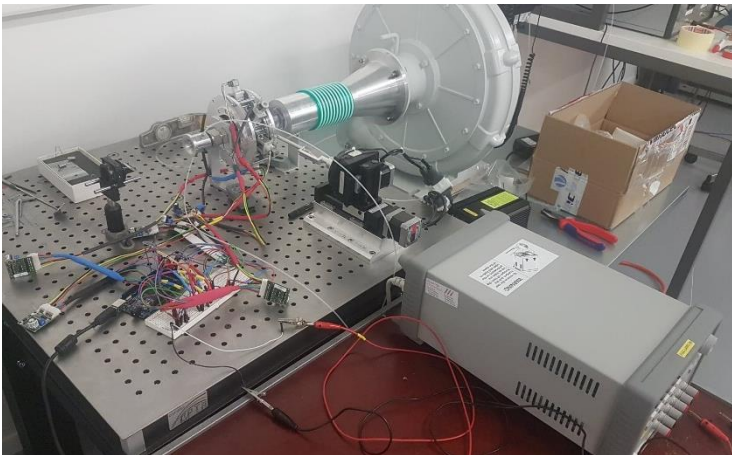


Figure 84: Mechanism final configuration with the electronic part assembled

## 7. New Mechanism Test Experiments

Once the mechanical and electronic design and assembly of the entire mechanism were finished, the last stage of this project included experimental tests with the new mechanism. As seen, the new solution is a mechanism that will allow more accurate control of the blade angle, from a theoretical point of view. In order to validate the new mechanism globally, it must be experimentally verified.

Therefore, tests were performed in the laboratory. The results are shown in figure 85. The conditions under which all the tests occurred are present in table 25.

Table 25: Inlet and Outlet pressures of the experiment with direct drive mechanism

Fluid: Air				
Angle Adjusted	Total Pressure(Pa)	$P_t - P_{static1}$ (Pa)	$P_t - P_{static2}$ (Pa)	Temperature(°C)
-8°	964300	0,0814	9,0143	25,9
0°	965000	0,0813	9,0128	26,7
+8°	965100	0,0811	9,0074	26,9

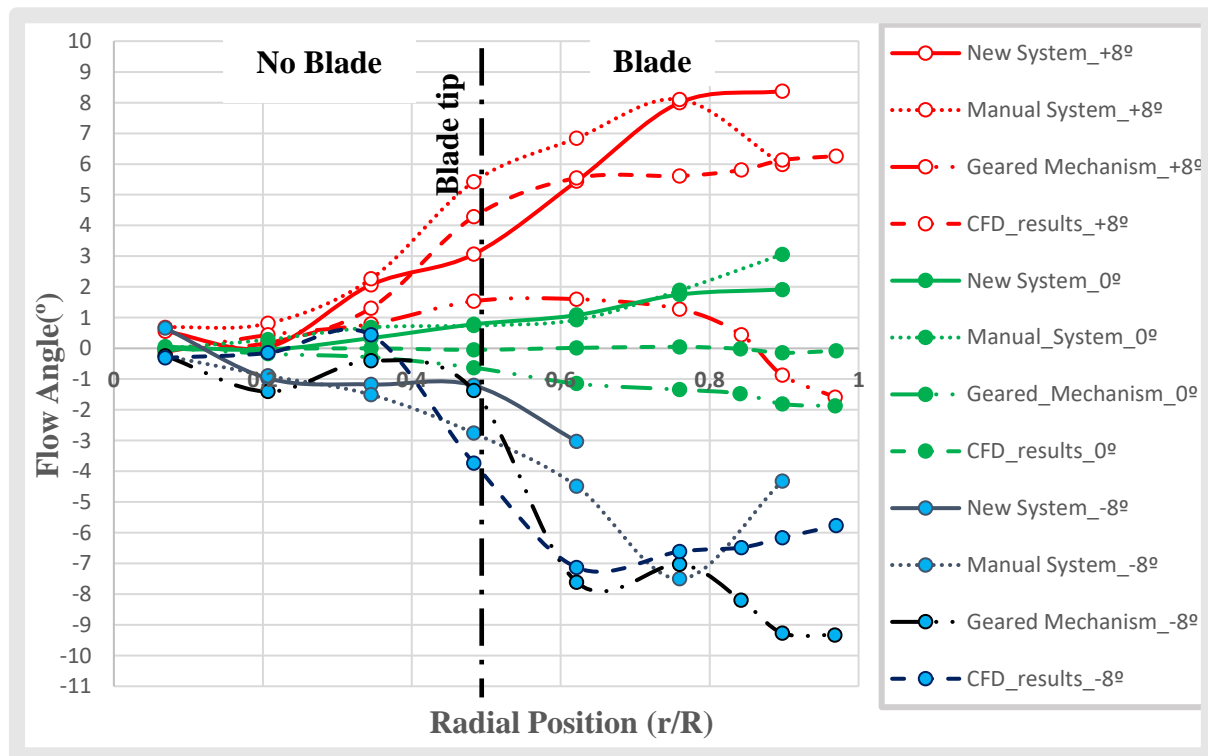


Figure 85: Deviation between tested mechanisms and CFD angle profile with error bars

Table 26: Mean absolute deviation between the tested mechanisms and CFD, function of the angle adjusted

<b>Blade Angle\ Absolute Mean Error of Mechanism</b>	<b>Automated Geared Mechanism</b>	<b>Manual Mechanism</b>	<b>Direct Drive Mechanism</b>
<b>-16°</b>	4,66	1,94	---
<b>-8°</b>	1,94	1,59	1,46
<b>0°</b>	1,34	1,69	1,40
<b>8°</b>	5,21	1,27	1,46
<b>16°</b>	2,12	2,27	---

Table 27: Mean absolute deviation between the tested mechanisms and CFD, function of the radial position

<b>Mean Absolute Deviation (°)</b>			
<b>Radial Position\ Mechanism</b>	<b>Geared</b>	<b>Manual</b>	<b>Direct Drive</b>
<b>0,069</b>	0,233	0,263	0,235
<b>0,207</b>	0,540	0,630	0,494
<b>0,345</b>	0,540	1,355	0,464
<b>0,483</b>	3,346	1,100	1,399
<b>0,622</b>	3,753	1,967	0,896
<b>0,760</b>	2,470	1,505	1,578
<b>0,898</b>	2,660	2,421	2,071

Due to time constraints and problems with the test bench, the mechanism could not be tested for -16° and +16° adjustment of the blade angle. For the same reason, the parameters calculated for the direct drive mechanism are based on a less data sample.

Based on the results obtained, it can be verified that the new mechanism allows the reduction of the deviation with CFD results regarding in the blade angle adjustment, compared to the adjustment made by the automated geared mechanism. For an adjustment of -8°, the error was reduced by 25% with the use of the direct-drive mechanism (table 26). For a setting of +8°, the deviation reduction is even more relevant when comparing the direct drive mechanism with the automated geared mechanism, reaching 72%.

In an overall analysis, it was possible to conclude that the new mechanism allowed an absolute mean error reduction in the IGVs adjustment of 30.75%, compared to the results obtained for the automated geared mechanism.

Regarding the comparison of the new design with the manual mechanism, the results are similar for the tested angles. The new mechanism can furthermore guarantee repeatability of results.

## 8. Conclusions

### 8.1. Achievements

While working on this project, several challenges in the field of problem analysis, precision design were faced and solved. The first significant step was to understand the influence of IGVs on compressor design and to realise the importance of the mechanism's precision in controlling IGVs and consequent generation of pre swirl.

As this was a work of redesigning a mechanism in order to rectify the drawbacks of previous mechanisms, it was essential to analyse and detect the sources of inaccuracy present in both the automated geared mechanism and the manual mechanism. This detected that the calibrator and the gear train backlash were responsible for more than 95% of the imprecision of the automatic system.

The results of the CFD simulations obtained by [1], were used as a way to assess the accuracy of the system. These results are fundamentally dependent on the position of the probe to IGVs. Significant discrepancies were observed between the CFD and the profile obtained using the geared mechanism, which was reduced with the use of the manual mechanism.

After analysing the mechanisms, it was concluded that the mechanisms involving gears require accurate and challenging assembly, being difficult to obtain repeatability and accuracy. A direct drive mechanism was then designed which, in addition to having an assembly that is unlikely to be subject to errors, also contributes to reducing the mechanical error of the mechanism by replacing mechanical components with electronics.

After the design and assembly of the mechanism, tests were carried out with the new mechanism that showed improved precision of blade angle adjustment. Therefore, it was concluded that the use of a direct drive mechanism could be implemented on a large scale in future applications involving precise control since it does not require a large investment compared to a mechanism that has more mechanical components.

It was concluded that the tests carried out are not the most adequate to assess the accuracy of the adjusted angle as it suffers post-processing and does not provide a direct result of the accuracy of the mechanism. However, a match can be established between the adjusted angle and the angle profiles obtained, which are very important for designing future compressors.

In order to design efficient compressors, it is necessary to fix the value of numerous variables. In this task, it is essential to note that the need to calibrate the system every time one wants to test a new mechanism is a source of error, even because it is dependent on the operator. In tasks where repeatability is desired, the operator must have a minimum influence on obtaining results. In this sense, the work performed fits in the perspective of a small step taken towards optimising in the future the design of small scale centrifugal compressors with the use of IGVs.

## 8.2. Future work

Future work on this topic should include several fields of research. Regarding the design of the control mechanism, some features can be improved in order to make the mechanism more accurate in test cycles.

Regarding the automated part of the mechanism, a display screen and push buttons were ordered. New code has been developed (annex [A.4](#)) in order to adjust the blades without using the computer. It is therefore necessary to set up the buttons on the Arduino. The manufacture of an electronic box by additive manufacturing process (3D printing) that can group and protect the cables present in the mechanism is also planned.

Although the current code (annex [A.4](#)) already allows relatively precise control of the blade angle, it can be improved. Because the code uses an existing library to control the blades, some parameters selected in control are likely to be optimized (speed, step angle). Therefore, the development of a specific code for the stepper motors that are being used would allow better use of their capabilities and would lead to higher accuracy of the system.

Regarding the manual part of the design, four of the six shafts are already working correctly and are perfectly aligned with the holes on which they have to rotate (figure [86](#)). The remaining two shafts need to be adjusted to the diameter of the section (drawing A.2.1 – annex [A.2](#)) that interacts with the hole in the inlet pipe in order to allow a smoother and more precise movement, which requires less torque.

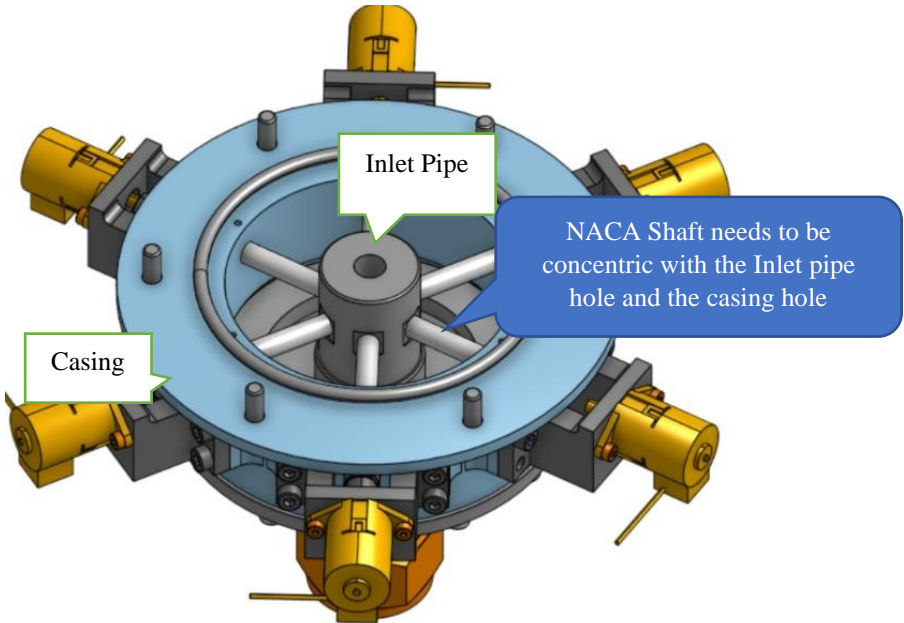


Figure 86: Problem prevents correct shaft rotation when adjusting the blade angle

**Fix the relative position of the 3 components**

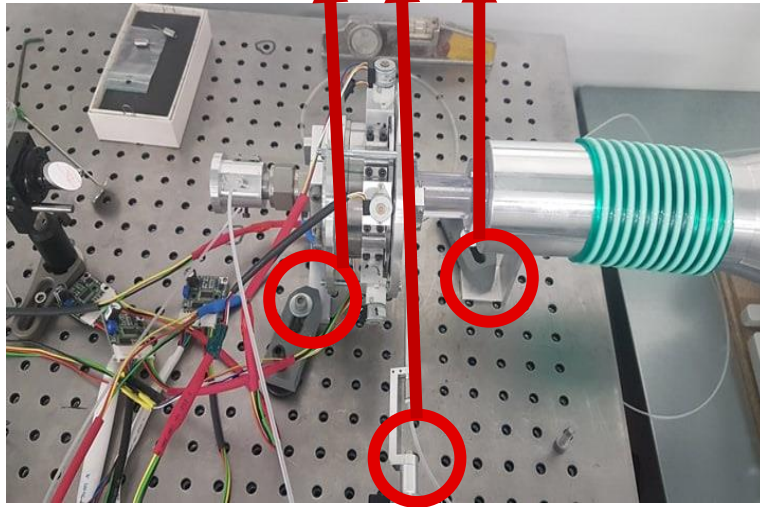


Figure 87: Relative position of the 3 components of the experimental design susceptible to large deviations

Finally, in order to be able to design future centrifugal compressors using the new mechanism, the experimental configuration needs to be improved so that it can be achieved repeatably every time the mechanism is changed. For this, the calibration of the entire system needs to be rethought. One suggestion would be to fix the 3 points marked in figure [87](#) by creating a specific table. In this way, the relative position of the 3 points would remain unchanged, and the performance of the test cycles would be less time consuming and more efficient.



## 8. References

- [1] FS Elliot [Online], Accessed at 19-05-2019. Available: <https://www.fs-elliott.com/inlet-guide-vane-and-inlet-butterfly-valves?locale=en>.
- [2] A. Aeschbacher, "Numerical and experimental performance investigations on a reduced scale centrifugal compressor by using variable inlet guide vanes", Unpublished report LAMD, EPFL, 2017.
- [3] Lin P. and Avelar V., "The different types of cooling compressors", [Online], Accessed at 12-04-2019 Available: [http://www.apc.com/salestools/VAVR-AE7T7G/VAVRAE7T7G\\_R0\\_EN.pdf](http://www.apc.com/salestools/VAVR-AE7T7G/VAVRAE7T7G_R0_EN.pdf).
- [4] Reagon R., Suhail R., Shashank N., Nag G. and Tej, V., "Study of Inlet Guide Vanes for Centrifugal Compressor in Miniature Gas-Turbines," International Journal of Scientific Research in Computer Science, Engineering and Information Technology, India, 2018.
- [5] Heinrich M., "Generic Optimization of Turbomachinery Components using a volute of a Transonic Centrifugal Compressor as a Case Study," T.U.Freiberg, 2016.
- [6] Rodgers C. "Impeller Stalling as Influenced by Diffusion Limitations", ASME. J. Fluids Eng. 1977;99(1):84-93. doi:10.1115/1.3448569.
- [7] Toussant M. and Podevin P., "Guide-Vanes upstream the impeller of centrifugal compressor", Conservatoire National des arts et Métiers, 2005.
- [8] Huang L., Liu Y. and Chen H., "Inlet Swirl on Turbocharger Compressor Performance" National Laboratory of Engine Turbocharging Technology, Tianjin, China, 2015.
- [9] Pillet M., "Design of a Variable Inlet Guide Vane mechanism for a small scale turbocompressor," Unpublished report LAMD, 2017.
- [10] Rusovici R., Feys J., Sepri P. AND Subramanian C. , "Smart Actuation of Inlet Guide Vanes for Small Turbine Engine," International Conference on Adaptive Structures and Technologies, 2014.
- [11] Kassin J., "Variable Inlet Guide Vanes Boost Centrifugal Air Compressor Efficiency", Compressed Air and Gas Institute. [Online]. Available: <https://www.airbestpractices.com/technology/air-compressors/variable-inlet-guide-vanes-boost-centrifugal-air-compressor-efficiency>
- [12] "Piller Blowers & Compressors" [Online], Accessed at 29-03-2019. Available: <https://www.piller.de/products-applications/blower-design/>
- [13] Sconfiatti R. A., "Geared Inlet Guide Vane for a centrifugal compressor. Patent US 8079808 B2," December 2011
- [14] Sishtla V., "Inlet Guide Vane Mechanism". United States Patente US2015/0377250 A1, 2015.
- [15] Sahin C., "Experimental evaluation of igv performance," Unpublished report at LAMD, EPFL, 2017.
- [16] "Farnell" [Online], Accessed at 05-05-2019. Available: <https://www.farnell.com/datasheets/1526460.pdf>
- [17] Nanotec. Product Catalog- Plug&Drive, pp. 14-36.
- [18] "Oriental Motor" [Online], Accessed at 29-04-2019. Available: <https://www.orientalmotor.com/stepper-motors/technology/speed-torque-curves-for-stepper-motors.html>.

- [19] “Backlash Instrumentation” [Online], Accessed at 18-03-2019. Available: <https://www.quora.com/What-is-backlash-in-instrumentation>.
- [20] K. S. Gears, “Gear Backlash” [Online], Accessed at 02-04-2019. Available: [https://khkgears.net/new/gear\\_knowledge/gear\\_technical\\_reference/gear\\_backlash.html](https://khkgears.net/new/gear_knowledge/gear_technical_reference/gear_backlash.html).
- [21] Wasilewski R. F., “How to install bevel gears for peak performance,” Arrow Gear Co.1994
- [22] “Nozag- Transmission” [Online], Accessed at 22-03-2019. Available: <https://www.nozag.ch/standard-program/Bevel+gears>.
- [23] KISSsoft, “KISSsysTutorials” [Online], Accessed at 20-03-2019. Available: <https://www.kisssoft.ch/english/downloads/KISSsysTutorials.php>.
- [24] “Backlash,” [Online]. Available: [https://www.kggear.co.jp/en/wp-content/themes/bizvektor-global-edition/pdf/TechnicalData\\_KGSTOCKGEARS.pdf](https://www.kggear.co.jp/en/wp-content/themes/bizvektor-global-edition/pdf/TechnicalData_KGSTOCKGEARS.pdf).
- [25] Schreiber C., “Alignment tool assessment. Internal report at LAMD,” LAMD, 2019.
- [26] "Global Fastener"[Online], Accessed at 14-05-2019. Available: [http://www.globalfastener.com/standards/detail\\_2660.html](http://www.globalfastener.com/standards/detail_2660.html)
- [27] Bhatia A., “Basic Fundamentals of Gear Drives”, 2014.
- [28] “Hybrid Linear Actuators- Nanotec” [Online], Accessed at 27-04-2019. Available: <https://en.nanotec.com/products/2271-hybrid-linear-actuators/>.
- [29] R. Schmid S., J. Hamrock B. and O. Jacobson B. , " Fundamentals of Machine Elements", Third Edition.
- [30] "Catiadoc" [Online], Accessed at 26-05-2019 Available: [http://catiadoc.free.fr/online/cfyuganalysis\\_C2/cfyuganalysis3dmeshpart.htm](http://catiadoc.free.fr/online/cfyuganalysis_C2/cfyuganalysis3dmeshpart.htm)
- [31] “ASM Aerospace Specification Metals Inc.” [Online], Accessed at 07-06-2019. Available: <http://asm.matweb.com/search/SpecificMaterial.asp?bassnum=MQ303H>.
- [32] Budynas R.G. and Nisbett J.K. , "Shigley's Mechanical Engineering Design". Ninth Edition
- [33] “Elastotech” [Online], Accessed at 05-06-2019. Available: <http://www.elastotechgaskets.com/static-seal-dynamic-seal.php>.
- [34] Bowman D., “Sealing A/C systems,” in *AUTOMOTIVE ENGINEERING INTERNATIONAL*, 2012.
- [35] Angst+Pfister, O-Ring Normatec. [Online], Accessed at 08-06-2019. Available: [http://catalog.minetti.com/Portals/0/pdf/AngstPfister/APSoseal@-Tecnologia\\_delle\\_tenute/NORMATEC](http://catalog.minetti.com/Portals/0/pdf/AngstPfister/APSoseal@-Tecnologia_delle_tenute/NORMATEC)
- [36] A. Direct, “Stepping Systems User Manual,” 2019, p. Appendix C.
- [37] “The Engineering ToolBox” [Online], Accessed at 05-06-2019. Available: [https://www.engineeringtoolbox.com/friction-coefficients-d\\_778.html](https://www.engineeringtoolbox.com/friction-coefficients-d_778.html).
- [38] McRoberts M., Arduino Starter Kit Manual, 2009.
- [39] SILVA A., T. R. Carlos, DIAS J. and SOUSA L., *Desenho Técnico Moderno*, Lisboa: Lidel- Edições Técnicas, 2004.

## A. Annex

### A.1. KISSsoft Procedure Analysis

1° Step: Compute all the information regarding gear train which is not present in the manufacturer's datasheet [24]

Table 28: Gear train dimensions computed in the automated mechanism

Parameter	Gear 1 (Pinion)	Gear 2 (Wheel)
$\Sigma$ - Shaft Angle (°)	90	
$\alpha''$ - Pressure Angle (°)	20	
M - Module (mm)	1	
Z - Number ofTeeth	15	45
D - Pitch Diameter (mm)	15	45
Da - Crown Diameter (mm)	16,9	45,6
Df - Root Diameter (mm)	12,625	44,25
Db - Base Diameter (mm)	14,25	13,5
Z' - Equivalent Number ofTeeth	15,7895	150
D' - Equivalent Pitch Diameter	15,7895	150
Da' - Equivalent Crown Diameter	17,7895	152
Df' - Equivalent Root Diameter	13,2895	147,5
Db' - Equivalent Base Diameter	15	45
$\delta$ (Primitive Angles) (°)	18,1949	72,5424
Pang (Angular Pitch) (°)	24	8
g - Geratriz	24,02	
h-Tooth Height (mm)	2,25	
ha – addendum (mm)	1	
hf – dedendum (mm)	1,25	
$\epsilon_a$ - addendum angle (°)	2,3840	
$\epsilon_f$ - dedendum angle (°)	2,9791	
j - root clearance (mm)	0,25	
P - Circular Pitch (mm)	3,1416	
S - tooth thickness (mm)	1,5708	
E - tooth range (mm)	1,5708	
i - gear ratio	3	

Basic data   Manufacturing   Reference profile   Tolerances   Modifications   Rating   Factors

---

Strength

Calculation method: Bevel gear ISO 10300:2001, Method B      Reference gear: Gear 1

Calculation method scuffing: according to calculation method      Power: P 0.0250 kW

Calculation method tooth flank fracture: No calculation      Torque: T<sub>1</sub> 0.1500 Nm

Driving gear: Gear 1

Working flank gear 1: right flank

---

Information

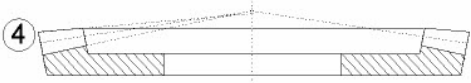


Figure 88: Data entry regarding the power of the system

## 2° Step: Prepare the simulation (Introducing the values of the gear train)

**Note:** Since the program does not have the exact model of the gears of the system used in its database, the method of entering all collected and possible data into the program was adopted in order for the program to calculate the missing parameters. This way it is expected that the final results can provide a general idea of the real backlash of the model.

The screenshot shows the 'Basic data' window in KISSsoft, with the 'Reference profile' tab selected. The 'Configuration' section shows the gear type as 'Standard, fig 4 (Pitch and Root apex in one point)'. The 'Geometry' section is divided into two columns for Gear 1 and Gear 2. The parameters and their values are as follows:

Parameter	Value	Unit
Mean normal module ( $m_{mn}$ )	1.0000	mm
Outer pitch diameter gear 2 ( $d_{a2}$ )	45.6000	mm
Pressure angle at normal section ( $\alpha_n$ )	20.0000	°
Gear 1 Profile	Zerol, right-hand (0°, with spiral teeth)	
Mean spiral angle gear 2 ( $\beta_{m2}$ )	0.0000	°
Addendum angle gear 2 ( $\theta_{a2}$ )	3.0170	°
Dedendum angle gear 2 ( $\theta_{r2}$ )	3.0170	°
Number of teeth ( $z$ )	15 (Gear 1), 45 (Gear 2)	
Facewidth ( $b$ )	5.0000	mm
Profile shift coefficient ( $x'_{mn}$ )	0.0000	
Tooth thickness modification factor ( $x'_{gmn}$ )	0.0000	
Quality (ISO 17485) ( $Q$ )	6	
Shaft angle ( $\Sigma$ )	90.0000	°

Figure 89: Basic data introduction about the gear train

It should be noted that in this type of system, the backlash of the model will depend heavily on how the system is mounted and on possible errors that occur in this mounting. After entering the basic data of the gear train system it is necessary to enter the power supplied to the system, in order to be able, after having chosen the calculation method, to obtain an analysis of the forces in the gears, as shown in figure 89. With these results, the number of cycles that the gear train could run without wear affecting the system can be calculated later. However, as it is not part of the main objective of this project, the same was not done.

After entering the system-related data in the program, the operator must go to Rough Sizing as shown in figure 90, check that the parameters are not in conflict with the place, and then go through the Fine Sizing step, where the various possible solutions are calculated (figure 91).

The screenshot shows the 'Rough sizing' dialog box in KISSsoft. The parameters and their values are as follows:

Parameter	Value	Unit	Checked
Transmission ratio ( $u$ )	3.0000		
Ratio facewidth to mean normal module ( $b/m_{mn}$ )	5.0000		
Ratio of outer cone distance to facewidth ( $R_a/b$ )	3.5000		
Mean spiral angle gear 2 ( $\beta_{m2}$ )	20.0000	°	
Mean normal module ( $m_{mn}$ )	1	mm	<input checked="" type="checkbox"/>
Number of teeth, gear 1 ( $z_1$ )	15.0000		<input checked="" type="checkbox"/>
Facewidth gear 2 ( $b_2$ )	5.0000	mm	<input checked="" type="checkbox"/>
Outer pitch diameter gear 2 ( $d_{a2}$ )	45.6000	mm	<input checked="" type="checkbox"/>

Buttons: Accept, Calculate, Cancel

Figure 90: Rough Sizing window on KISSsoft

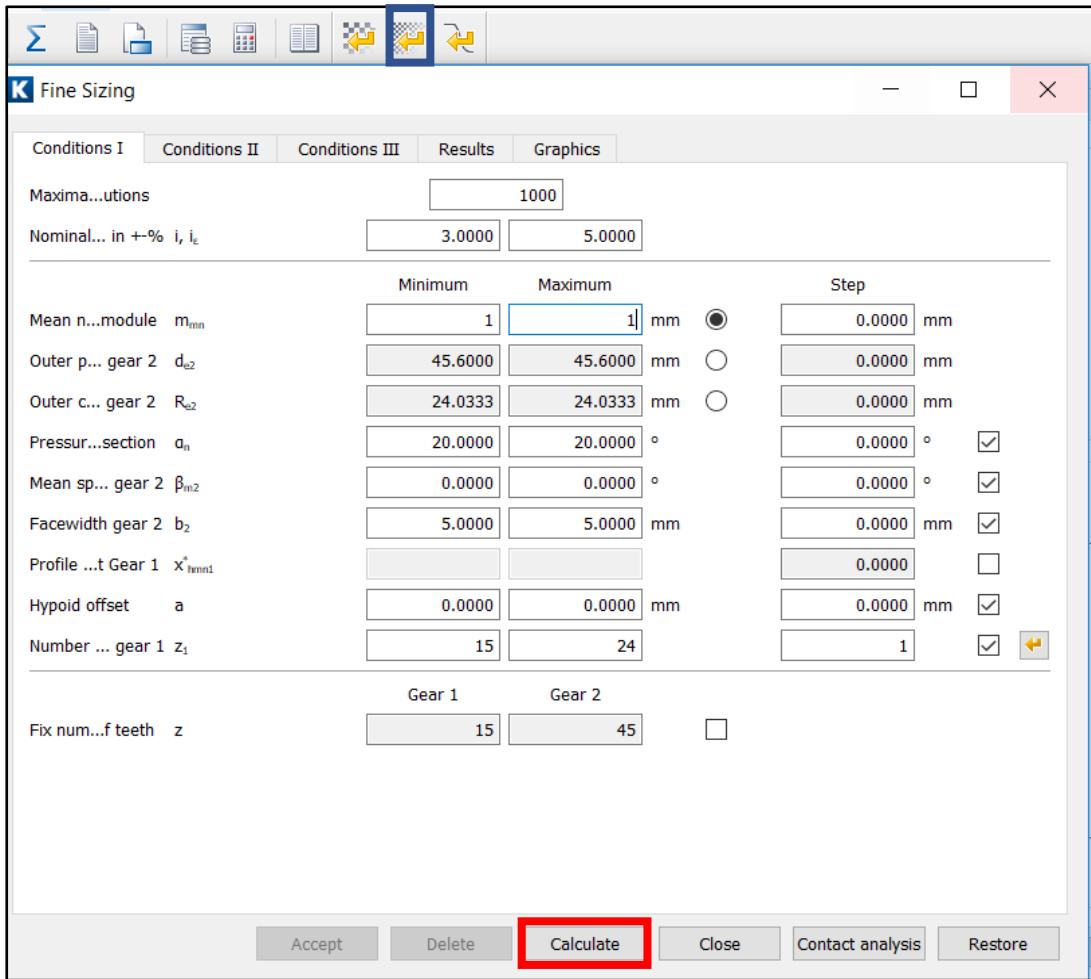


Figure 91: Fine Sizing window on KISSsoft

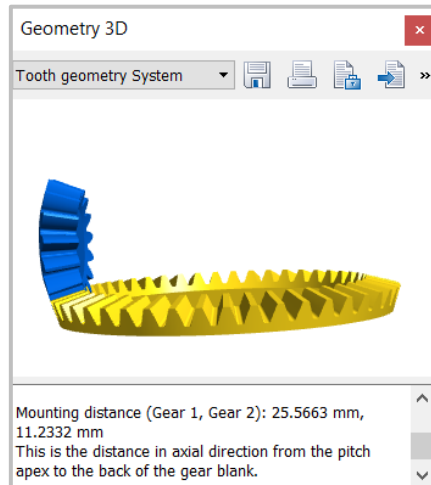
After the calculations made by the program, it is possible to obtain multiple solutions that meet the data of the gear train, and the user can choose one of the various solutions generated and that are more similar to the original version of the gear train (figure 92).

Nr.	av [mm]	b <sub>1</sub> [mm]	b <sub>2</sub> [mm]	m <sub>min</sub> [mm]	α <sub>n</sub> [°]	β <sub>m2</sub> [°]	z <sub>1</sub>	z <sub>2</sub>	z <sub>3</sub>
0	0.000	5.000	5.000	0.908	20.000	0.000	15	45	
1	0.000	5.000	5.000	1.000	20.000	0.000	15	43	
2	0.000	5.000	5.000	1.000	20.000	0.000	15	44	
3	0.000	5.000	5.000	1.000	20.000	0.000	15	45	
4	0.000	5.000	5.000	1.000	20.000	0.000	15	46	
5	0.000	5.000	5.000	1.000	20.000	0.000	15	47	
6	0.000	5.000	5.000	1.000	20.000	0.000	16	46	
7	0.000	5.000	5.000	1.000	20.000	0.000	16	47	
8	0.000	5.000	5.000	1.000	20.000	0.000	16	48	
9	0.000	5.000	5.000	1.000	20.000	0.000	16	49	
10	0.000	5.000	5.000	1.000	20.000	0.000	16	50	
11	0.000	5.000	5.000	1.000	20.000	0.000	17	49	
12	0.000	5.000	5.000	1.000	20.000	0.000	17	50	
13	0.000	5.000	5.000	1.000	20.000	0.000	17	51	
14	0.000	5.000	5.000	1.000	20.000	0.000	17	52	
15	0.000	5.000	5.000	1.000	20.000	0.000	17	53	
16	0.000	5.000	5.000	1.000	20.000	0.000	18	52	
17	0.000	5.000	5.000	1.000	20.000	0.000	18	53	
18	0.000	5.000	5.000	1.000	20.000	0.000	18	54	
19	0.000	5.000	5.000	1.000	20.000	0.000	18	55	
20	0.000	5.000	5.000	1.000	20.000	0.000	18	56	
21	0.000	5.000	5.000	1.000	20.000	0.000	19	55	
22	0.000	5.000	5.000	1.000	20.000	0.000	19	56	
23	0.000	5.000	5.000	1.000	20.000	0.000	19	57	
24	0.000	5.000	5.000	1.000	20.000	0.000	19	58	
25	0.000	5.000	5.000	1.000	20.000	0.000	19	59	
26	0.000	5.000	5.000	1.000	20.000	0.000	20	57	

Figure 92: Solutions computed by KISSsoft for gear train

### Step 3: Generate the results of the analysis

A Z70 file is generated, which gives the operator an extensive analysis report of the chosen system. Among the results provided by the program, it is possible to obtain the expected values for the system backlash. The corresponding mounting distances should also be obtained.



Axial displacement for the predefined backlash:			
Required backlash due to axial displacement (mm)	[Delj]	0.020	
Additional backlash per gear (mm)	[Delj1,2]	0.002	0.018
Required axial displacement per gear (mm)	[alf1,2]	0.009	0.026
Backlash for the predefined axial displacement:			
Change of assembly distance (mm)	[alf1,2]	0.100	0.100
Additional backlash per gear (mm)	[Delj1,2]	0.023	0.069

Figure 93: Intended results from KISSsoft analysis

## A.2. Technical Drawings

In this annex, are presented the drawings sent to the workshop to manufacture the parts. They have been realized by considering the manufacturing process and the clearances necessary for the proper functioning of the mechanism. For a better understanding by the reader, little explanations are also given about why we should use the geometric tolerance used in each drawings [39].

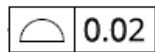
### A.2.1.- 0012\_Naca\_Shaft

The part that contains the machined Naca profile 0012 and that interacts with three parts of the system: coupling, casing and inlet pipe. Due to this fact needs to be very precise. In this drawing, it is essential to note the presence of dimensions necessary to be inspected by the operator in order to check the feasibility of the assembly between the 0012\_Naca Shaft and the parts mentioned above.

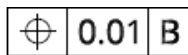
**Datum References:** A → Center axis of the vanned shaft

B → Surface that sits on the inlet pipe

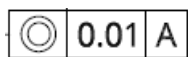
### Geometric Tolerances used



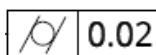
**Profile of a surface:** the Naca surface must be contained between two surfaces tangential to spheres of diameter 0,02 mm whose centers are located on the surface with the geometrically perfect shape.



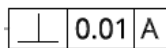
**Position (in our case of a line and not of a point):** the line shall be contained within a tolerance zone defined by two parallel lines spaced apart from each other by 0.01 mm and symmetrically located relative to the theoretically exact position. Plan B serves to indicate the direction of the tolerance lines.



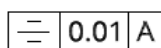
**Concentricity:** The axis of the cylinders entering the inlet pipe hole and in the coupling part must be within a cylindrical tolerance range of 0.01 mm diameter, coaxial with the vanned shaft center axis.



**Cylindricity:** the outer surface of the cylinder shall be contained between two coaxial cylinders which are 0,02 mm apart.



**Perpendicularity:** the line that defines the surface that will sits against the inlet pipe shall be contained between two parallel lines, which are 0.01mm apart. These 2 lines are perpendicular to the center axis of the vanned Shaft.



**Symmetry:** the axis of the hole into which the calibrator will enter must be contained between two parallel lines 0.01 mm apart and positioned symmetrically in relation to the A axis.

All these tolerances are important so that the axes are oriented perpendicularly with precision to the direction of flow.

## A.2.2.- Casing\_6s

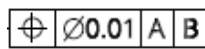
As happens with 0012\_Naca\_Shaft, this drawing also has dimensions that must be adjusted according to the parts that connect with the casing. Therefore, its manufacturing must not be independent of the other parts and may have to be adjusted slightly after manufacturing at the CNC. This part will also be responsible for allocating the O-rings that will seal the entire module, so it is also crucial that the roughness of the connection surfaces to other parts is limited.

**Datum References:** A → Center axis of the casing

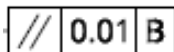
B → Top surface of the casing that links to the inlet pipe

C → Axis of lateral holes where the blades shaft passes

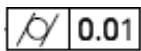
### Geometric Tolerances used



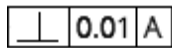
**Position:** the axis of each hole must be located within the circular tolerance zone of 0.01 mm diameter, where the axes of the tolerance zone are positioned in relation to the distance they are from planes A and B.



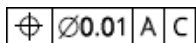
**Parallelism:** the surface of the casing that sits on the volute must be contained between two parallel surfaces, which are 0.01 mm apart. These two surfaces are parallel to the surface that serves as a reference (B).



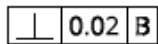
**Cylindricity:** the inner surface of the cylinder must be contained between two coaxial cylinders which are 0,01 mm apart.



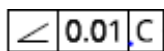
**Perpendicularity:** the line delimiting the casing surface that contacts the inlet pipe line shall be contained between two parallel lines, which are 0,01 m apart. These 2 lines are perpendicular to the axis A that serves as a reference.



**Position:** the drilling axis of goupille must be located within the circular tolerance zone of 0.01 mm diameter, where the axes of the tolerance zone are positioned in relation to the distance they are from planes A and C.



**Perpendicularity:** the line delimiting the casing's contact surface with the fixation\_moteur shall be contained between two parallel lines which are 0.02 mm apart. These two lines are perpendicular to plane B.



**Angularity:** The axes of the 6 holes that allocate the Naca shafts, must be contained between 2 parallel lines between themselves and away from 0.01mm, relative to the referential C.

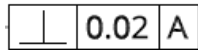


### A.2.3.- Fixation\_Moteur

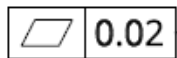
Part used to fix the stepper motor to the casing. In this case, the centre bore needs to be very precise and with low roughness so as not to cause possible lateral deviations in the motor coupling that lead to the defective shaft rotation movement.

**Datum References:** A → External surface of Fixation\_Moteur, where the stepper motor will settle

#### Geometric Tolerances used



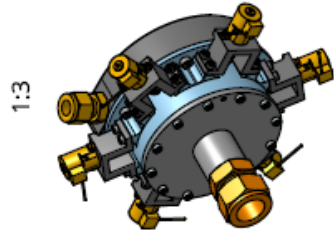
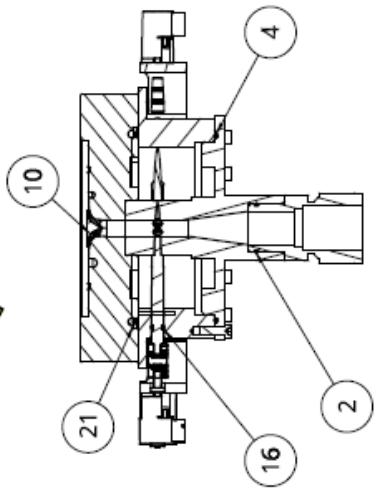
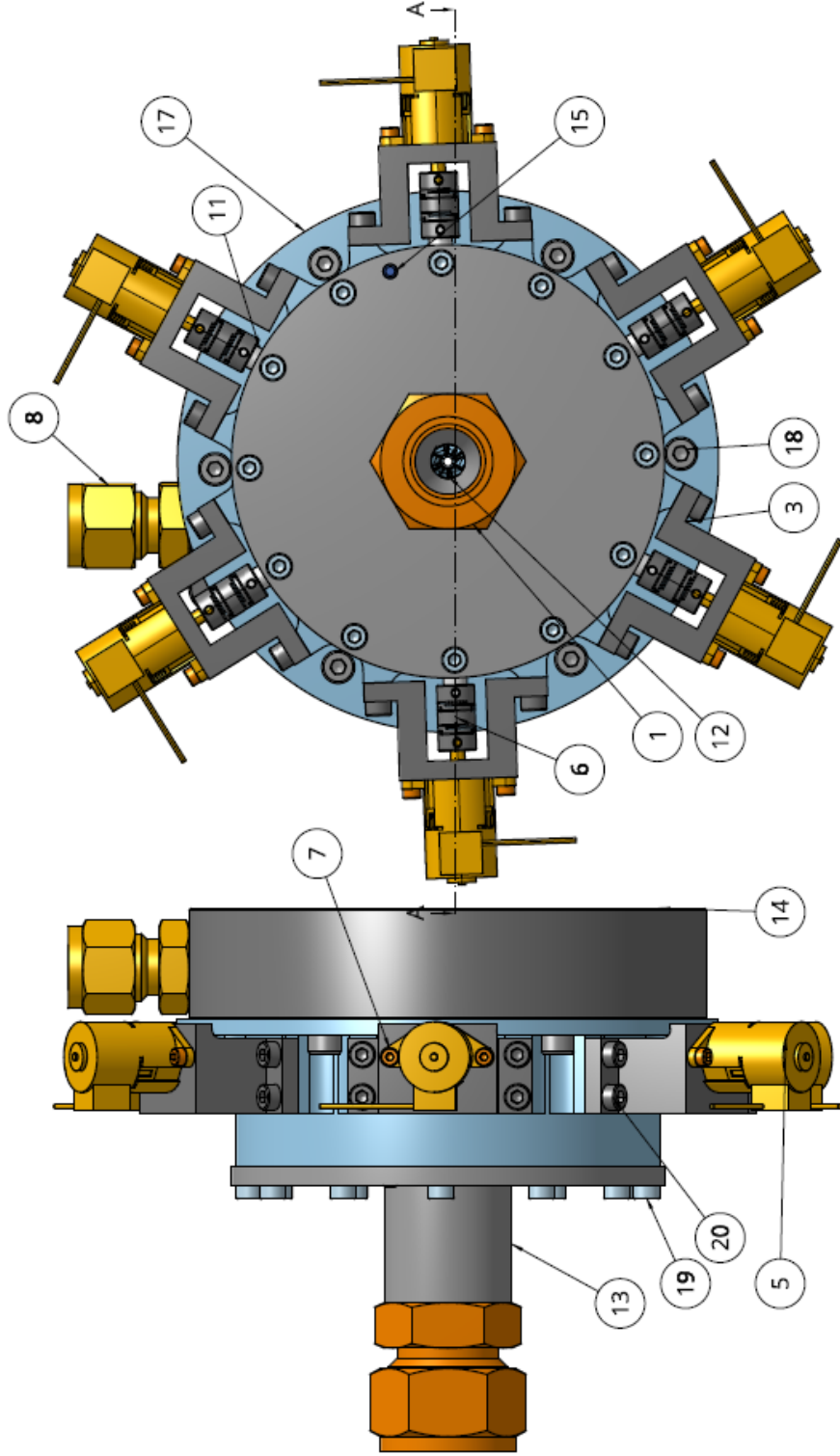
**Perpendicularity:** The axis of the centre hole must be contained between two parallel lines, which are 0.02 m apart. These two lines are perpendicular to the axis delimiting the outer surface of the workpiece.



**Flatness:** The external surface of the part shall be contained between two parallel planes which are 0.02 mm apart.

### A.2.4.- Volute

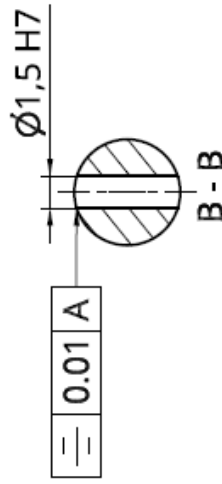
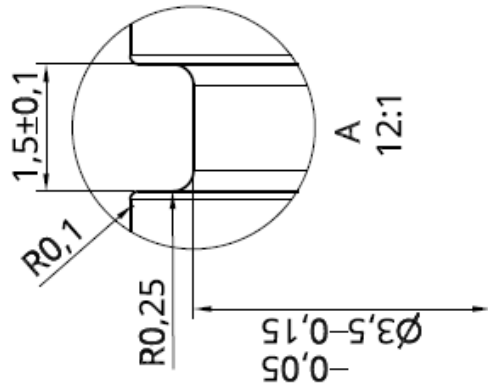
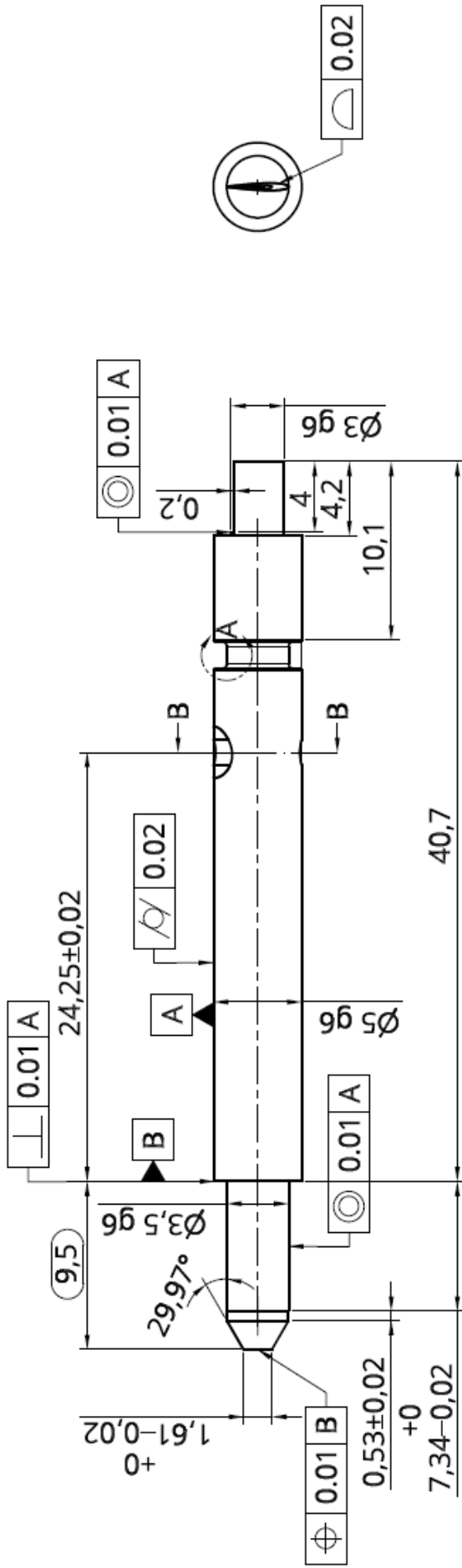
Due to the costs, volute is a part that was reused from the old Pillet design [2]. There was only the need to add two holes to the previous part in order to allow the connection with the casing that was changed compared to the previous design.



Item No.	Quantity	Part number	Description
1	1	SS_1210_1_8W	
2	1	O-ring_18_5_1	
3	6	Fixation Moteur	
4	1	O-ring_74_1_5_1	
5	6	Stepper Motor	
6	6	Coupling	
7	12	M2 x 6mm	
8	1	SS_600_1_6W	
9	1	O-ring_14_5_1	
10	1	Impeller	
11	6	0012 Naca Shaft	
12	6	Profil 0012	
13	1	Inlet Pipe	
14	1	Volute	
15	1	Goupille	
16	6	O-ring_3_5_1	
17	1	Casing	
18	6	M4 x 12 mm	
19	12	M3 x 10 mm	
20	24	M3x 8mm	
21	1	O-ring 74_3_1	

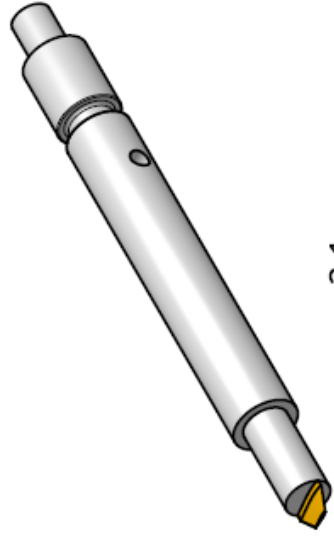
VIGV-Assembly				Description	
Ref.	Q'ty	Description	Unit	Issue	Version
19-LAMD-DR-010	1	19-LAMD-DR-010	UNIT	001	000
Author	19-01-2018	Page	1/1	Draw Date	..
Appr. by	AWD	Drawn		Draw Date	..
Per. app.	19-01-2018	Control		Drawn	..
				Scale	1:1
				Material	

19-LAMD-DR-010  
STP-IGN-LAMD  
VIGV-Assembly



Tolérances générales ISO 2768 - fH  
 Chanfreins: 0.3x 45° MAX  
 Rayons: R0.2 MAX

Profil NACA 0012



2:1

Rep.	Quantité	Désignation	Matériau	Acier Inox 1.4305	Dimensions
6		0012_Naca_Shaft			Valeur g) 3:1
Rep.	Quantité	Désignation	Matériau	Acier Inox 1.4305	Dimensions
6		0012_Naca_Shaft			Valeur g) 3:1
Rep.	Quantité	Désignation	Matériau	Acier Inox 1.4305	Dimensions
6		0012_Naca_Shaft			Valeur g) 3:1
Rep.	Quantité	Désignation	Matériau	Acier Inox 1.4305	Dimensions
6		0012_Naca_Shaft			Valeur g) 3:1

19-LAMD-DR-010

0012\_Naca\_Shaft

STI-IGM-LAMD

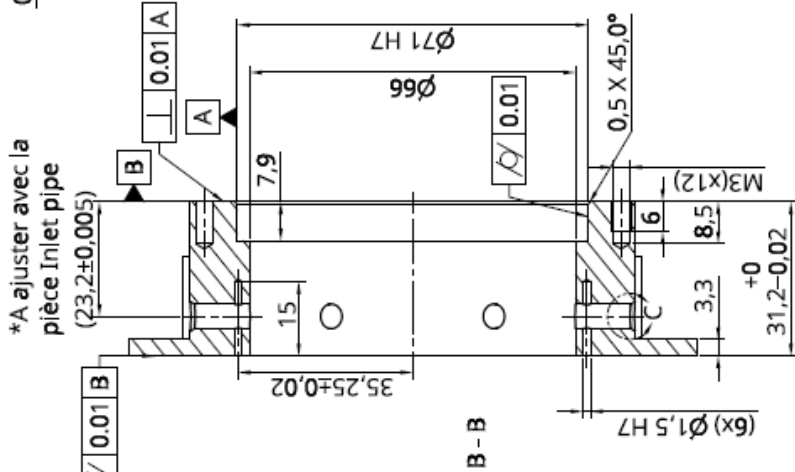
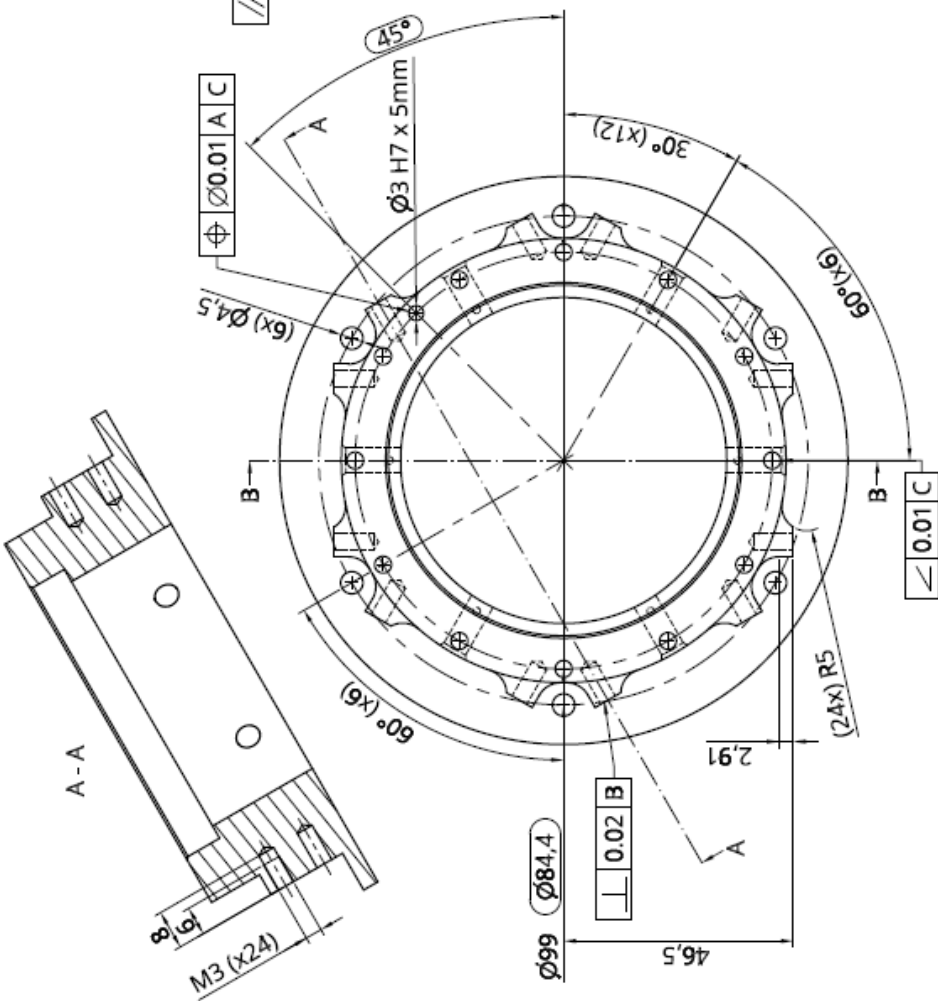
0012\_Naca\_Shaft

0012\_Naca\_Shaft

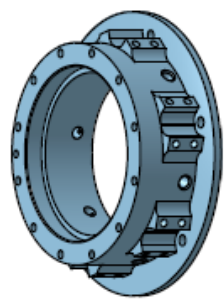
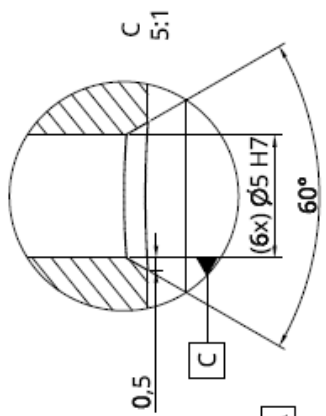
0012\_Naca\_Shaft

0012\_Naca\_Shaft

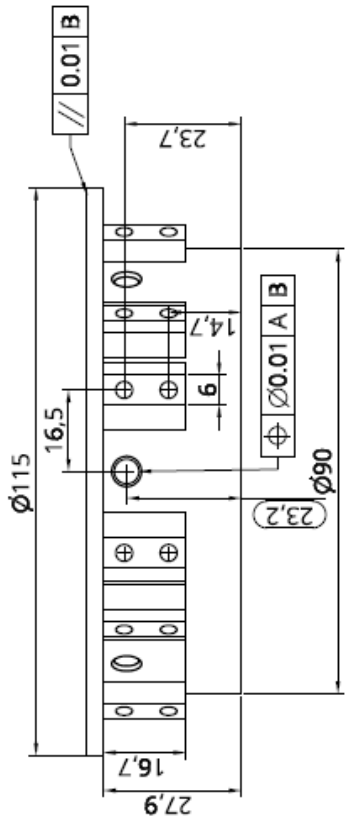
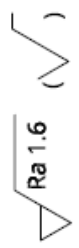
0012\_Naca\_Shaft



\*A ajuster avec la  
pièce Inlet pipe  
(23,2±0,005)



1:2



Tolerance: 99 Max: ISO 2768 - FH  
Revised: RD.2 MAX

Part	Quantity	Case No.	Case Title	Revision	Date
1	1		Casing	1	

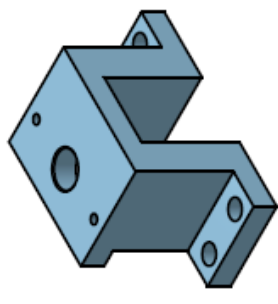
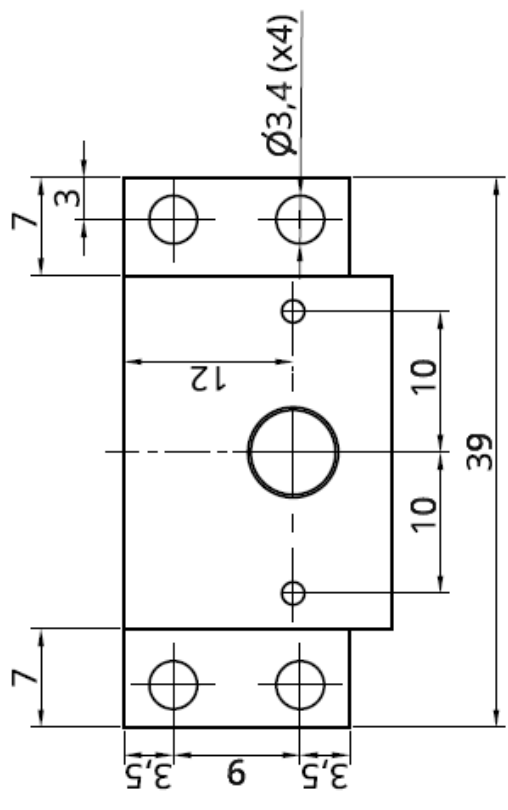
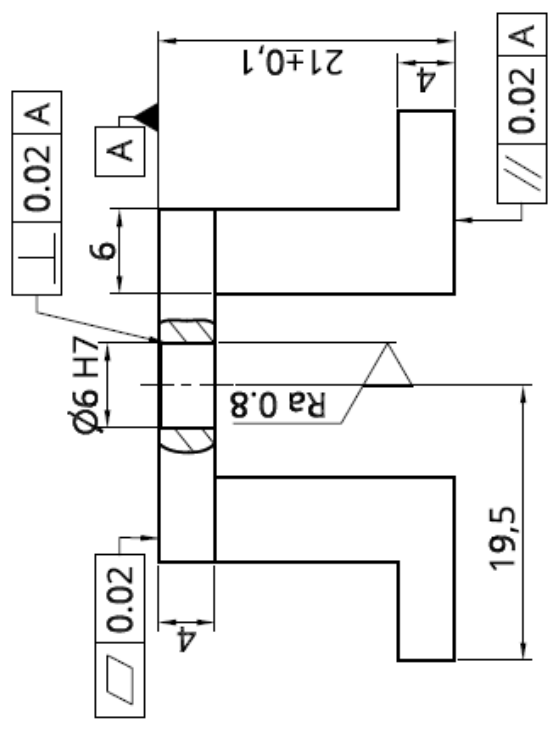
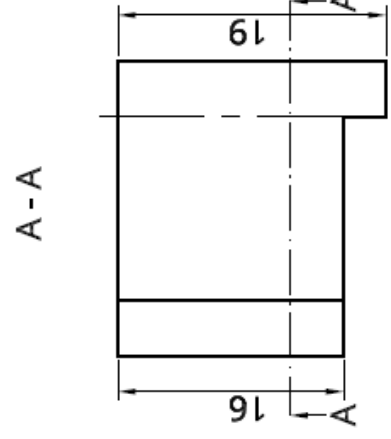
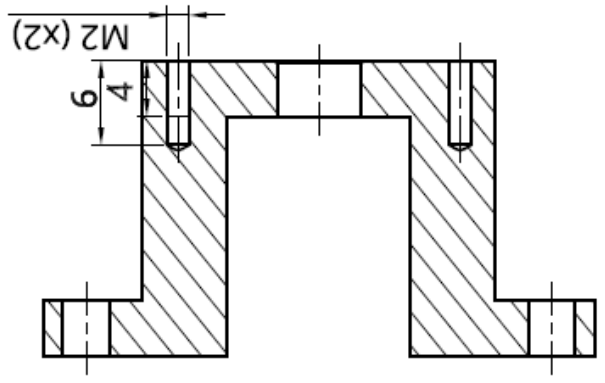
  

Author	Checked	Approved	Drawn	Scale
				1:1

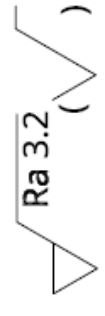
19-LAND-038-10

Casing\_6s



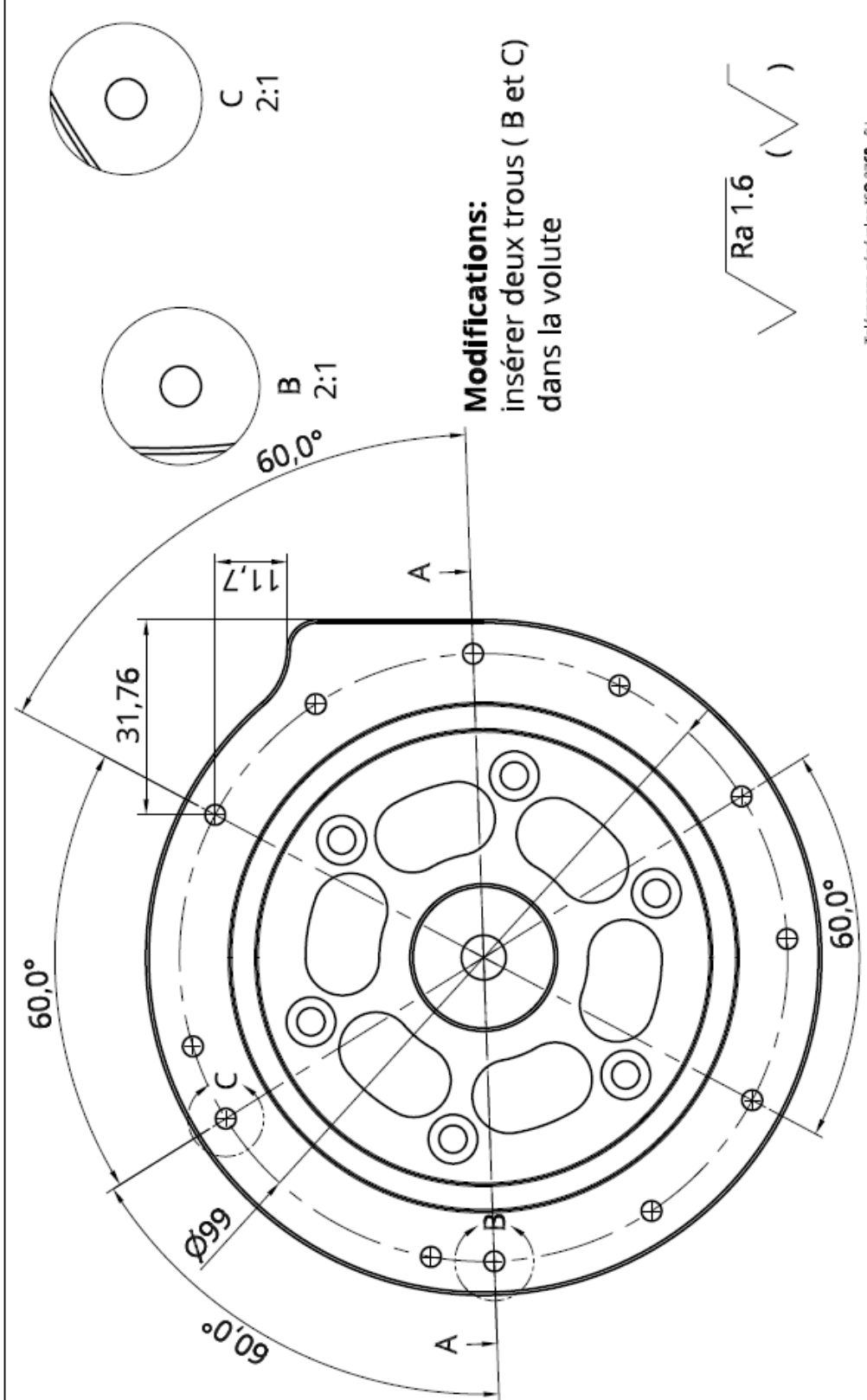


1:1



Tolérances générales: ISO 2768 - FH  
 Chanfreins: 0,3x45° MAX  
 Rayons: R0,2 MAX

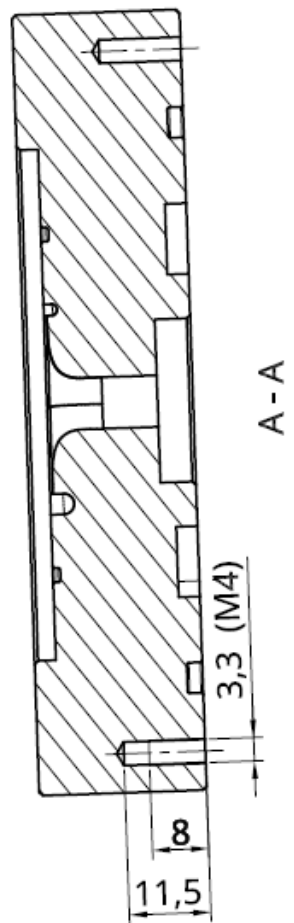
6		Fixation Moteur		Aluminium		Dimensions	
Rep.	Quantité	Dénomination	Matière	Masse (g)	—		
Nom Resp.	David Ribeiro	Nom					
Telephone	+41 21 88 5486	Projet.	VIGV				
Laboratoire	LAMD	Destinée	David Ribeiro				
Prof. resp.	Jürg Schaffmann	Contrôle	2019/08/17				
			<b>Fixation_Moteur</b>				
19-LAMD-DR-010			ST-IGM-LAMD				
			Numéro de pièce				
			Echelle 2:1				





**Modifications:**  
insérer deux trous ( B et C )  
dans la volute

$\sqrt{Ra\ 1.6}$  (  $\nabla$  )

Tolérances générales ISO 2768 - fh  
Chamfreins: 0.3x 45° MAX  
Rayons: R0.2 MAX



A - A

Rep.	Quantité	Volume_VIGV	Aluminium 7075-T6	Dimensions
1				
Rep.	Quantité	Désignation	Matériau	Version
1	1	Volute	Aluminium 7075-T6	1.1
Nom Resp.	David Ribeiro	Nom		
Téléphone	+31 21 69 54 09	Projet	WGV	
Laboratoire	LAMD	Dessiné	David Ribeiro	
Prof. resp.	Jürg Schiffmann	Contrôle	...	Echelle 1:1
				Numero de dep.
				
<p>19-LAMD-DR-010</p>				
<p>Volute</p>				

### A.3. Technical data of the motor, controller and arduino

#### SMC11

Compact Microstep Controller



#### TECHNICAL DATA

Operating voltage	12-35 VDC
Max phase current	1.0 A (1/1 step (1.25 A with cooling block), 1.4 A (microstep (1.8 A with cooling block)))
Current setting	Via potentiometer
Operating type	Bipolar
Operating mode	1/1, 1/2, 1/4, 1/8 (precis)
Protection function	Overcurrent, overvoltage and over-temperature
Step frequency	0 to 200 kHz
Current reduction	Switchable to 40%
Input signals	0 V active (L = 0.8 V; 3.5 V < H < 6 V or open)
Temperature range	0 to + 40°C
Connector	4ST connector
Weight	10 g
Fastening type	2 boreholes of Ø18.05 mm for M2.5 - mounted directly on the stepper motor

#### VERSIONS

Type	Min. Operating Voltage V	Max. Operating Voltage V	Rated Current A	Subsize for Stepper Motors	Interface	Weight kg
SMC11	12	35	1.4	Stepper Motors	4ST-Quadcan Chy	0.01

#### ORDER IDENTIFIER

SMC11	= 1/8 step mode
SMC11-2	= 1/16 step mode

#### ACCESSORIES

ZK4700/50	Charging Capacitor
ZK-SMC11	Connection cable

#### CAUTION

We recommend using a back-up capacitor of sufficient size to stabilize the operating voltage.

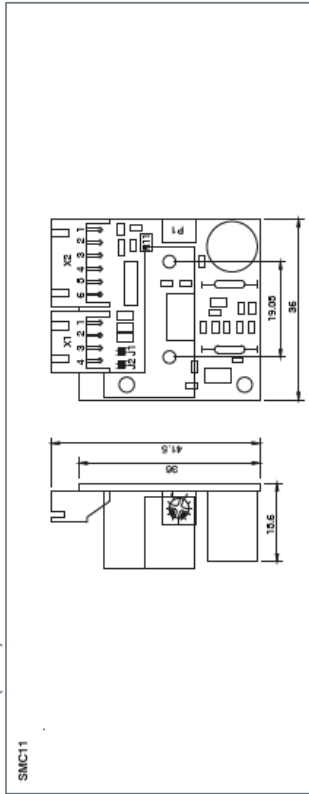
#### SMC11

Compact Microstep Controller

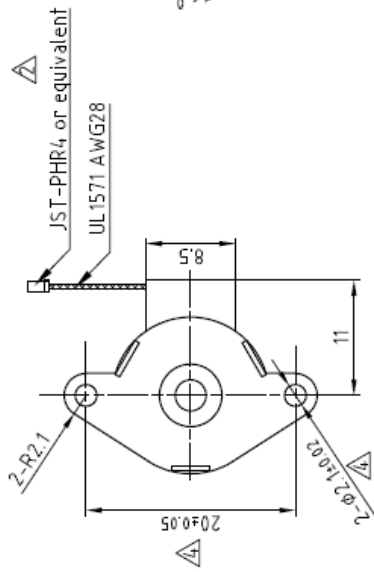


#### DIMENSIONS (IN MM)

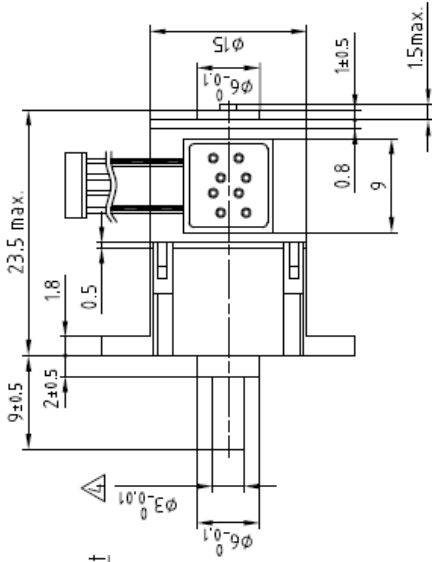
SMC11



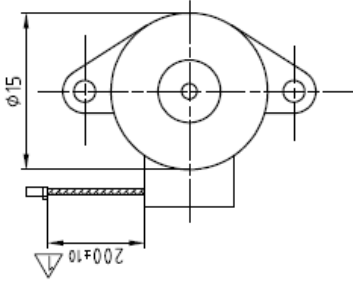
Front view and mounting



Side view

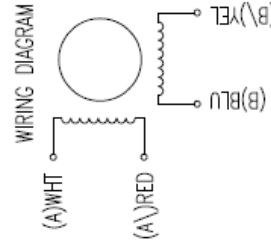


Rear view



SPECIFICATION	CONNECTION	BIPOLAR
VOLTAGE (VDC)		5
AMPS/PHASE		0.5
RESISTANCE/PHASE (Ohms)@25°C		10±7%
INDUCTANCE/PHASE (mH) @1KHz		2.3±20%
HOLDING TORQUE (Nm) [lb-in]		0.2 [1.76]
GEAR RATIO		1:102.5
STEP ANGLE (°)		18/102.5
STEP ACCURACY (NON-ACCUM)		±7%
ROTOR INERTIA (Kg-m <sup>2</sup> ) [lb-in <sup>2</sup> ]		1.0x10 <sup>-7</sup> [3.416x10 <sup>-4</sup> ]
WEIGHT (Kg) [lb]		0.012 [0.026]
TEMPERATURE RISE: MAX.80°C (MOTOR STANDSTILL; FOR 2 PHASE ENERGIZED)		
AMBIENT TEMPERATURE -10°~ 50°C [14°F ~ 122°F]		Δ
INSULATION RESISTANCE 100 MΩhm (UNDER NORMAL TEMPERATURE AND HUMIDITY)		
INSULATION CLASS E 120° [248°F]		
DIELECTRIC STRENGTH 500VAC FOR 1 MIN. (BETWEEN THE MOTOR COILS AND THE MOTOR CASE)		
AMBIENT HUMIDITY MAX. 85% (NO CONDENSATION)		

TYPE OF CONNECTION (EXTERN)	MOTOR			
	CONNECTOR PIN NO.	LEADS	WINDING	
A	1	WHT	A	
A\	2	RED	A\	
B	3	BLU	B	
B\	4	YEL	B\	



FULL STEP 2 PHASE-Ex., WHEN FACING MOUNTING END (X)

STEP	A	B	A\	B\	CCW	CW
1	+	+	-	-	↑	↓
2	-	-	+	+	↓	↑
3	-	+	-	+	↑	↓
4	+	-	+	-	↓	↑



4	change tolerance	27.04.17	A.S.	APVD	S.H.a.	14.01.08	STEPPING MOTOR
3	REMOVE LOAD SPEC.	28.02.14	J.D.	CHKD			
2	CONNECTOR TYPE	12.07.12	J.W.	DRN	J.W.	11.01.08	DWG.NO
REV	DESCRIPTION	DATE	DRN	SIGNATURE		DATE	

General tolerances DIN ISO 2768-mH	Work piece edge DIN ISO 13715
---------------------------------------	----------------------------------

Surface specification DIN ISO 1302	DATE	DRN
---------------------------------------	------	-----

SPG1518M0504-102



# Arduino MEGA 2560

Microcontroller board with ATmega2560



Microcontroller board with ATmega2560

Technical specification

microcontroller	ATmega2560
operating voltage	5V
Input voltage (recommended)	7-12V
Input voltage (limit)	6-20V
Digital I / O pins	54 (15 of them PWM output)
Analog input pins	16
DC Current via I / O pin	20mA
DC Current for 3.3V pin	50mA
Flash memory	256 KB of which 8 KB for boot loader
SRAM	8 KB
EEPROM	4 KB
Clock speed	16 MHz
length	101.52 mm
width	53.3 mm
mass	37 g

## A.4. Arduíno Control Routine

### A.4.1. Version without buttons on breadboard

```
Minha_versao $
#include <Stepper.h>

const int stepsPerRevolution = 1000;

//Initializes the library using ports 22 through 45 to
//ligacao ao motor
//Stepper myStepper(stepsPerRevolution, 8,10,9,11);
//arduino UNO 1- positivo 2- enable 3-direction 4-clock 5- negativo 6 - current down (ground);
  Stepper Motor1(stepsPerRevolution, 22,24,23,25);
  Stepper Motor2(stepsPerRevolution, 26,28,27,29);
  Stepper Motor3(stepsPerRevolution, 30,32,31,33);
  Stepper Motor4(stepsPerRevolution, 34,36,35,37);
  Stepper Motor5(stepsPerRevolution, 38,40,39,41);
  Stepper Motor6(stepsPerRevolution, 42,44,43,45); //Arduino Mega
// Stepper Motor ( ground, clock, ground, direction)
//Stepper(int number_of_steps, int motor_pin_1, int motor_pin_2, int motor_pin_3, int motor_pin_4)

void setup()
{
  //Determines the initial engine speed
  Motor1.setSpeed(300);
  Motor2.setSpeed(300);
  Motor3.setSpeed(300);
  Motor4.setSpeed(300);
  Motor5.setSpeed(300);
  Motor6.setSpeed(300);
}

void loop()
{
  //Turns the motor in clockwise (positive steps) or counterclockwise (negative steps), i steps.
  //With these parameteres each i=333 steps--> correspond to turn 1 degree;
  for (int i = 0; i<=1350; i++)
  {
    delay(5000); // 5-second pause
    Motor1.step(-1);
    Motor2.step(-1);
    Motor3.step(-1);
    Motor4.step(-1);
    Motor5.step(-1);
    Motor6.step(-1);
    delay(0);
  }
  delay(20000); //20-second pause
}
```

#### A.4.2. Version with buttons on breadboard

```
#include <Stepper.h>

const int stepsPerRevolution = 1000;
#define step_button_CCW 46
#define step_button_CW 47
#define step_button_CCW 48
#define step_button_CW 49

int status_button_step_step_CCW=0;
int status_button_step_step_CW=0;
int status_button_continuous_CCW=0;
int status_button_continuous_CW=0;

//Start the library using ports 22 to 45 to
//the motor connection
//Stepper myStepper(stepsPerRevolution, 8,10,9,11);
//arduino UNO 1- positivo 2- enable 3-direction 4-clock 5- negativo 6 - current down (ground)
  Stepper Motor1(stepsPerRevolution, 22,24,23,25);
  Stepper Motor2(stepsPerRevolution, 26,28,27,29);
  Stepper Motor3(stepsPerRevolution, 30,32,31,33);
  Stepper Motor4(stepsPerRevolution, 34,36,35,37);
  Stepper Motor5(stepsPerRevolution, 38,40,39,41);
  Stepper Motor6(stepsPerRevolution, 42,44,43,45); //Arduino Mega
//Stepper(int number_of_steps, int motor_pin_1, int motor_pin_2, int motor_pin_3, int motor_pin_4)

void setup()
{
  //Determines the initial stepper motor speed
  Motor1.setSpeed(300);
  Motor2.setSpeed(300);
  Motor3.setSpeed(300);
  Motor4.setSpeed(300);
  Motor5.setSpeed(300);
  Motor6.setSpeed(300);
  pinMode(button_step_step_CCW, INPUT);
  pinMode(button_step_step_CW, INPUT);
  pinMode(button_continuous_CCW, INPUT);
  pinMode(button_continuous_CW, INPUT);
}

void loop()
{
  //Turns the motor in clockwise i steps
  status_button_step_step_CCW=digitalRead(button_step_step_CCW);
  status_button_step_step_CW=digitalRead(button_step_step_CW);
  status_button_continuous_CCW=digitalRead(button_continuous_CCW);
  status_button_continuous_CW=digitalRead(button_continuous_CW);
```

```

//step-by-step clockwise
if(status_button_step_step_CCW==LOW)
{
  Motor1.step(1);
  Motor2.step(1);
  Motor3.step(1);
  Motor4.step(1);
  Motor5.step(1);
  Motor6.step(1);
  while(digitalRead(button_step_step_CCW)==LOW)
  {
  }
}
else
//step-by-step counterclockwise
if(status_button_step_step_CW==LOW)
{
  Motor1.step(-1);
  Motor2.step(-1);
  Motor3.step(-1);
  Motor4.step(-1);
  Motor5.step(-1);
  Motor6.step(-1);
  while(digitalRead(button_step_step_CW)==LOW)
  {
  }
}
else
//Continuous counterclockwise mode (while the user is pressing the button the motor rotates)
if(status_button_continuous_CW==LOW)
{
  while(digitalRead(button_continuous_CCW)==LOW)
  {
  }
}
else
//Continuous clockwise mode (while the user is pressing the button the motor rotates)
if(status_button_continuous_CW==LOW)
{
  while(digitalRead(button_continuous_CW)==LOW)
  {
  }
}
}

```

---

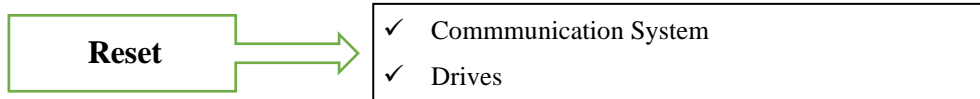
## A.5. Procedure to place baldes (automated part)

1. Check all wiring connections to the Arduino and breadboard (see diagram in [6.4](#) subsection and SMC11-2 controller manual);  
Note: Cable purple -> clock (control show many steps)  
Cable grey -> direction (control the direction)
2. Set the controller potentiometer to the desired step angle of the stepper motor (do not exceed level 4, so as not to burn the motors);
3. Send the code to the Arduino (routine present in annex [A.3](#));
4. Adjust the electrical parameters of the power supply unit
  - Output On/Off
  - Select +25V
  - Adjust voltage (12V or 24V—Better with 24V, more torque provided by the stepper motor)
  - Press Voltage/Current
  - Adjust current (Display limit 0,5 A)
5. Connect crocodile wires to positive and neutral breadboard wires;
6. Connect banana wires to the power source;
7. The system will be running, and it will be possible to see the variation in the current supplied (generally between 0.200 and 0.300 V) - 0.05 per stepper motor as the motors run;
8. After placing the blades in the desired position, remove at least one of the banana cables connected to the power source and perform the procedure of running the experiment ([annex A.6](#)).

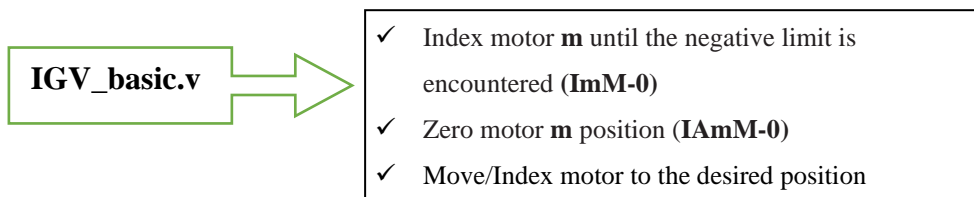
## A.6. Procedure to run the experiment (after placing blade angle)

Before performing the test and after the system has already been properly set up (i.e., IGVs angle correctly adjusted) some steps must always be taken.

1. Register the rpm of the blower;
2. Register the information relative to pressure, temperature and humidity of the room;
3. Check if all equipment is in order to be used;



1. Run the routine *IGV\_basic.vi*;



2. Run *cDAQ\_basic.vi*

